



TECHNICAL UNIVERSITY OF CRETE

SCHOOL OF MINERAL RESOURCES ENGINEERING

---

**Geostatistical Analysis of Porosity,  
Permeability and Production Data from  
Burbank Oil Field (Oklahoma, USA)**

---

*Author:* Ioannis Tsepetakis

*Advisory Committee :*

Professor D. T. Hristopulos (supervisor), School of Mineral  
Resources Engineering, TUC

Professor Nikolaos Varotsis , Assistant PhD Andreas Pavlides

August 18, 2020



# Dedication

*My family, my friends for full support...*

# Abstract

This thesis focuses on the analysis of data from a hydrocarbon reserve located in Burbank, Oklahoma. The study is based on the analysis of porosity, thickness and permeability data of a reservoir. Parameters were calculated for empirical models which relate the porosity and the permeability in porous media. Spatial analysis was also performed, based on two methods of linear spatial interpolation. One method belongs to the Kriging family and the other was the inverse distance weighting (IDW) method. These were applied with a view to estimating oil supplies in the reserve under normal conditions (OOIP) for specific flow units of the reservoir. In this thesis, the following units were examined: FU3, FU5, FU8, FU9 and FU10. The FU5 flow unit is extensively analysed and the others are presented in the Annex. Understanding of the spatial sequence is expected to improve plans for oil field development. It can provide a better picture of the financial risks at an early stage, and is therefore able to be of use when making investment decisions.

The first part of the thesis concerns the investigation of empirical formulae, namely the Kozeny-Carman, Timur and Coates models. Comparison of the models was performed on the basis of their adaptation to existing data. As performance criteria, the root mean square error (RMSE) and the Spearman's rank correlation coefficient were used. Based on these measures, the Timur model demonstrated better adaptation to porosity - permeability data.

In the second part, geostatistical analysis of the reservoir thickness in a flow unit was undertaken. Thickness combined with porosity make a contribution to the calculation of reserves and optimal exploitation planning. Different variogram models were examined and it was found that the spherical model was optimal. Point interpolation was applied to the data and the ordinary kriging stochastic interpolation algorithm was used. This methodology is the most reliable method of linear estimation when enough data is available. At the other extreme, there is the inverse distance weighting (IDW) method which uses an empirical exponent for the distance (it usually takes arbitrary values between 1 and 3). The IDW method is a quicker way of estimating specific drillings in the same flow unit.

---

The results of the spatial interpolation were evaluated using statistical validation measures. The IDW method resulted in better spatial estimation than the kriging based on the RMSE. Lastly, the OOIP was determined on the basis of an empirical formula that relates porosity to thickness and the technical characteristics of the reservoir (e.g : porosity, water saturation " $S_w$ " or oil formation volume factor " $B_o$ "). Using both the Kriging and the IDW methods, volumetric calculations showed 10,484,000 barrels for the first method and 9,565,300 barrels for the other method, respectively. The comparison of the methods was based on the (RMSE) between kriging and IDW total Oil in place (OOIP) results. Unlike IDW, Kriging provides the ability to construct uncertainty maps of point estimates. Under suitable assumptions on the priors, kriging gives the best linear unbiased prediction of the intermediate values. In future projects with a similar theme, it is recommended that simulation also be used, to ensure better control of spatial variations.

## Περίληψη

Η παρούσα εργασία επικεντρώθηκε στην ανάλυση δεδομένων από κοίτασμα υδρογονανθράκων που βρίσκεται στην πολιτεία της Οκλαχόμα των Ηνωμένων Πολιτειών και συγκεκριμένα στο Burbank . Η μελέτη βασίζεται στην ανάλυση δεδομένων πορώδους, πάχους και διαπερατότητας ενός ταμιευτήρα. Οι ιδιότητες αυτές είναι βασικές παράμετροι στην μηχανική του πετρελαίου και μπορούν να διερευνηθούν με την επιστήμη της γεωστατιστικής. Υπολογίστηκαν εμπειρικές εξισώσεις άλλα και συγκεκριμένα μοντέλα τα οποία συσχετίζουν το πορώδες και την διαπερατότητα σε πορώδη μέσα. Επίσης χρησιμοποιήθηκαν αλλά και αναλύθηκαν δύο οικογένειες μεθόδων χωρικής παρεμβολής. Η μία ανήκει στην οικογένεια Kriging και η άλλη είναι μέθοδος αντίστροφης απόστασης (IDW) . Κατόπιν, παρουσιάστηκαν εφαρμογές εκτίμησης αποθεμάτων πετρελαίου στο κοίτασμα σε κανονικές συνθήκες (OOIP) σε συγκεκριμένες ρεολογικές μονάδες του ταμιευτήρα.

Ο ταμιευτήρας καθορίζεται από 79 χερσαίες γεωτρήσεις μικρού βάθους. Οι ρεολογικές μονάδες είναι γνωστές στην πετρελαϊκή βιομηχανία ως «flow units». Μία γεώτρηση μπορεί να διέρχεται από περισσότερες από μία ρεολογικές μονάδες. Στην διπλωματική εξετάστηκαν οι μονάδες: FU3 με 94 δεδομένα, FU5 με 103 δεδομένα, FU8 με 110 δεδομένα, FU9 με 110 δεδομένα, FU10 με 104 δεδομένα. Η παρούσα διπλωματική χρησιμοποιεί τα δεδομένα της ρεολογικής μονάδας FU5 και οι υπόλοιπες έχουν αναλυθεί στο παράρτημα.

Στις γεωεπιστήμες συχνά είναι διαθέσιμο μόνο ένα δείγμα χωρικά άτακτων δεδομένων, όπως για παράδειγμα ένα σύνολο μετρήσεων συγκεντρώσεως ενός ρύπου στην ατμόσφαιρα. Οι σημαντικότερες αιτίες που περιορίζουν τη λήψη μετρήσεων ως επί το πλείστον, είναι το κόστος, αλλά και το ενδεχόμενο τα σημεία δειγματοληψίας να είναι δυσπρόσιτα. Παρόμοιοι περιορισμοί υπάρχουν και σε αλλά επιστημονικά πεδία, όπως στην επεξεργασία σήματος, ή σε ιατρικές εφαρμογές. Η εκτίμηση των τιμών της υπολογίσιμης ιδιότητας στα σημεία που δεν υπάρχουν μετρήσεις, πραγματοποιείται με χωρική παρεμβολή. Η κατανόηση της χωρικής αλληλουχίας αναμένεται να βελτιώσει τα σχέδια αξιοποίησης πετρελαϊκών κοιτασμάτων. Δίνει μια καλύτερη εικόνα του οικονομικού κινδύνου σε πρώιμο στάδιο, έτσι ώστε να χρησιμοποιηθεί για να ληφθούν επενδυτικές αποφάσεις.

Το πρώτο σκέλος της διπλωματικής αφορά στη διερεύνηση εμπειρικών εξισώσεων και συγκεκριμένα στα μοντέλα Kozeny - Carman, Timur και Coates , τα οποία συσχετίζουν το πορώδες και την διαπερατότητα σε πορώδη μέσα. Αξίζει να σημειωθεί ότι τα συγκεκριμένα μοντέλα χρησιμοποιούνται ευρέως για τον ποσοτικό προσδιορισμό της διαπερατότητας σε σημεία που είναι ανέφικτος ο υπολογισμός κορεσμού σε νερό ( $S_w$ ) .Ωστόσο, αυτά τα εμπειρικά μοντέλα δεν περιλαμβάνουν την δομή των πετρωμάτων,

---

την χωρική κατανομή υγρών στο χώρο των πόρων του πετρώματος ή την επίδραση της κατανομής ορυκτών αργίλου στην διαπερατότητα. Η σύγκριση των μοντέλων έγινε με βάση την προσαρμογή τους στα υπάρχοντα δεδομένα. Χρησιμοποιήθηκε η ρίζα μέσης τετραγωνικής απόκλισης (RMSE) ως κριτήριο επίδοσης και ο συντελεστή συσχέτισης Spearman . Με βάση τα μέτρα αυτά, το μοντέλο Timur επέδειξε καλύτερη προσαρμογή στα δεδομένα πορώδους - διαπερατότητας.

Στο δεύτερο σκέλος αυτής της διπλωματικής εργασίας εκπονήθηκε γεωστατιστική ανάλυση του πάχους του πετρώματος σε μια ρεολογική μονάδα (flow unit). Το πάχος σε συνδυασμό με το πορώδες συμβάλλουν στον υπολογισμό των αποθεμάτων και στην επιλογή του κατάλληλου σχεδιασμού για την εκμετάλλευση. Πραγματοποιήθηκε καθορισμός της ρεολογικής μονάδας με υπολογισμό διαφορετικών μοντέλων βαριογράμμάτων. Βρέθηκε ότι το σφαιρικό μοντέλο ήταν το βέλτιστο μοντέλο βαριογράμματος. Η ανάλυση ενός βαριογράμματος χαρακτηρίζει τη χωρική συνέχεια ενός συνόλου δεδομένων. Τα μονοδιάστατα στατιστικά στοιχεία για δύο σύνολα δεδομένων όπως το πορώδες και το πάχος, μπορεί να είναι σχεδόν ίδια, αλλά η χωρική συνέχεια μπορεί να είναι αρκετά διαφορετική.

Στα πλαίσια της γεωστατιστικής ανάλυσης διεξήχθη σημειακή παρεμβολή στα δεδομένα και χρησιμοποιήθηκε ο στοχαστικός αλγόριθμος παρεμβολής του κανονικού kriging. Η μεθοδολογία αυτή είναι ο πιο αξιόπιστος γραμμικός τρόπος εκτίμησης όταν υπάρχουν αρκετά δεδομένα. Στον αντίποδα, υπάρχει η μέθοδος αντίστροφης απόστασης (IDW) που χρησιμοποιεί ένα εμπειρικό εκθέτη (συνήθως παίρνει τιμές αυθαίρετα μεταξύ 1 και 3). Η μέθοδος IDW αποτελεί ταχύτερο τρόπο εκτίμησης για τις συγκεκριμένες γεωτρήσεις στην ίδια ρεολογική μονάδα. Τα αποτελέσματα της χωρικής παρεμβολής αξιολογήθηκαν χρησιμοποιώντας στατιστικά μέτρα επικύρωσης (Validation Measures). Αυτές οι συγκρίσεις έδειξαν ότι με εκθέτη 1,5 για το πορώδες και 2,5 για το πάχος η μέθοδος αντίστροφης απόστασης (IDW) οδήγησε σε καλύτερη χωρική εκτίμηση από το kriging , σύμφωνα με μέτρο επίδοσης την ρίζα μέσης τετραγωνικής απόκλισης (RMSE) . Προσδιορίστηκε το ΟΟΙΡ (συνολική ποσότητα πετρελαίου στο κοίτασμα σε κανονικές συνθήκες) βάση εμπειρικής εξίσωσης που συνδέει το πορώδες με το πάχος και τεχνικά τα χαρακτηριστικά του ταμιευτήρα. Κάνοντας χρήση τόσο της μεθόδου του Kriging όσο και του IDW, οι ογκομετρικοί υπολογισμοί έδειξαν 10,484,000 για την μία και 9,565,300 βαρέλια για την άλλη αντίστοιχα. Η διαφορά είναι 9.6 ή 918,700 βαρέλια. Η σύγκριση των μεθόδων έγινε με βάση τα στατιστικά μέτρα απόδοσης και συγκεκριμένα την ρίζα μέσης τετραγωνικής απόκλισης (RMSE). Σε αντίθεση με την IDW, το Kriging παρέχει την δυνατότητα να κατασκευαστούν χάρτες αβεβαιότητας των σημειακών εκτιμήσεων. Σε μελλοντικές εργασίες με παρόμοια θεματολογία προτείνεται επιπλέον χρήση προσομοίωσης για καλύτερο έλεγχο των χωρικών διακυμάνσεων.

---

Η εργασία αυτή ακολουθεί την εξής δομή: Στο πρώτο κεφάλαιο γίνεται ανάλυση των στόχων και του κινήτρου αυτής της διπλωματικής εργασίας. Ακόμα, γίνεται η εισαγωγή σε βασικά χαρακτηριστικά των γεωτρήσεων πετρελαίου. Στο δεύτερο κεφάλαιο παρουσιάζεται η θεωρία που απαιτείται για την κατανόηση ενός ταμειευτήρα πετρελαίου και σχετικοί όροι. Στο τρίτο κεφάλαιο εισάγονται τα τυχαία πεδία, ο ορισμός τους αλλά και το θεωρητικό υπόβαθρο το οποίο χρησιμοποιείται στην διπλωματική. Στο τέταρτο κεφάλαιο εισάγονται εμπειρικά μοντέλα για την συσχέτιση της διαπερατότητας και του πορώδους. Γίνεται εκτίμηση των παραμέτρων τους από τα δεδομένα και αξιολόγηση των μοντέλων. Το πέμπτο κεφάλαιο παρουσιάζει στοχαστικές και αιτιοκρατικές μεθόδους χωρικής παρεμβολής και συγκρίνει την εφαρμογή τους στην εκτίμηση της συνολικής ποσότητας πετρελαίου στο κοίτασμα σε κανονικές συνθήκες (OOIP).



# Acknowledgements

Over the last six years I managed to fulfil one of the most challenging and hard working tasks of my life. It's the time that you realise that nothing is easy, and in order to succeed in your dreams, you need to go the extra mile to make that work.

First of all, I would like to heartily thank my advising committee, my project advisor Professor D. T. Hristopoulos, for the opportunity to work with him upon an intriguing topic and for the productive cooperation that we have had during this period. Furthermore, Professor N. Varothis for the useful advice and comments that he provided me with. Last but not least Dr A.Pavlidis for his support and guidance throughout this project.

Of course, nothing would have been possible without the support of my family and my close friends. With this opportunity, I would like to thank my mother, for her constant and unconditional support. And of course, no words can express how grateful i am for my partner, Olga, who has been by my side both in good and bad times, for many years now. Furthermore, I acknowledge the person to whom I owe the most, my father, who managed through his continuous guidance to convert one of the world's most impatient person, to a more patient, persistent and determined one.

Last but not least, I would also like to express my gratitude to the members of the Geostatistics Laboratory of the Mineral Resources Engineering School of Technical University of Crete for their invaluable help during this thesis.

# Contents

<b>1</b>	<b>Motivation and Drilling Engineering</b>	<b>1</b>
1.1	Motivation . . . . .	1
1.2	History of Drilling . . . . .	3
1.3	The Drilling Team . . . . .	3
1.4	Drilling Rigs . . . . .	6
1.4.1	Land Rigs . . . . .	8
1.5	Burbank Region . . . . .	8
1.5.1	Burbank Stratigraphy . . . . .	11
<b>2</b>	<b>Reservoir Characterization</b>	<b>13</b>
2.1	Preliminaries . . . . .	13
2.1.1	Creation of liquid hydrocarbons . . . . .	14
2.1.2	Immigration of hydrocarbons . . . . .	14
2.1.3	Classification of hydrocarbon reservoirs . . . . .	15
2.1.4	Storage conditions . . . . .	15
2.1.5	Well logs . . . . .	17
2.2	Reservoir Heterogeneity . . . . .	19
2.3	Oil Terminology . . . . .	23
2.3.1	Net pay zone . . . . .	23
2.3.2	Gross thickness zone . . . . .	23
2.3.3	Porosity . . . . .	23
2.3.4	Determining permeability . . . . .	25
2.3.5	Oil formation volume factor . . . . .	25
2.3.6	Water saturation . . . . .	26
2.4	Original Oil In Place (OOIP) . . . . .	26
2.5	Flow unit . . . . .	28
<b>3</b>	<b>Random Fields</b>	<b>30</b>
3.1	Geostatistics . . . . .	30
3.2	Random field . . . . .	31

3.3	Randomness . . . . .	32
3.4	Spatial interpolation . . . . .	33
3.5	Covariance . . . . .	33
3.5.1	Covariance Versus Variogram . . . . .	34
3.6	Statistical homogeneity . . . . .	34
3.6.1	Statistical isotropy . . . . .	35
3.6.2	Statistical anisotropy . . . . .	35
3.6.3	Trend model . . . . .	35
3.6.4	Trend removal . . . . .	36
3.6.5	Variogram models . . . . .	36
3.6.6	Theoretical variogram model . . . . .	37
3.6.7	Kriging . . . . .	38
3.6.8	Simple kriging . . . . .	39
3.6.9	Ordinary kriging . . . . .	40
3.7	Spatial Model Validation . . . . .	41
3.7.1	Validation measures . . . . .	42
3.8	Inverse Distance Weight Method . . . . .	44
<b>4</b>	<b>Relation Between Permeability-Porosity</b>	<b>46</b>
4.1	Introduction . . . . .	46
4.1.1	Permeability importance for Data modeling . . . . .	47
4.1.2	Permeability and importance of grain size . . . . .	47
4.2	Permeability Empirical Models . . . . .	48
4.2.1	Kozeny–Carman . . . . .	48
4.2.2	Empirical models . . . . .	49
4.3	Preliminary data analysis . . . . .	50
4.4	Results and discussion . . . . .	51
<b>5</b>	<b>Use of Geostatistics in Reservoir Description</b>	<b>56</b>
5.1	Introduction . . . . .	56
5.2	Preliminary data analysis . . . . .	58
5.3	Kriging . . . . .	60
5.3.1	Ordinary kriging implementation . . . . .	60
5.3.2	Porosity and thickness trend analysis . . . . .	60
5.3.3	Variogram analysis . . . . .	61
5.3.4	Kriging maps - reserves estimation . . . . .	62
5.3.5	Total oil in place (OOIP) analysis . . . . .	63
5.3.6	IDW and kriging comparison . . . . .	68
5.4	Synopsis . . . . .	71
<b>6</b>	<b>Conclusions and Suggestions for Further Research</b>	<b>75</b>

6.1	Conclusions . . . . .	75
6.1.1	Future work . . . . .	77
<b>7</b>	<b>Appendix</b>	<b>82</b>

# List of Figures

1.1	Edwin L. Drake (Giddens 1975). Used with permission from the Pennsylvania Historical and Museum Commission Drake Well Museum Collection, Titusville, Pennsylvania. Adapted from [23]. . . . .	4
1.2	Cable-tool rig schematic. After Brantley (1940).Figure retrieved from Adapted from [23]. . . . .	5
1.3	Well classification.Figure retrieved from [23]. . . . .	6
1.4	Drilling operations in the Chinook Field, Gulf of Mexico (courtesy of Petrobras), Alaska (courtesy of Minerals Management Service), and Brazil's Amazon jungle (courtesy of Petrobras).Figure retrieved from [23]. . . . .	7
1.5	The rotary drilling process (Bourgoyne et al. 1991).Figure retrieved from [23]. . . . .	9
1.6	Rig with cantilever derrick (Derrick Engineering Company 2010) and Mobile rig with portable mast (GEFCO 2007),Courtesy of GEFCO .Figure retrieved from [23]). . . . .	10
1.7	Burbank oil Field.Figure retrieved from [36]. . . . .	11
1.8	Oklahoma oil Field.Figure retrieved from [36] . . . . .	12
2.1	Stages of hydrocarbon creation with total a oil and Gas geological background Figure retrieved from [28]. . . . .	14
2.2	Schematic Integration's of all relevant data that create a reservoir interpolation Figure retrieved from [20] . . . . .	15
2.3	Well logging records the events, subsurface formations, and depth measurements of geologic formations during drilling. Adapted from [38].	19
2.4	Burbank well Logs Example. Adapted from [36]. . . . .	20
2.5	Scales of Reservoir Heterogeneities.Figure retrieved from [37]. . . . .	21
2.6	Vertical heterogeneities. a)top-view, b)front-view. Figure retrieved from [21] . . . . .	22
2.7	Effect of gigascopic Heterogeneities on Performace.Figure retrieved from [10]. . . . .	23

2.8	Gross thickness and net thickness. Figure retrieved from [3]. . . . .	24
2.9	Heterogeneities can be measured from small-scale measurement of grain-size distribution at a microscopic level to large-scale geological at a basin level. Figure retrieved from [10]. . . . .	25
2.10	Volumetrics is an integration of geological fluid and the modeled relationships. Figure retrieved from [39]. . . . .	27
2.11	Four possible conditions for isotropy/anisotropy and homogeneity/heterogeneity. Note that what is apparent at one scale may not be apparent at another. For example, when viewed close up, a sample may appear homogeneous and isotropic (lower left), yet from afar it may be heterogeneous and isotropic (lower right). Here, heterogeneity is expressed as bed boundaries. Figure retrieved from [7] . . . . .	29
3.1	The three principal parameters of the variogram [40] . . . . .	38
4.1	Permeability Norm Plot of Flow Unit 5 . . . . .	52
4.2	Porosity Norm Plot of Flow Unit 5 . . . . .	52
4.3	Porosity Histogram of Flow Unit 5 . . . . .	53
4.4	Permeability Histogram of Flow Unit 5 . . . . .	53
4.5	Timur, Kozeny-Carman, Coates Equation . . . . .	54
5.1	Flow Chart for Total Oil in Place (OOIP) Processing . . . . .	57
5.5	Thickness Variograms of Flow Unit 5 . . . . .	62
5.6	Porosity Variograms of Flow Unit 5 . . . . .	62
5.7	Multiplication Porosity and Thickness Variogram of Flow Unit 5 . . . .	63
5.12	Total Oil in Place of Flow Unit 5 multiplication . . . . .	69
5.13	Total Oil in Place (bbl) . . . . .	70
5.15	IDW OOIP of Flow Unit 5 . . . . .	74
5.16	IDW Simulations for flow units 5 . . . . .	74

# List of Tables

3.1	Common models of trend functions (1D)	36
4.1	Data statistics of flow unit 5	51
4.2	Validation Measures (RMSE,Pearson) on Empirical Models	55
5.1	Trend Values for data statistics of flow unit 5	58
5.2	Detrended data statistics of flow unit 5	58
5.3	Detrended data statistics of flow unit 5	60
5.4	Variogram Parameters Thickness	61
5.5	Variogram Parameters Porosity	63
5.6	Variogram Parameters with $((\log(\%) \cdot (m)))$	68
5.7	Thickness Variogram Errors (RMSE(m))	68
5.8	Porosity Variogram Errors (RMSE(%))	69
5.9	Multiplication Porosity and Thickness Variogram Variogram Errors RMSE( $(\log(\%) \cdot (m))$ )	69
5.10	Kriging of Porosity (Validation Measures)	69
5.11	Kriging of Thickness (Validation Measures)	70
5.12	Kriging of Multiplication $((\log(\%) \cdot (m)))$	70
5.13	Total Oil In Place in bbl for each method	71
5.14	Validation Measures IDW of Thickness with Power index (1,1.5,2,2.5,3)	71
5.15	Best Power index (2.5) Thickness	71
5.16	Validation Measures IDW of Porosity with Power index (1,1.5,2,2.5,3)	72
5.17	Best Power index (2.5) Porosity	72

# Chapter 1

## Motivation and Drilling Engineering

I know nothing except the fact  
of my ignorance.

---

Socrates

### 1.1 Motivation

Envision an amazing source of energy whose location is known but not easily accessible. Now imagine that this energy will be used to provide means of transportation for every person living on Earth. In addition, envision that this incredible energy will also allow every product, natural or industrialized, to be transported from or into virtually any place on the face of our planet. As a consequence of that, this energy will somehow be an important part of every venture in every country of the world.

During the last decades, geostatistical approaches have been successfully applied in different environmental and earth sciences disciplines. Geostatistics methods that can be applied in difficult situations, such as sparse measurements, is able to provide space time predictions for variables with reserves estimation and provides evaluation of the uncertainty of the results.

Nowadays, geostatistical methods are at the core of new research methodologies that are being proposed. Because of the uncertainties involved, probability approaches are required to enable oil resources managers to undertake analyses of risk under scenarios of oil production. Mathematical techniques are being developed to



construct probability distributions for specified outcomes. Most studies of oil estimation methods they provide uncertainty. The combination of different techniques - methods gives a high level of trust. And lastly increased or decreased the availability of oil stocks.

Many interpolation and approximation methods were developed in order to predict values of spatial phenomena at unsampled locations. For a review of the interpolation methods utilized in Geosciences. In general, the methods can be classified into two classes depending whether randomness is taken into account:

**Deterministic spatial interpolation methods** Randomness is not taken into account. There is no assessment of prediction errors. Examples of such interpolation methods are: nearest neighbors, triangular irregular network related interpolations, natural neighbors<sup>3</sup>, inverse distance weighting, regression models, several spline-based models and Fourier series interpolation models.

**Stochastic spatial interpolation methods** Randomness is taken into account. Assuming random errors, these methods provide an assessment of prediction errors. This is the key advantage of the stochastic methods. Examples of stochastic (or geostatistical) interpolation methods are the several flavors of kriging and its extensions: Simple, Ordinary, Universal, Block, Indicator etc.

This thesis is motivated by the need for accurate interpolation methodologies that can help to determine the spatiotemporal variability of well logs data. Thus, below we introduce spatiotemporal methodologies applied on field data from Burbank oil field. It is necessary to understand quantitatively the variations in the spatial distribution in order to optimize exploitation plans, correctly assess investment risks, and timely compensate for spatial variations in the quality of the energy product.

Geostatistical analysis is commonly used for reserves estimation. However, the exploitation lasts for several years. The price of the product, the oil exploration costs, the environmental reclamation cost, the cost to expropriate the land and other costs usually fluctuate significantly during the duration of the exploitation. For example, the price of crude oil was nearly halved between 5 years now almost 40\$ per barrel [17]. Changes in costs or product price could render unprofitable the exploitation of certain parts of the oil that were considered profitable based on previous economic estimates thus changing the reserves.

At this point, this chapter introduces the fundamentals aspects of the drilling. It covers the basic definitions related to drilling engineers, importance and the procedure for drilling operations. The applications and history of drilling are also outlined. The systematic approach and the introduction to casing sets are discussed. Finally, the aspects of sustainable drilling operation will be introduced.

## 1.2 History of Drilling

Oil and gas drilling are not new, in fact, they have already been occurring for many centuries. The first evidence of wells purposely drilled for production of hydrocarbons, was in China during the 4th century, as well as wells purposely drilled for oil production in Japan during the 7th Century. In Europe, the first oil well drilled activity was found in Pechelbronn, France, in 1745, where petroleum mining from oil sands had, in fact been taking place since 1498. After that, many wells were drilled, mostly using rudimentary hand tools, in Europe, North America, and Asia where an oil well was drilled in 1848 on the Aspheron Peninsula northeast of Baku. Following the Baku well, various shallow oil wells were drilled in Europe during the next decade. Obviously, in this thesis, we are going to describe methods that are completely different from those prehistoric ones, more modern techniques and equipment are used nowadays, however it is important to highlight where it all started.

There are many different versions about where the first well of the modern oil industry was drilled. Depending on the historian, locations and dates will vary widely. Also, there are many different depictions about what should be considered a modern well and what would differentiate it from a well that, even though it has produced oil, was not actually drilled having that as a primary goal.

Generally, without dueling about whom, where, and when, which would be rather ineffectual, we will mention some important milestones and pioneers that have contributed to the advancement of the modern oil industry in those early days. In 1858, in Oil Springs (then part of the township of Enniskillen), Ontario, Canada, a rudimentary 49-ft (14.93-m) well was dug by James Miller Williams with the intention to produce “kerosene” for lamps. Even though this is considered to be one of the pioneer ventures of the North American oil industry, the Williams well did not represent any significant advance as far as drilling technology is concerned. A true milestone for the drilling industry and probably the world’s most widely recognized drilling milestone occurred in 1859. In that year, in Titusville, Pennsylvania, USA, Edwin L. Drake [1.1](#) drilled what is, so far as known or documented, the first well purposely planned for oil in the United States. Even though there is evidence of oil and gas wells that had been drilled in the United States for as long as 40 years prior to the Drake well, most of those early wells were actually originally drilled in search of potable water or brine [\[23\]](#).

## 1.3 The Drilling Team

Modern well drilling is an activity that involves many specialists and usually various companies. The expertise and number of engineers and technicians involved



Figure 1.1: Edwin L. Drake (Giddens 1975). Used with permission from the Pennsylvania Historical and Museum Commission Drake Well Museum Collection, Titusville, Pennsylvania. Adapted from [23].

in the planning and execution of a drilling operation will depend on the type of well being drilled, its purpose, the well location, its depth, and the complexity of the operation. A well drilled with the purpose of discovering a new petroleum reservoir is called an exploration (or wildcat) well. Wildcat wells are the very first ones drilled in a certain unexplored area. After a wildcat well has shown the potential of a reservoir to be productive, appraisal wells may be drilled to obtain more information about the reservoir and its extension. Once a newly discovered reservoir is considered economically viable, a development plan is established and development wells are drilled to produce the oil and gas present in the reservoir. Besides the most common exploration and development wells, special wells may be drilled for a variety of purposes including stratigraphic tests and blowout relief presents an overall classification of wells according to their purpose.

The rights for a company to explore a certain area must be secured before any activity is carried out. Due to the high risk involved in the business, it is not uncommon to have two or more companies forming a consortium for the venture. Normally in that case, one company—the operating partner—will lead the operation while the other partners, who will have proportional participation in all expenses and profits, may or may not have a say on the operational procedures depending on the clauses accorded in the joint operating agreement (often referred to as the JOA) [23].

Prior to any drilling activity, seismic and geologic studies are carried out in order to determine the best location for the first exploration well. Those studies are

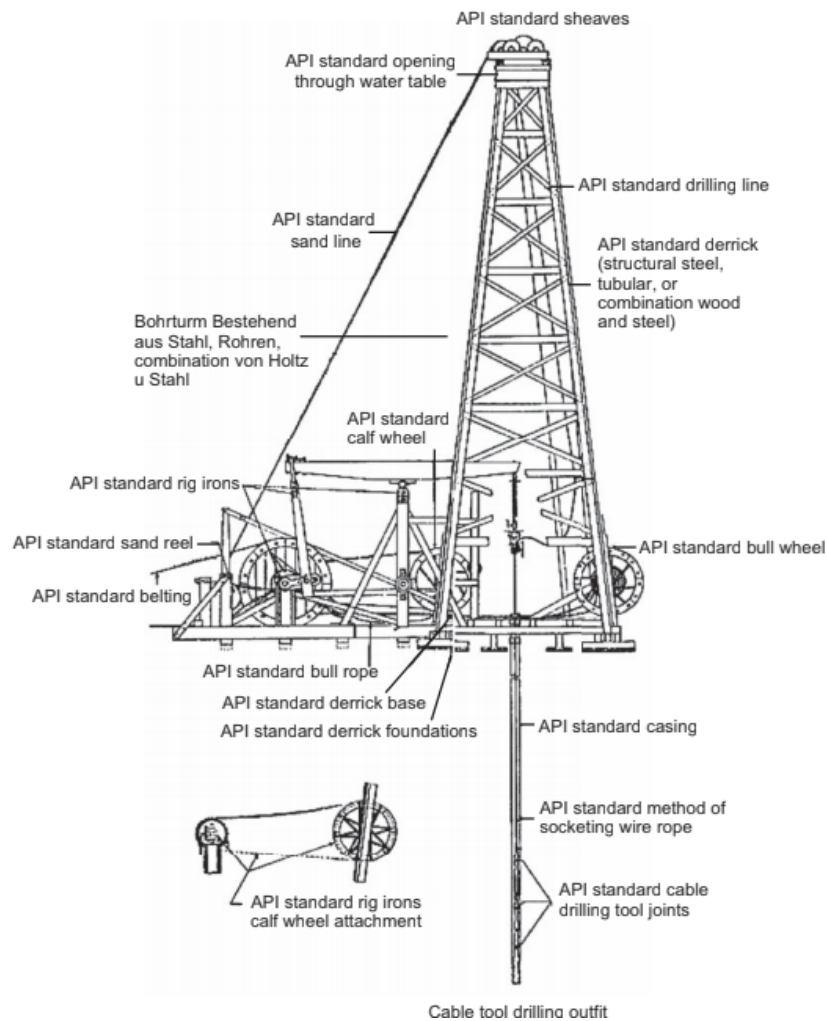


Figure 1.2: Cable-tool rig schematic. After Brantley (1940). Figure retrieved from Adapted from [23].

Objective	Trajectory	Environment
<ul style="list-style-type: none"> <li>• Exploration <ul style="list-style-type: none"> <li>◦ Wildcat</li> <li>◦ Appraisal</li> <li>◦ Extension</li> </ul> </li> <li>• Development</li> <li>• Injection</li> <li>• Special purpose <ul style="list-style-type: none"> <li>◦ Stratigraphic</li> <li>◦ Blowout relief</li> </ul> </li> </ul>	<ul style="list-style-type: none"> <li>• Vertical</li> <li>• Directional <ul style="list-style-type: none"> <li>◦ Inclined</li> <li>◦ Horizontal</li> <li>◦ Long reach</li> <li>◦ Special design</li> </ul> </li> </ul>	<ul style="list-style-type: none"> <li>• Onshore</li> <li>• Offshore</li> </ul>

Figure 1.3: Well classification. Figure retrieved from [23].

performed by a company's geological team, which usually is responsible for recommending locations for wildcat wells, while the reservoir team will be responsible, on a later phase, for locating development wells. In either situation, the drilling team will be responsible for the planning and execution of the operation including its budget (cost estimation) and contingency plans. Leading a drilling operation is not an easy task. Normally, the oil company that owns the exploration rights for the area, or the operating partner in case of a consortium, assembles a drilling team that in turn will prepare the detailed well design and the drilling program and establish operational procedures according to local regulations and the company's own health, safety, and environment (HSE) policy. This is done in order to conduct drilling operations in the most safe, clean, and economical way. The drilling operation itself generally will be carried out by a drilling contractor that may be hired specifically for a certain well or on a long-term contract. The contractor will be responsible for performing the operations according to the well program using the equipment and procedures specified in the contract 1.4, shows an offshore location in the North Sea, an operation in western Canada, and another in Brazil's Amazon jungle [23].

## 1.4 Drilling Rigs

Currently, rotary drilling is the standard oil well drilling method for the drilling industry, with almost all operations being performed by rotary-drilling rigs. Rigs will vary widely in size, drilling capability, level of automation, and environment in which they can operate. Nevertheless, the basic rotary-drilling process is the same for all types of rigs as shown in 1.5, the well is drilled using a bit that, under a downward force and rotation, breaks the rock into small pieces. The force is provided by the



Figure 1.4: Drilling operations in the Chinook Field, Gulf of Mexico (courtesy of Petrobras), Alaska (courtesy of Minerals Management Service), and Brazil's Amazon jungle (courtesy of Petrobras). Figure retrieved from [23].

weight of pipes placed above the drilling bit, while rotation generally is provided at surface by equipment that rotates the drill string, which in turn transmits rotation to the bit. As the bit drives into the ground, deepening the well, new pipes are added to the drill string. The small pieces of rock (cuttings), resulting from the bit action, are transported to surface by a fluid (drilling fluid or mud) that is constantly pumped into the hollow drill string all the way to the bottom of the hole, where it passes through small orifices placed at the bit, and returns to surface carrying the cuttings through the annular space formed between the well and the drill string. Once reaching the surface, the cuttings are separated from the fluid, which is treated for reuse. Generally, rotary rigs are classified as either land rigs or marine rigs [1.3](#), shows rig classification under those categories.

### **1.4.1 Land Rigs**

Land rigs, in a broad sense, can be categorized as conventional and mobile. Mobile rigs tend to be more easily transported, while the conventional rigs will take longer to be moved from one location to another [1.6](#). Conventional rigs normally use a standard derrick that needs to be built on location before drilling the well and is usually dismantled before moving to the next location. In the past, quite often the derrick was left standing above the well after it began production in case workovers became necessary however, today's modern rigs are usually built so that the derrick can be easily disassembled and moved to the next wellsite. There also are special rigs that are built in a way that rig pieces, when disassembled, will never exceed a certain weight, allowing transportation by helicopter. Those rigs, also called heli-transportable rigs, are used in remote areas with no road infrastructure and also on jungle operations.

Mobile rigs have a cantilever derrick or a portable mast that is raised and lowered as a whole rather than being constructed piecemeal. The rig-up and rig-down operation is less time-consuming than on conventional rigs [\[23\]](#).

## **1.5 Burbank Region**

The first oil produced in Osage County was on its eastern line, near Bartlesville, Oklahoma. This was found at a depth of 1,600 feet, near the base of the Pennsylvanian series. It is the most widespread and prolific of any oil sand in the county. The western limit of this sand, as now known, may be shown by a northeast- southwest line nearly through the center of the county. Because developments started in the eastern part of the county and worked west, operators, after drilling many dry holes west of the center of the county, became reluctant to drill even on well-known

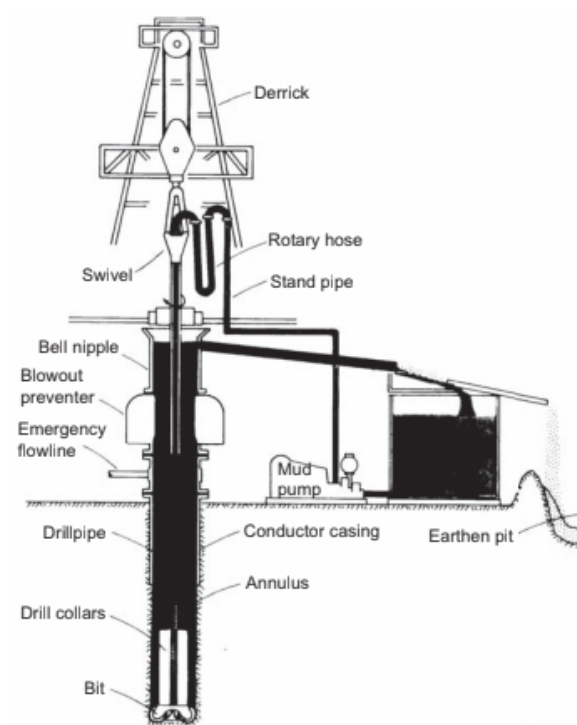


Figure 1.5: The rotary drilling process (Bourgoyne et al. 1991).Figure retrieved from [23].





Figure 1.6: Rig with cantilever derrick (Derrick Engineering Company 2010) and Mobile rig with portable mast (GEFCO 2007), Courtesy of GEFCO .Figure retrieved from [23]).

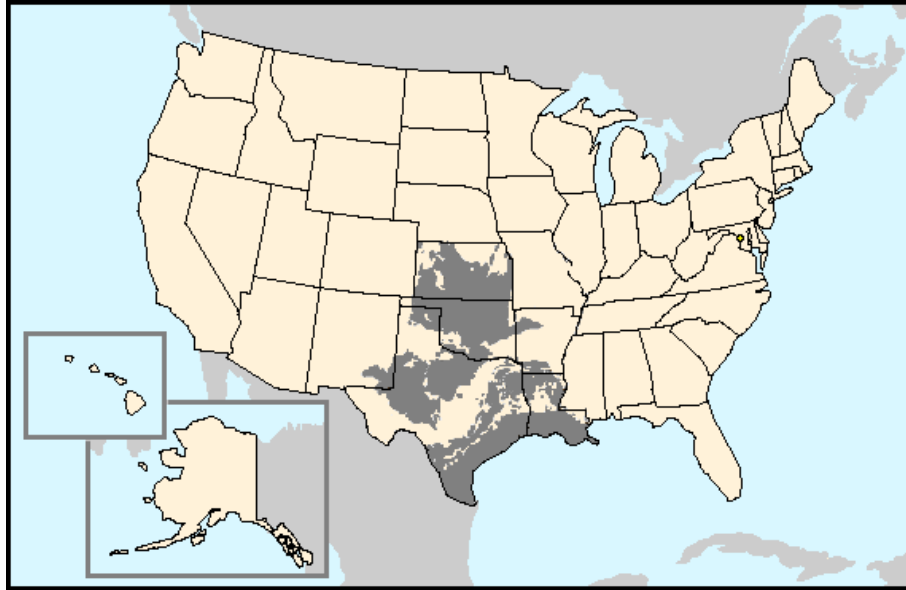


Figure 1.7: Burbank oil Field. Figure retrieved from [36].

anticlines in the western Osage, in which the Burbank field is located. It was not until the Marland Oil Company drilled in its first well in the Burbank field in May, 1920 [26].

An incorporated town in western Osage County, Burbank is situated just north of U.S. Highway 60, twenty-two miles west of the Osage County seat of Pawhuska and 122 miles northeast of Oklahoma City 1.7. Burbank was established on the Eastern Oklahoma Railway in 1903 and evolved as a farming and ranching community. The town had approximately two hundred residents when oilman Ernest W. Marland discovered the Burbank oil field north and east of town on May 14, 1920. As a result, Burbank became a 'boom' town and a center of oil-field activity [36].

The Burbank Field produced more than thirty-one million barrels of oil in 1923. The Phillips Petroleum Company and the Sinclair Oil and Gas Company built large refineries near town 1.8. Burbank declined with the oil boom during the Great Depression. Agriculture subsequently supported the local economy. Burbank was a community of 155 citizens in 2000 [36].

### 1.5.1 Burbank Stratigraphy

The stratigraphy of Osage County has been so thoroughly studied by all of the oil companies operating in that district, and also has been described so completely in several publications, particularly those of the United States Geological Survey,

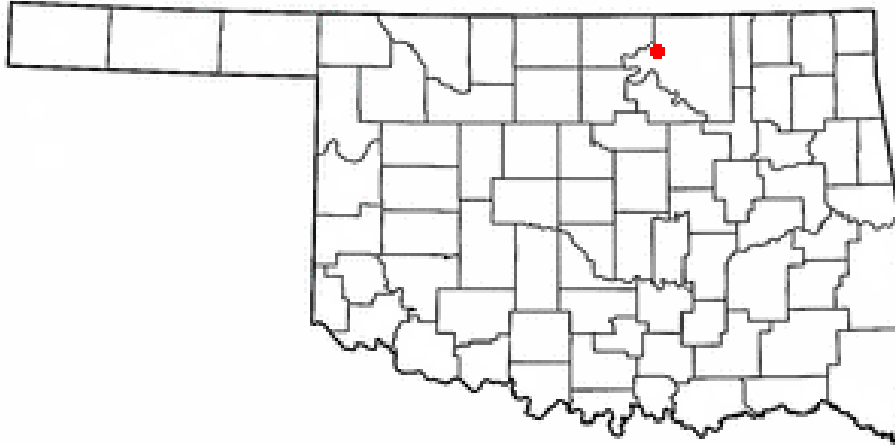


Figure 1.8: Oklahoma oil Field. Figure retrieved from [\[36\]](#)

that space will not be taken here to describe the different members in detail ??.

The surface rocks of the entire county, with the exception of a small area in the northwest part, are of Pennsylvanian age Permian rocks overlies the Pennsylvanian conformable in that area. The contact of the Permian and Pennsylvanian extends northeast and southwest, through the eastern side of the Burbank field, so that most of the limestones used in working the surface structure are of Permian age. The total thickness of the Pennsylvanian series in Osage County is about 2,900 feet. It contains several different producing horizons in different parts of the county, be one field producing from several horizons at the same time [\[26\]](#), [\[36\]](#).

# Chapter 2

## Reservoir Characterization

Omnia bona quoad perora  
"All prospects look good until  
drilled"

---

Motto used by Anadarko in  
1994 following their sub-salt  
drilling in the Gulf of Mexico

### 2.1 Preliminaries

As reservoir is defined as a porous, permeable and sedimentary rock which contains an economically exploitable concentration of hydrocarbons. It is surrounded by impenetrable rock (cap rock) and usually by a aquifer. Most reservoir rocks are sandstones and carbonates. These consist of a solid structure (matrix) and a pore space that include both fissures and fractures of the rock. When filling the reservoir, oil or gas migrating from the parent rock displaces some of the pre-existing water in the pores. However, some of the water remains in the porous space in contact with the hydrocarbon phase. Therefore, the part of the rock whose porous space is occupied by hydrocarbons and residual water can be defined as a reservoir. The main properties of the permeable rock that make the amount of hydrocarbons exploitable are the high permeability and the high porosity of the rock as well as the saturation in fluids.

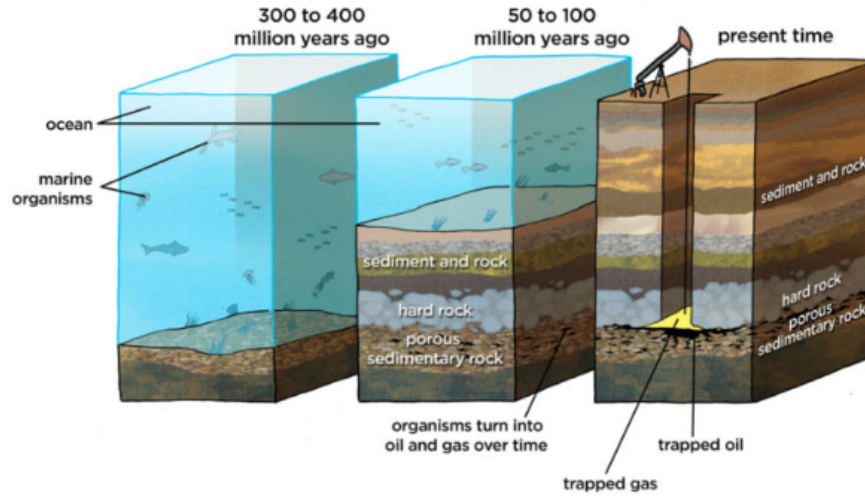


Figure 2.1: Stages of hydrocarbon creation with total a oil and Gas geological background Figure retrieved from [28].

### 2.1.1 Creation of liquid hydrocarbons

Organic residues of plants and marine organisms have been maintained without contact with oxygen in sedimentary layers 2.1. During the first stage of their transformation, microorganisms convert part of the organic material into methane. As the depth of the layer increases, the temperature increases at the same time, resulting in the inhibition of the microbial activity corresponding to the end of the transgenesis. At that time the thermal transformations become significant and the formed kerogenes degraded in the early stages of degeneration into smaller and more volatile molecules the bitumens which in turn are converted into smaller molecules of liquid and gaseous phase [34].

### 2.1.2 Immigration of hydrocarbons

The formation of hydrocarbon molecules in the sedimentary rocks creates an increase in the pressure in the formation which, when it exceeds the strength of the rock, forms cracks through which quantities of hydrocarbons are discharged into the surrounding space. These cycles, that is to say an increase in the pressure of the parent rock-cracking-discharge of hydrocarbons, can be repeated many times during maturation. Primary migration is very slow and occurs through a porous medium usually poorly permeable until the hydrocarbons encounter more favorable flow conditions, so that secondary migration becomes much faster [34].

The flow of hydrocarbons into the permeable layers during secondary migration

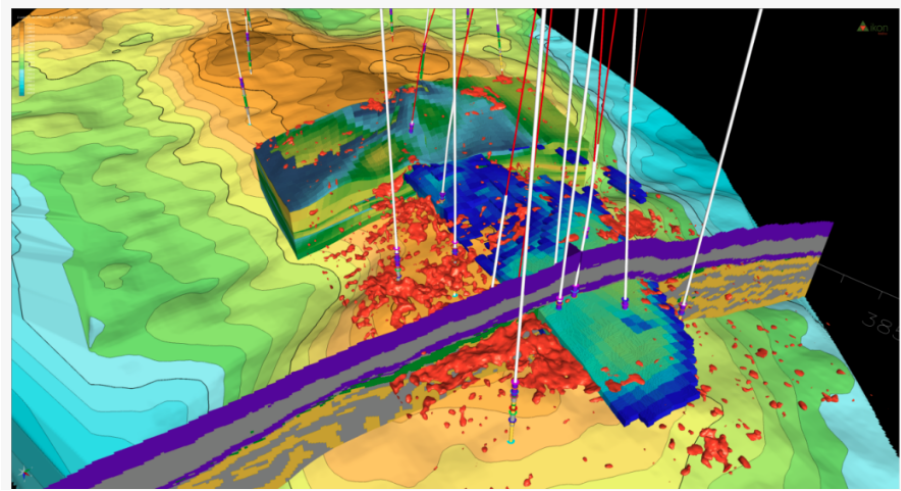


Figure 2.2: Schematic Integration's of all relevant data that create a reservoir interpolation Figure retrieved from [20]

is mainly regulated by gravity forces because hydrocarbons having a lower water density than formation water displace them downward while they move upward.

### 2.1.3 Classification of hydrocarbon reservoirs

The classification of hydrocarbon reservoirs is based on the fluid contained inside them. Oil reservoir: In oil reservoirs, the temperature of the reservoir is lower than the critical temperature of the liquid contained in it. Gas reservoir: In gas reservoirs, the temperature of the reservoir is higher than the critical temperature of the fluid contained in it.

Near-Critical Reservoir: In reservoirs at the critical point, the temperature of the reservoir is close to the critical temperature of the fluid contained in it. At the critical point, the phases of the phases disappear.

### 2.1.4 Storage conditions

The prerequisites for the creation of a commercially exploitable hydrocarbon concentration are: a mature parent rock, a rock / reservoir, an migration channel between the parent rock and the reservoir as well as an impenetrable cap-rock superstructure. Finally, it is necessary to create conditions for trapping hydrocarbons 2.2.

*Reservoir pressure:* the fluid pressure contained in the porous medium is divided into normal , Abnormal Pressure and Subnormal Pressure.

*Normal pressure* : at a given depth is the hydrostatic pressure of a water column from the surface to the formation. It can be considered that the normal pressure is equal to the hydrostatic pressure of the water in the pores of the formation.

The concentration of salt in the water affects the hydrostatic pressure as the value of the pressure level depends on the density of the water and the temperature. This price for clean water is 9.79 kPa / m (0.433) while the usual price range for reservoir water is from 10 kPa / m (0.442) to 10.59 kPa / m (0.478). Excessive pressure at a given depth means that the pressure is greater than the hydrostatic pressure of a water column (normal pressure). These pressures are dangerous when the drilling pressure of the formation is higher than the pressure inside the well. Then, the extra pressure (kick) will be channeled into the drilling system and can cause complete loss of the well as well as losses in human resources. One mechanism responsible for the overpressure observed in many reservoirs is the rapid compression of slate, the bound water of which does not manage to escape in order to restore hydrostatic equilibrium. There have also been reports of hypertension due to the weight of ice from glaciers buried above the deposit. Deep pressure at a given depth means that the pressure is lower than normal pressure and may potentially cause loss-circulation problems of drilling mud.

### **Trapping**

The upward movement of the hydrocarbons migrating continues until the flow encounters impermeable rock where the capillary inlet pressures in the pores can not be overcome by the buoyancy forces.

The traps of hydrocarbon fluids are either structural, such as antigens, transitions, salt blocks, etc., or stratigraphic. In order for a deposit to be exploitable, the formation of the rock should create traps in which large quantities of oil have accumulated [34].

### **Detection**

The detection of hydrocarbon reservoirs is carried out in various stages and by various research methods distinguished in :

- Surface research
- Geological research
- Geophysical research

Surface research can only provide clues, while geological research is the first phase of the systematic search for oil. Of particular importance is the correlation of the geological formations of the area under investigation with the corresponding forma-

tions of neighboring oil producers, which have therefore been studied intensively. Finally, geophysical research, with its three basic methods (magnetic, gravimetric and seismic), gives extraordinarily interesting information on the geological structure of the subsoil before even the extremely expensive exploration drills are carried out.

### **Research drilling - test**

After the results of the above research efforts have been taken into account and evaluated, and if no obvious evidence arises, the point at which the first drilling will take place is chosen. The drill rig with all the auxiliary equipment is installed in the correct position and the preparations are completed.

The four basic functions that take place during the drilling are [34]:

- Hoisting,
- Rotating,
- Circulating,
- Controlling,

### **2.1.5 Well logs**

Drilling evaluation techniques are beneficial and allow a real-time characterization of the drilled formations. These techniques require expensive high-technology sensors to be inserted in the bottomhole assembly, while performing high resolution records [1], [31], [40]. For this reason, a brief introduction of the main types of logs will be presented.

#### **Wireline Logging**

This mechanism is a continuous measurement of formation properties with electrically powered instruments to infer properties and make decisions about drilling and production operations. The record of the measurements, typically a long strip of paper, is also called a log. Measurements include electrical properties (resistivity and conductivity at various frequencies), sonic properties, active and passive nuclear measurements, dimensional measurements of the wellbore, formation fluid sampling, formation pressure measurement, wireline-conveyed sidewall coring tools, and others.

For wireline measurements, the logging tool (or sonde) is lowered into the open wellbore on a multiple conductor, contra-helically armored wireline cable. Once the tool string has reached the bottom of the interval of interest, measurements are taken



on the way out of the wellbore. This is done in an attempt to maintain tension on the cable (which stretches) as constant as possible for depth correlation purposes. (The exception to this practice is in certain hostile environments in which the tool electronics might not survive the downhole temperatures for long enough to allow the tool to be lowered to the bottom of the hole and measurements to be recorded while pulling the tool up the hole. In this case, "down log" measurements might be conducted on the way into the well, and repeated on the way out if possible.) Most wireline measurements are recorded continuously while the sonde is moving. Certain fluid sampling and pressure-measuring tools require that the sonde be stopped, increasing the chance that the sonde or the cable might become stuck.<sup>[7]</sup>

### **Logging While Drilling (LWD)**

The Logging-While-Drilling (LWD) formation evaluation sensors acquire downhole data while drilling, collecting mainly petrophysical data. The measuring elements are part of the instrumented Bottom Hole Assembly, also called BHA, the drilling collars; pulses of the signals are transmitted to the surface via the mud column. 2.3

The advantages of LWD are:

1. Access to real time information.
2. Mud invasion does not have an effect on measurements.
3. The LWD tools is more serviceable for collecting data from tough structural environments, such as deviated wells, horizontal wells or an unstable borehole.
4. The LWD sensor provides information about the well's placement and stability while minimizing the risk of a stuck pipe, thus a safer and more efficient hole is drilled.

However, there are factors restricting the LWD tool's efficiency and those are mentioned below:

1. Data transmission/recording may be affected by the speed's telemetry or by the existence of pumped mud into the drill string.
2. Limited memory size.
3. Most LWD tools are powered by batteries with limited battery life that fluctuates from 40 to 90 hours depending on the tool.
4. LWD tool's placement in the bit have to be taken into consideration due to some technical limitations. For instance, ROP's productiveness and sufficiency can possible be influenced by the location of the tool in the drill string.

### **Measurements While Drilling (MWD)**

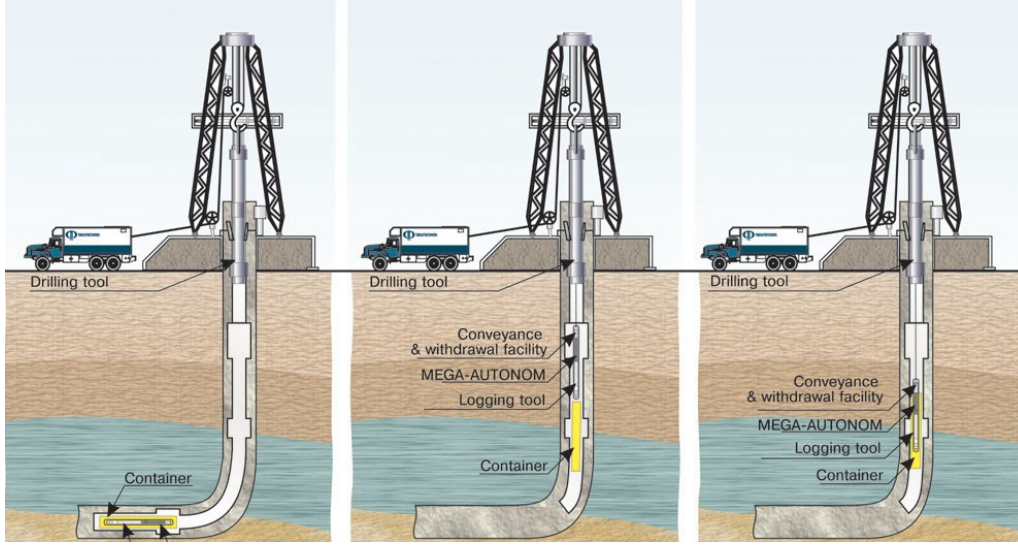


Figure 2.3: Well logging records the events, subsurface formations, and depth measurements of geologic formations during drilling. Adapted from [38].

The Measurement While-drilling formation evaluation technique measures data which is near the bit, without interrupting the standard drilling operations. The recorded information reaches the surface by the exact mechanism of transmission of the LWD tool (mud pressure pulses) 2.3.

The advantages of MWD are:

1. Real time directional drilling operations monitoring.
2. Advantageous use in wellbore completion.
3. Estimation of drilling formation properties and drilling parameters, such as the bottom hole pressure, the torque and the weight on the bit, in the interest of optimizing the drilling process.

## 2.2 Reservoir Heterogeneity

Reservoir is defined as a variation in reservoir properties as a function of space. 2.5 Ideally, if reservoirs were homogeneous, measuring a reservoir property at any location would allow a full description of the reservoir. The properties may include permeability, porosity, thickness. saturation faults , and fractures, rock and rock characteristics. For a proper description, these reservoir properties as a function of spatial location must be predicted. [10]

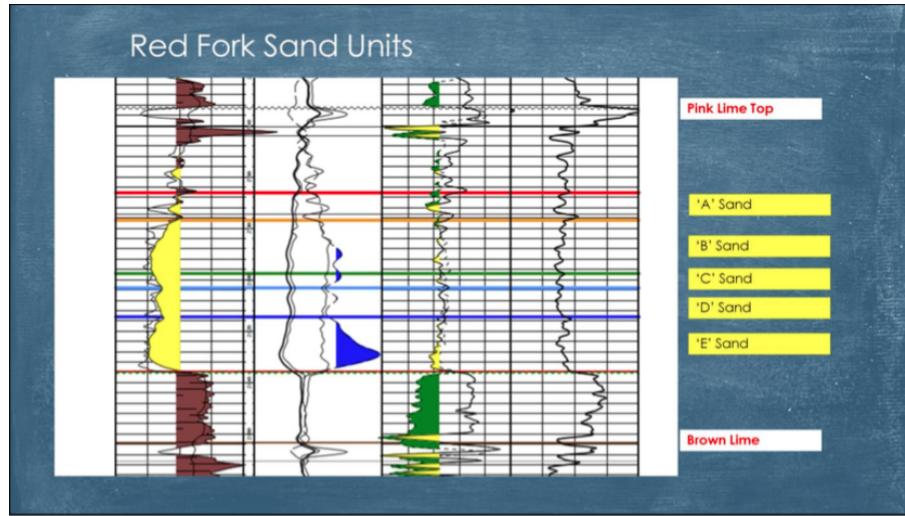


Figure 2.4: Burbank well Logs Example. Adapted from [36].

**Macroscopic heterogeneities** are those measured at a core level. Hence, they are also called core-level heterogeneities. They include core measurements (such as relative permeability, porosity, saturation and wettability of the rock), petrophysical properties (such as permeability and capillary pressure), and some log data.

**Microscopic heterogeneities** are that measured at a micro. They can also be called pore-level heterogeneities. These heterogeneities include pore and grain-size distributions, openings, and rock lithology and mineralogy.

**Megascopic Heterogeneities** are the heterogeneities at have the same order of magnitude as a reservoir simulator gridblock, which is typically several feet in breadth and the properties measured on this scale include some log data; pressure-transient data, such as repeat formation tests (RFTs); and residual-oil-saturation measurements with single well-tracer tests. Some seismic data can also be considered to be on this scale.

**Gigascope heterogeneities** are those measure data and inter-well reservoir scale .The properties measured on this scale include permeability measurements from well-test and inter-well tracer tests. In addition, surface seismic data and major fault locations also can be considered of gigascope heterogeneities.

### Effect on Reservoir Performance

The scales of heterogeneities are also important because different heterogeneities affect reservoir performance differently. Microscale heterogeneities create preferential-flow-path channels. These are pore-level heterogeneities. Because of pore-level heterogeneities, displacing fluids may take preferential paths and by pass some hydro-


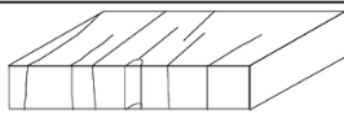



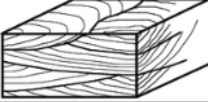
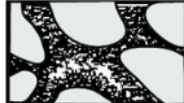
Scale	Reservoir heterogeneity types	
Giga (>300 m)	Sealing to nonsealing faults	
	Fracturing	
Mega (10–100 m)	Genetic unit boundaries	
	Permeability zonation within genetic units	
Macro (in meters)	Baffles within genetic units	
	Sedimentary structures	
Micro ( $\mu\text{m}$ )	Microscopic heterogeneity	

Figure 2.5: Scales of Reservoir Heterogeneities. Figure retrieved from [37].

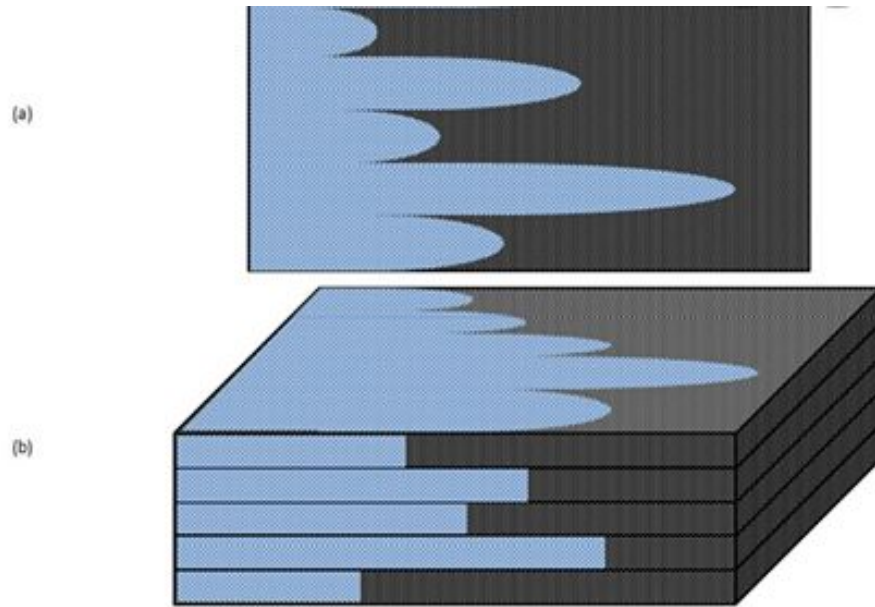


Figure 2.6: Vertical heterogeneities. a)top-view, b)front-view. Figure retrieved from [21]

carbons. Figure 2.6 shows the impact of vertical heterogeneities. The hydrocarbons left behind result in a reduced displacement efficiency: the higher the amount the lower the displacement.

The displacement efficiency directly impacts the the reservoir. The oil behind is called trapped or residual oil. For a typical water-wet reservoir in a dual-pore system. Water enters the smaller pore, displaces the oil from it. and leaves oil behind in the larger pore. Once water forms a continuous path, the discontinuous oil left behind can be displaced only by modifying the capillary forces between oil and displacing fluid

Microscale and megascale heterogeneities results in preferential paths for displacing fluids on a larger scale. Owing to stratification in the vertical direction, oil in preferentially displaced by the displacing fluid. 2.7 The displacing fluids moves preferentially through high permeability regions, leaving behind significant amounts of oil in the lower-permeability strata. Because of the preferential flow paths, the displacing fluids reaches the producing well without reaching all parts of the reservoir. Once preferential paths are established, the displacing fluid short-circuits through these paths, leaving behind bypassed oil [10].

Gigascope heterogeneities cause some oil sources to remain uncontacted 2.9. These sand lenses are not connected with each other. If a drilled well intersects any of

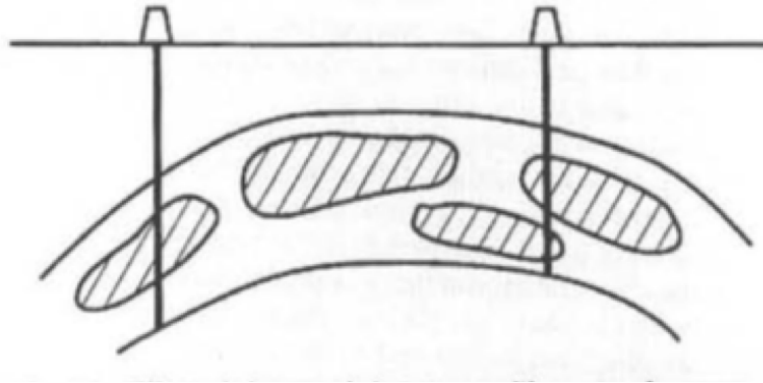


Figure 2.7: Effect of gigascope Heterogeneities on Performace. Figure retrieved from [10].

these lenses, the hydrocarbons can be produced from these lenses. However, if the lens is not in contact with any of the drilled wells, the oil in that lens cannot be extracted unless an infill well is drilled. The oil left behind in the isolated parts of the reservoir is called untapped oil. Extraction efficiency of these reservoirs can be improved by drilling infill wells [10].

## 2.3 Oil Terminology

### 2.3.1 Net pay zone

Net pay (net productive) is thickness of those intervals in which porosity and permeability are known or supposed to be high enough for the interval to be able to produce oil or gas. Water and gas is not included to the net pay thickness [3].

### 2.3.2 Gross thickness zone

Gross thickness (also referred to reservoir thickness) its thickness of stratigraphically space in which the reservoir beds occur. In other words, it's thickness of the whole reservoir. Also its common another terminal Net oil bearing thickness, it includes those intervals in which oil is present in such saturation that the interval may be expected to produce oil, if penetrated by a properly completed well [3].

### 2.3.3 Porosity

Porosity is defined as a measure of the capacity of reservoir rocks to contain or store fluids. The fluids stored in the pore spaces within the reservoir rocks could be gas,



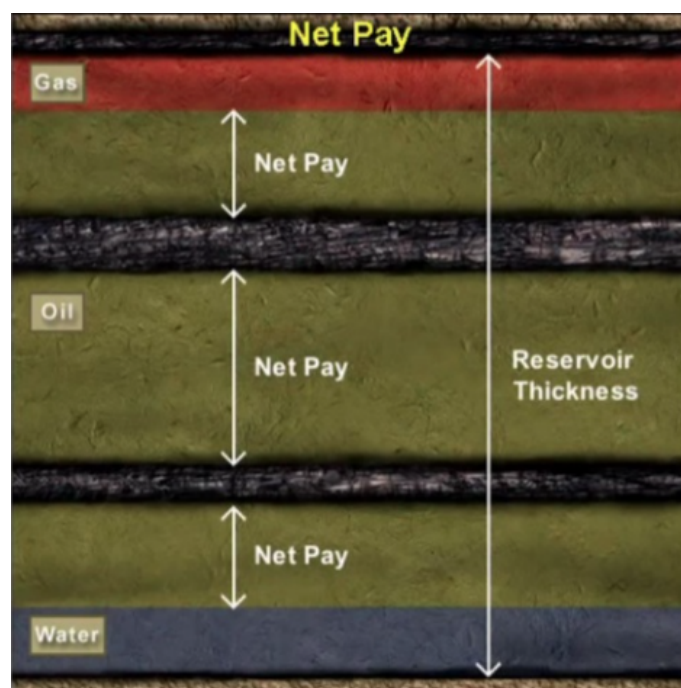


Figure 2.8: Gross thickness and net thickness. Figure retrieved from [3].

oil, and water. High porosity values indicate high capacities of the reservoir rocks to contain these fluids, while low porosity values indicate the opposite. Consequently, porosity data are routinely used qualitatively and quantitatively to assess and estimate the potential volume of hydrocarbons contained in a reservoir. For instance, in a discovery well that shows the presence of hydrocarbons in the reservoir rocks, the set of data that is reviewed at least qualitatively to evaluate reservoir potential is porosity data acquired with either logging-while-drilling (LWD) tools or by running wireline tools. Porosity data are obtained from direct measurements on core samples and/or indirectly from well logs. In most cases, porosity data from core samples are used to validate or calibrate porosity data from well logs. Porosity data are also used in reservoir characterization for the classification of lithological facies, and the assignment of permeabilities using porosity-permeability transforms. Since porosity data are very important in many reservoir engineering calculations, this book begins by reviewing basic concepts in the determination of rock porosities. This review is concise and serves to refresh the reader with the many sources of porosity data that exist through applications of different formation evaluation tools. [10]

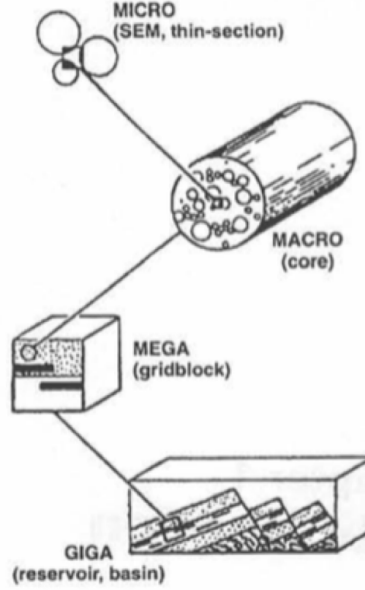


Figure 2.9: Heterogeneities can be measured from small-scale measurement of grain-size distribution at a microscopic level to large-scale geological at a basin level. Figure retrieved from [10].

### 2.3.4 Determining permeability

Point-by-point permeability values are needed over the reservoir interval at the well-bores for several purposes. First, the distribution and variation of the permeabilities are needed by the engineers to develop completion strategies. Second, this same information is needed as input to the geocellular model and dynamic-flow calculations (e.g., numerical reservoir-simulation models). For both of these, the first consideration is the location of shales and other low-permeability layers that can act as barriers or baffles to vertical flow. A second consideration is the nature of the permeability variation (i.e., whether the high - permeability rock intervals occur in specific layers and the low - permeability intervals occur in other layers, or that there is so much heterogeneity that the high and low-permeability intervals are intimately interbedded with each other). [10]

### 2.3.5 Oil formation volume factor

The volumetric coefficient of formation of a liquid phase (Oil Formation Volume Factor or  $B_o$  or FVF) is defined as the ratio of the volume occupied by a liquid mixture (including dissolved gases) in the conditions of formation ( $V_o$  in reservoir conditions



) to the volume of liquid that will remain after the mixture has normalized on the surface ( $V_o$  in standard barrels) (when dissolved gases have been released). [34]

$$\frac{V_0^{RES}}{V_0^{STB}} \left( \frac{bbl}{STB} \right) \quad (2.1)$$

The rate takes values greater than the unit. For pressures above the saturation point it increases decreasing pressure while below the boiling point it decreases.

### 2.3.6 Water saturation

The fraction of water in a given pore space. It is expressed in volume/volume, percent or saturation units. Unless otherwise stated, water saturation is the fraction of formation water in the undisturbed zone. The saturation is known as the total water saturation if the pore space is the total porosity, but is known as effective water saturation if the pore space is the effective porosity. If used without qualification, the term usually refers to the effective water saturation.

Water saturation ( $S_w$ ) estimates are of prime importance for reserves estimation, reservoir development and reservoir management. Traditionally,  $S_w$  has been derived from the Archie equation with formation resistivity or thermal neutron capture cross-section (Sigma, S) in stand-alone mode. Either the resistivity or S approach requires good knowledge of formation water salinity which can be difficult, particularly in instances of unknown and/or mixed salinities. When resistivity and S-logs are unaffected by fluid invasion, one can simultaneously compute  $S_w$  and salinity from the two measurements as has been done recently using wireline logs acquired in flowing wells.[25]

Most oil and gas reservoirs are water wet; water coats the surface of each rock grain. A few reservoirs are oil wet, with oil on the rock surface and water contained in the pores, surrounded by oil. Some reservoirs are partially oil wet. Oil wet reservoirs are very poor producers as it is difficult to get the oil to detach itself from the rock surface. It is fairly easy to take a core sample, clean it and dry it, then make the rock oil wet. However, reservoir rocks are seldom clean and dry, so that same rock in situ will often be water wet.

## 2.4 Original Oil In Place (OOIP)

The volume of hydrocarbon contained in a reservoir is a function of pore volume and water saturation ( $S_w$ ). Reservoir size and porosity determine pore volume. Pore throat size (see Pore and pore throat sizes) distribution, pore geometry, and hydrocarbon column height determine  $S_w$ . Estimating hydrocarbon volume in place

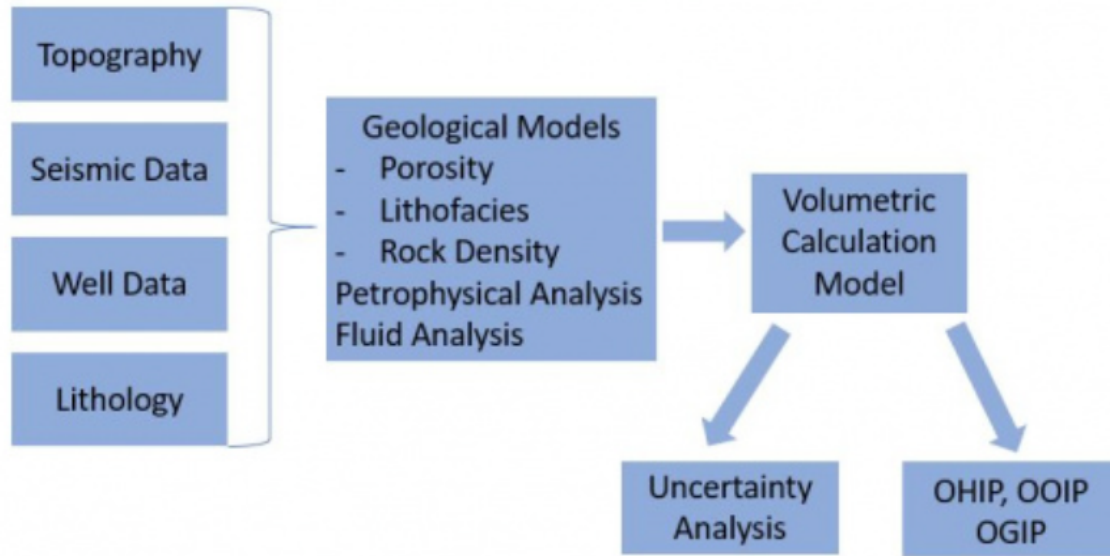


Figure 2.10: Volumetrics is an integration of geological fluid and the modeled relationships. Figure retrieved from [39].

before drilling a well is a matter of predicting pore volume and  $S_w$ . Recovery of hydrocarbons depends on the efficiency of the reservoir drive mechanism. Predicting recovery depends on predicting reservoir quality and reservoir drive. 2.10

$$OOIP = \frac{7.758 \cdot A \cdot h \cdot ng \cdot (\phi/100)(1 - S_w)}{B_o} \quad (2.2)$$

1. A= is surface area of a block
2. h =gross thickness (m),
3. ng= net to gross ratio
4.  $\phi$ = porosity (%)
5.  $S_w$ = water saturation
6.  $B_o$ =formation volume factor
7. 7.758 = conversion factor from acre-ft to bbl

## 2.5 Flow unit

A rock volume with identifiable fluid flow characteristics that can be modeled, including heterogeneity or anisotropy as shown in figure [2.11](#).

Flow units are popular means of characterizing or zoning a reservoir. A flow unit is defined as a mappable portion of the total reservoir, within which geologic and petrophysical properties that effect the flow of fluids are consistent and predictably different from the properties of other reservoir rock volumes. Flow units have the following characteristics in common:

- A flow unit is a specific volume of a reservoir. It is composed of one or more reservoir - quality lithologies and any nonreservoir - quality rocks types within that same volume , as well as the fluids they contain.
- A flow unit is correlative and mappable at the interwell scale.
- A flow unit zonation is recognizable on wireline logs.
- A flow unit may be in communication with other flow units. (However, flow units based on lithostratigraphic characteristics are not always in pressure communication.

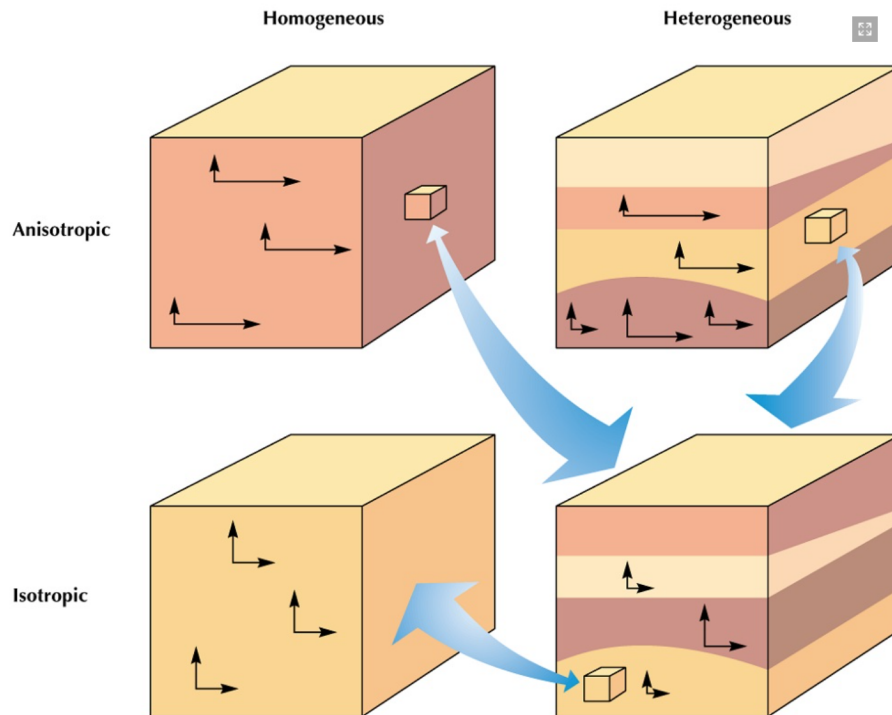


Figure 2.11: Four possible conditions for isotropy/anisotropy and homogeneity/heterogeneity. Note that what is apparent at one scale may not be apparent at another. For example, when viewed close up, a sample may appear homogeneous and isotropic (lower left), yet from afar it may be heterogeneous and isotropic (lower right). Here, heterogeneity is expressed as bed boundaries. Figure retrieved from [7]

# Chapter 3

## Random Fields

*G. de Marsily started the defense of his hydrogeology thesis by showing the audience a jar filled with fine sand and announced “here is a porous medium.” Then he shook the jar and announced “and here is another,” shook it again and said “and yet another.” Indeed, at the microscopic scale the geometry is defined by the arrangement of thousands of individual grains with different shapes and dimensions, and it changes as the grains settle differently each time. Yet at the macroscopic scale we tend to regard it as the same porous medium because its physical properties do not change. This is an ingenious illustration of the notion of a random function in three-dimensional space*

### 3.1 Geostatistics

Geostatistics is a class of statistics used to analyze and predict the values associated with spatial or spatiotemporal phenomena. It incorporates the spatial (and in some cases temporal) coordinates of the data within the analyses. Many geostatistical tools were originally developed as a practical means to describe spatial patterns and interpolate values for locations where samples were not taken. Those tools and methods have since evolved to not only provide interpolated values, but also measures of uncertainty for those values. The measurement of uncertainty is critical to informed decision making, as it provides information on the possible values (outcomes) for each location rather than just one interpolated value. Geostatistical analysis offers mechanisms to incorporate secondary datasets that complement a (possibly sparse) primary variable of interest, thus allowing the construction of more accurate interpolation and uncertainty models [4], [14].

Geostatistics is widely used in many areas of science and engineering, for example

in climate [2], reserves estimation [12], Renewable energy studies [11].

The *mining industry* uses geostatistics for several aspects of a project: initially to quantify mineral resources and evaluate the project's economic feasibility, then on a daily basis in order to decide which material is routed to the plant and which is waste, using updated information as it becomes available [12].

In the *environmental sciences*, geostatistics is used to estimate pollutant levels in order to decide if they pose a threat to environmental or human health and warrant remediation.

Relatively new applications in the field of soil science focus on mapping soil nutrient levels (nitrogen, phosphorus, potassium, and so on) and other indicators (such as electrical conductivity) in order to study their relationships to crop yield and prescribe precise amounts of fertilizer for each location in the field [22].

*Meteorological applications* include prediction of temperatures, rainfall, and associated variables (such as acid rain). Most recently, there have been several applications of geostatistics in the area of *public health*, for example, the prediction of environmental contaminant levels and their relation to the *incidence rates of cancer*, [2].

In all of these examples, the general context is that there is some phenomenon of interest occurring in the landscape (the level of contamination of soil, water, or air by a pollutant; the content of gold or some other metal in a mine; and so forth).

Exhaustive studies are expensive and time consuming, so the phenomenon is usually characterized by taking samples at different locations. Geostatistics is then used to produce predictions (and related measures of uncertainty of the predictions) for the unsampled locations [15], [14], [4].

## 3.2 Random field

A random field (RF) is characterized by its finite-dimensional distributions (also called here spatial distribution for short), namely the set of all multidimensional distributions of  $k$ -tuples  $(X(s_1), X(s_2), \dots, X(s_k))$  for all values of  $k$  and all configurations of the points  $s_1, s_2, \dots, s_k$ . Even if a very large number of realizations of a random function were available, the combinatorial possibilities are such that, in practice, one could calculate sample multidimensional distributions only for the simplest  $k$ -tuples. When a single realization is available, which is the common case, these distributions cannot be determined, except under an assumption of stationarity which introduces repetition in space: Two configurations of points that are identical up to a translation are considered as statistically equivalent. Since the sample points are unevenly distributed, the only (nearly) identical configurations

that can be found are pairs of sample points. A large part of the book is therefore dedicated to methods involving only the knowledge of two point statistics [4].

The complete knowledge of the multivariate distributions, required for the nonlinear techniques. For linear methods, which are the most widely used, it suffices to know the second-order moments. These are the focus of the present chapter [4].

The main tool is the variogram. We will distinguish three main definitions:

- The variogram of the random function, or theoretical variogram, whose knowledge is required for further analysis
- The variogram of the regionalized variable, or regional variogram, which could be calculated if we knew the value of the regionalized variable at every point of its domain of study and
- The sample variogram, which can be calculated from the data.

Our task can therefore be split into two phases:

- Compute a sample variogram that best approximates the regional variogram and
- Fit a theoretical model to this sample variogram.

In applications, a sample is usually not a point but a volume such as a core, that is, a piece of rock characterized by its shape, size, and location. Shape and size define the support of the sample. If it is very small and the same for all the data we can assume it as a point. We will adopt that point of view throughout this thesis [4].

### **3.3 Randomness**

Randomness characterizes phenomena in which the knowledge of a situation with absolute precision is impossible due to various constraints. Some of these constraints are intrinsic due to the intense spatial and temporal variability of the phenomenon or imposed by the experimental process (limited resolution, accidental errors), or caused by fluctuations in environmental factors (eg. temperature and humidity). In these cases, the value of the measured property at various points in the space is determined by a probability distribution function, which determines the probability of occurrence for each possible result [15].

## 3.4 Spatial interpolation

It is usual to estimate the values of a regionalized variable at places where it has not been measured. Typically, these places are the nodes of a regular grid laid out on the studied domain, the interpolation process being then sometimes known as “gridding.” Once grids are established, they are often used as the representation of reality, without reference to the original data. They are the basis for new grids obtained by algebraic or Boolean operations, contour maps, volumetric calculations, and the like. Thus the computation of grids deserves care and cannot rely on simplistic interpolation methods. The estimated quantity is not necessarily the value at a point, in many cases a grid node is meant to represent the grid cell surrounding it. This is typical for inventory estimation or for numerical modeling. Then we estimate the mean value over a cell, or a block, and more generally some weighted average [4].

In all cases the goal is for the estimates to be “accurate.” This means, firstly, that on the average our estimates are correct, they are not systematically too high or too low.

This property is captured statistically by the notion of unbiasedness. It is especially critical for inventory estimation and was the original motivation for the invention of kriging. The other objective is precision, and it is quantified by the notion of error variance, or its square root the standard deviation, which is expressed in the same units as the data. The geostatistical interpolation family of kriging is composed by different methods, such as: simple kriging, ordinary kriging, universal kriging, intrinsic kriging, and so on, depending on the underlying model. The general approach is to consider a class of unbiased estimators, usually linear in the observations, and to find the one with minimum uncertainty, as measured by the error variance. This optimization involves the statistical model established during the structural analysis phase, and there lies the fundamental difference with standard interpolation methods: These focus on modeling the interpolating surface, whereas geostatistics focuses on modeling the phenomenon itself [4].

## 3.5 Covariance

The Covariance function, or simply covariance  $c_x(s_1, s_2)$  of a random field  $X$  is a measure of how much the fluctuation of the field at point  $s_1$  influences the fluctuation of the field at the point  $s_2$  [18], [41].



$$C_x(s_1, s_2) = E[(X(s_1) - E[X(s_1)])(X(s_2) - E[X(s_2)])] = E[X(s_1)X(s_2)] - E[X(s_1)]E[X(s_2)] \quad (3.1)$$

in the above  $E[\cdot]$  denotes the expectation over the ensemble of the random field states. It follows from equation (3.1) that  $c(0) = \sigma_2$ , where  $\sigma_2$  is the variance of the random field  $X$ . For two random vectors  $X_1, X_2$ , the covariance matrix is [18][41]

$$C(X_1, X_2) = E[(X_1 - E[X_1])(X_2 - E[X_2])^T] = E[X_1 X_2^T] - E[X_1]E[X_2]^T, \quad (3.2)$$

where  $X^T$  is the transpose of vector  $X$ . The element  $C_{i,j}$  of the covariance matrix is equal to the covariance  $C(X_i, X_j)$  as defined in equation [18], [41].

### 3.5.1 Covariance Versus Variogram

We will consider two classes of random functions: stationary random functions and intrinsic random functions. Throughout thesis, unless stated otherwise, stationarity means second order stationarity. Covariance of a Stationary Random Function [15], [4].

A stationary random function (SRF)  $Z(x)$  is characterized by its mean

$$m = E[Z(x)] \quad (3.3)$$

and its covariance function (or covariance for short)

$$C(r) = E[Z(x) - m][Z(x + r) - m] \quad (3.4)$$

## 3.6 Statistical homogeneity

A random field  $X(s)$  is statistically homogeneous in the weak sense if the mean value (expectation) is constant, meaning that  $m_X(s) = m_X$  and the covariance function depends only on the distance vector  $r = s_1 - s_2$  between two points i.e.,  $c_X(s_1, s_2) = c_X(r)$ . The second condition guarantees that the variance of a statistically homogeneous field is constant. Hence, the dependence of the value of random field  $X(s)$  on other locations  $s_i$ , is determined only by the distance between  $s_i$  and  $s$  and not by the actual coordinates of these locations [35], [4], [14], [16].

These above conditions define statistical homogeneity in the weak sense. A random field is statistically homogeneous in the strong sense if the multidimensional for  $N$  points, where  $N$  is any positive integer, remains unchanged by transformations that change the location of the points without changing the distances between them. Practically, statistical homogeneity implies that there are no spatial trends, so that the spatial variability of the field can be attributed to fluctuations around a constant level equal to the mean value. In practice it is difficult [8], [4].

### 3.6.1 Statistical isotropy

*Isotropy* implies uniformity in all directions. A field is statistically isotropic if it is statistically homogeneous and its covariance function depends only on the distance  $r$ , but not on the direction of the distance vector  $r$ . Therefore, if the covariance function is isotropic, the field is by definition statistically homogeneous, but not vice versa [14], [15].

### 3.6.2 Statistical anisotropy

*Anisotropy* On the contrary, implies that the spatial variability depends on the direction. The covariance of an anisotropic random field depends on both the distance  $r$  and the direction of vector  $r$ . A random field is considered anisotropic if the directional covariances have different sill or correlation length values [14], [15].

### 3.6.3 Trend model

Random fields can be represented as  $X(s) = m_X(s) + X'(s)$ . The function  $m_X(s)$  is the trend function that represents the deterministic spatial correlations between the data, which are usually of long range.  $X'(s)$  is a random field that corresponds to the fluctuations of  $X(s)$  around the trend. The expectation of the fluctuation is  $E[X'(s)] = 0$ .

In many applications there is no theoretical evidence to suggest a particular type of analytic trend model. Because the concept of trend  $m_X(s)$  is usually associated with a smoothly varying component of the variability of  $X(s)$  in space, it is typically modeled with low-order polynomials [14], [15].

### 3.6.4 Trend removal

Sometime its common to take into consideration that the data gathered through logging is liable to sampling or measurement error. That is, real data often exhibit more complicated trend models. By means of simplicity, the trend function  $u_x$  will be modelled by low-order polynomials of the coordinators of the series data points in order to ensure consistency of interpretation of the spatial direction in the data. On the other hand, to examine under which possible circumstances the effect of a trend on a variogram might be by-passed to allow a sufficient analysis of the data. In following figure some common 1D trend models are shown. The selection of the best trend model is done by means of Least Squares Errors (LSE).

Model	Equation
Mean	$u_x = a_0$
Linear	$u_x = a_0 + a_1x$
Quadratic	$u_x = a_0 + a_1x + a_2x^2$
Cubic	$u_x = a_0 + a_1x + a_2x^2 + a_3x^3$
Quartic	$u_x = a_0 + a_1x + a_2x^2 + a_3x^3 + a_4x^4$

Table 3.1: Common models of trend functions (1D)

### 3.6.5 Variogram models

Geostatistical analysis is based on the variogram function  $\gamma(s, s + r)$ , where  $s$  is the position vector and  $r$  the lag (distance) vector. The variogram describes the spatial correlations of the spatial random field  $X(s)$ . It is defined by means of the following equation in which  $E[\cdot]$  denotes the expectation over the ensemble of the random field states [14], [15], [4].

$$\gamma(r) = \frac{1}{2}E[\{X(s) - X(s + r)\}^2] \quad (3.5)$$

In equation it is assumed that the random field is either statistically stationary or that it has stationary increments, so that the variogram depends only on  $\mathbf{r}$  and not on  $\mathbf{s}$ . For the quality parameters of coal this assumption is generally true. If the random field is stationary, the variogram function is connected to the covariance  $C(\mathbf{r})$  as follows [14], [15], [4].

$$\gamma(r) = C(0) - C(\mathbf{r}) \quad (3.6)$$

It follows from equation that  $\gamma(0) = 0$ . As explained in section 2.1.2,  $C(0) = \sigma_2$ , where  $\sigma_2$  is the variance of the random field. As  $|\mathbf{r}| \rightarrow \infty$ ,  $C(\mathbf{r}) \rightarrow 0$ , hence the variogram of a stationary random field has a sill equal to the variance  $\sigma_2$  of the random field. In practice, the experimental variogram, which is estimated from the data, may show a discontinuity at the origin equal to  $C_0$ . This represents unresolvable fluctuations or measurement errors and is known as the nugget effect, where  $C_0$  is the nugget variance. The correlation length or characteristic length is a normalization parameter of the distance  $\mathbf{r}$  thus defining the interval within which the field value at one point significantly affects the value at another point [35], [15], [4], [14], [5].

### **Nugget**

The existence of nugget effect (or nugget) (as referred in figure: 3.1) is related to the fluctuation of the short range variability in the data. The nugget is equal to the intersection of the variogram with the y-axis of the graph. If the nugget is larger in comparison with the sill then that indicates too much noise and really small spatial correlation. Notice that below the intersection point no information can be obtained for interpretation [40].

### **Sill**

The sill (as referred in figure: 3.1) of a variogram is the inflection point of the curve at which levels off and represents the variance of the variables. Positive or negative spatial correlation occurs when the data points are below or above the sill, respectively. The existence of trends in the data can be indicated by the behavior of the variogram curve based on the sill. In that case, the trends have to be proceed accordingly [40].

### **Range**

The distance (as referred in figure: 3.1) at which the variogram's value points level off to the sill is known as the range and is a maximum correlation length estimation between two sampling points at separation distance  $h$ . One remark is that spatial correlation can be calculated if the point distances are greater than the range, but is practically zero [40].

## **3.6.6 Theoretical variogram model**

To emulate the variogram at any distance, theoretical variogram models are fit on the experimental variogram. Some commonly used theoretical variogram models include the exponential, gaussian and spherical models.

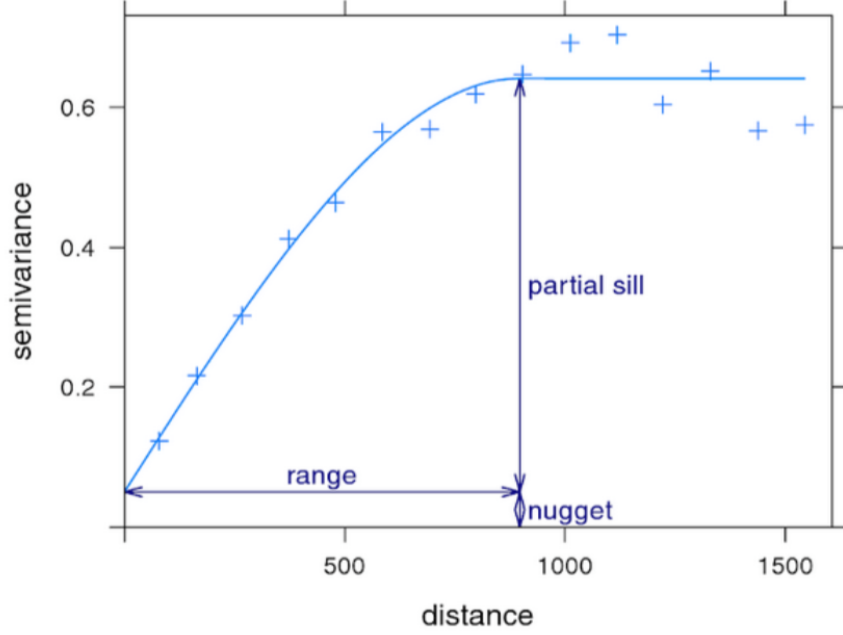


Figure 3.1: The three principal parameters of the variogram [40]

Their respective equations are listed below. The symbol  $\sigma^2$  denotes the variance,  $\|r\|$  is the Euclidean norm of the lag vector  $r$ , and  $\xi$  is the correlation length [15], [4], [5], [14], [8].

Exponential

$$\gamma(r) = \sigma^2[1 - \exp [(-\|r\|/\xi)] \quad (3.7)$$

Gaussian

$$\gamma(r) = \sigma^2[1 - \exp [(-\|r\|^2/\xi^2)] \quad (3.8)$$

Spherical

$$\gamma(r) = \begin{cases} \sigma^2[1.5(\|r\|/\xi) - 0.5(\|r\|/\xi)^3], & \text{if } \|r\| \leq \xi \\ \sigma^2, & \text{if } \|r\| \geq \xi \end{cases} \quad (3.9)$$

### 3.6.7 Kriging

Kriging involves a family of stochastic spatial interpolation methods that can be used to estimate the value of a random field  $X(u)$  at an unmeasured point  $u$  by means of a linear combination of the measurements at  $n$  nearby points  $s_1, \dots, s_n$ . These points ideally involve all the sampling locations. If this choice leads to too-heavy computational load, the neighboring points are restricted to those found within a

kriging neighborhood which is defined by the user. The estimation process is usually repeated at every node of a grid suitably defined for the particular application. This allows the creation of maps representing the isopleth contours of the random field. For example, if the yearly precipitation is measured in a few stations distributed in an area, kriging methods can be used to create a map of precipitation in a grid that encompasses the entire area. These maps can be accompanied by an estimate of reliability, which determines the uncertainty of the estimation at each point. The predicted value of the field at the estimation point is expressed according to the following linear combination: [4], [14], [29], [35], [6].

$$\hat{X}(u) = \sum_{i=1}^n \lambda_i X(s_i). \quad (3.10)$$

In equation ...,  $\hat{X}(u)$  is the estimation at the unmeasured point  $u$ , and  $\lambda_i$  are linear weights that correspond to each of the  $n$  points in the kriging neighborhood. The prediction error is  $\epsilon(u) = (X(u) - \hat{X}(u))$ . In kriging methods, the linear weights  $\lambda(i)$  are calculated by minimizing the error variance of equation

$$\sigma^2(u) = \text{Var}[X(u) - \hat{X}(u)]. \quad (3.11)$$

The variance may be minimized under constraints as in the case of ordinary kriging. This leads to a linear system of equations which is expressed in terms of the covariance or the variogram. In contrast with deterministic methods, such as inverse distance weights, Kriging provides a measure of prediction uncertainty based on the kriging variance  $\sigma^2(u)$

### 3.6.8 Simple kriging

Simple kriging(SK) is applied if the mean  $m_X$  is known and constant throughout the random field, i.e. ( $E[X(s)] = m_X$ ). If  $X'(s) = X(s) - m_X$ , the kriging estimator is defined by the following equation: [15], [35], [5]

$$\hat{X}(u) = m_x + \sum_{i=1}^{n(u)} \lambda_i X'(s_i). \quad (3.12)$$

Since  $E[X'(s)] = 0$  by definition the error variance of equation becomes

$$\sigma^2(u) = E[\{X(u) - \hat{X}(u)\}^2] \quad (3.13)$$

After minimization over the weights, the system of  $n(u)$  linear equations used to calculate the linear kriging weights  $\lambda_i$  is expressed by the system of equations shown in

$$\sum_{j=1}^{n(u)} \lambda_j c_x(s_i - s_j) = c_x(s_i - u), \quad i = 1, \dots, n(u). \quad (3.14)$$

The above system of linear equations may also be expressed as the matrix.

$$C_{i,j} \lambda_i = C_{i,u} \quad (3.15)$$

The matrix  $C_{i,j}$ , represents the covariance matrix between the data points.

The vector  $C_{i,j}$  represents the values of the covariance function between the sample points  $s_i$  and the estimation point  $u$ . Since  $c_x(0) = \sigma_x^2$ , the linear system is equivalent to

$$\begin{bmatrix} \sigma^2 & \dots & c_x(s_1 - s_n) \\ c_x(s_1 - s_n) & \dots & c_x(s_1 - s_n) \\ \vdots & \vdots & \\ c_x(s_1 - s_n) & \dots & \sigma_x^2 \end{bmatrix} \cdot \begin{bmatrix} \lambda_1 \\ \lambda_2 \\ \vdots \\ \lambda_n \end{bmatrix} = \begin{bmatrix} c_x(s_1 - u) \\ c_x(s_2 - u) \\ \vdots \\ c_x(s_n - u) \end{bmatrix} \quad (3.16)$$

The reliability of the prediction is determined by the square root of the variance of the estimation error  $\sigma_2(u)$ . The quantity  $\sigma_{E,SK}(u)$  is the standard deviation of the Gaussian distribution that describes the random variable  $\hat{X}(u)$ .

$$\sigma_{E,SK}^2(u) = \sigma_x^2 - \sum_{i=1}^{n(u)} \sum_{j=1}^{n(u)} C_{u,i} C_{i,j}^{-1} C_{j,u} \quad (3.17)$$

### 3.6.9 Ordinary kriging

Ordinary kriging (OK) is applied if the mean  $m_X(u)$  is constant but unknown inside the local neighborhood of the estimation point. The mean  $m_X(s)$  may vary from neighborhood to neighborhood if the ordinary kriging is not applied over the entire domain [5], [14], [29], [35], [6]. The unknown local mean is removed from the linear estimator by forcing the sum of the kriging weights to be equal to one. This constraint enforces the zero bias condition. The ordinary kriging estimator  $\hat{X}(u)$  is thus written as

$$\hat{X}(u) = \sum_{i=1}^{n(u)} \lambda_i X(s_i). \quad (3.18)$$

$$\text{with } \sum_{i=1}^n \lambda_i = 1 \quad (3.19)$$

In the case of ordinary kriging, the minimum mean square error should be calculated using the constraint imposed by the zero bias condition of equation 3.21. The minimization of the error variance under the zero bias condition makes use of the Lagrange multiplier method for constrained optimization [18]. These conditions lead to the linear system of equations 3.20 and 3.21 for the linear weights, where the constant  $\mu$  is the Lagrange parameter [4], [14], [29], [35], [6].

$$\sum_{j=1}^{n(u)} \lambda_j c_x(s_i - s_j) + \mu = c_x(s_i - u), \quad i = 1, \dots, n(u). \quad (3.20)$$

$$\sum_{i=1}^{n(u)} \lambda_i = 1 \quad (3.21)$$

$$\begin{bmatrix} \sigma^2 \dots & c_x(s_1 - s_n) & 1 \\ c_x(s_1 - s_n) \dots & c_x(s_1 - s_n) & 1 \\ \vdots & \vdots & \vdots \\ c_x(s_1 - s_n) & \sigma_x^2 \dots & 1 \\ 1 \dots & 1 & 0 \end{bmatrix} \cdot \begin{bmatrix} \lambda_1 \\ \lambda_2 \\ \vdots \\ \lambda_n \\ \mu \end{bmatrix} = \begin{bmatrix} c_x(s_1 - u) \\ c_x(s_2 - u) \\ \vdots \\ c_x(s_n - u) \\ 1 \end{bmatrix} \quad (3.22)$$

$$\sigma_{E,OK}^2 = \sigma_x^2 \sum_{j=1}^{n(u)} \lambda_j c_x(s_i - s_j) - \mu = c_x(s_i - u), \quad i = 1, \dots, n(u). \quad (3.23)$$

The Lagrange parameter  $\mu$  is always negative  $\mu < 0$ . As such,  $\sigma_{E,OK}(u)$  is always greater than  $\sigma_{E,OK}$

### 3.7 Spatial Model Validation

Cross-validation (CV) —a popular strategy for algorithm selection— is a model validation technique for assessing the predictive performance of a statistical spatial model. It is mainly used in settings where the goal is prediction, and one wants to estimate how accurately a predictive model will perform in practice. The goal of cross-validation is to estimate the expected level of fit of a model to a data set that is independent of the data (training sample) that were used to train the model. It can be based on any quantitative measure of fit that is appropriate for the data and the model. Most forms of cross-validation are straightforward to implement so long as an implementation of the prediction method is available. In particular, the



prediction method needs only to be available as a “black box”; there is no need to have access to the internals of its implementation [13].

The main idea behind CV is to split data, once or several times, in order to estimate the accuracy and reliability of each algorithm. In leave-p-out cross validation (LPOCV), part of the data (the training sample) is used for training each algorithm, while the remaining data p (the validation sample) is used to evaluate the predictive performance of the algorithm.

**Leave-one-out cross-validation** (LOOCV or LVO), is a particular case of leave – p – out cross-validation with  $p = 1$ . It can be shown that the CV error estimate is an almost unbiased estimate of the true error expected on an independent test set [30]. LVO cross-validation does not face the computational constraints of general LPO cross-validation because  $C_1^n = n$  [2].

### 3.7.1 Validation measures

The spatial model’s performance is evaluated using certain statistical measures. These measures include the following: the mean error (bias) (ME), the mean absolute error (MAE), the root mean square error (RMSE), Pearson’s correlation coefficient ( $\rho$ ) and Spearman’s (rank) correlation coefficient ( $r_S$ ).

For the following measures,  $\hat{x}(s_i)$  and  $x(s_i)$  are the estimated (based on the  $N - 1$  data that do not include point  $s_i$ ) and true value of the field at point  $s_i$ . The quantity  $\bar{x}(s_i)$  denotes the spatial average of the data and  $\bar{\hat{x}}(s_i)$  the spatial average of the estimates [4], [14], [29], [35], [6].

#### Mean error (bias) (ME)

The mean error is calculated as follows:

$$ME = 1/N \sum_{i=1}^N [\hat{x}(s_i) - x(s_i)] \quad (3.24)$$

This measure calculates the bias of the predictor. Particularly high positive or negative values of this error imply a systematic error that leads to inaccuracy.

#### Mean absolute error (MAE)

The mean absolute error is calculated as follows:

$$MAE = 1/N \sum_{i=1}^N |\hat{x}(s_i) - x(s_i)| \quad (3.25)$$

This measure calculates the accuracy and precision of the predictor. All individual differences are weighted equally by MAE.

### Root mean square error (RMSE)

The root mean square error is calculated as follows:

$$RMSE = \sqrt{1/N \sum_{i=1}^N [\hat{x}(s_i) - x(s_i)]^2} \quad (3.26)$$

RMSE also calculates the accuracy and precision of the predictor. Since the errors are squared before they are averaged, the RMSE gives a higher weight to large errors. As such, the RMSE is preferable to MAE when large errors are particularly undesirable.

### Pearson's correlation coefficient ( $\rho$ )

The correlation coefficient, ( $\rho$ ), is the statistic that is most commonly used to summarize the relationship between two variables. The formula for Pearson's linear correlation coefficient ( $\rho$ ) is

$$\bar{\rho}_{x, \hat{x}} = \frac{\sum_{i=1}^N [x(s_i) - \overline{x(s_i)}][\hat{x}(s_i) - \overline{\hat{x}(s_i)}]}{\sqrt{\sum_{i=1}^N [x(s_i) - \overline{x(s_i)}]^2} \sqrt{\sum_{i=1}^N [\hat{x}(s_i) - \overline{\hat{x}(s_i)}]^2}} \quad (3.27)$$

The correlation coefficient ( $\rho$ ) provides a measure of the linear relationship between two variables. This relation can best be illustrated in terms of a scatterplot. If ( $\rho$ ) = +1, the scatterplot is a straight line with a positive slope; if ( $\rho$ ) = -1, the scatterplot is a straight line with a negative slope. For  $|\rho| < 1$  the scatterplot appears as a cloud of points that becomes more diffuse as  $|\rho|$  decreases from 1 to 0. The value of ( $\rho$ ) is often a good indicator of how successful a linear prediction one variable from the other with a linear equation would be [4], [14], [29], [35], [6], [41].

### Spearman (rank) correlation coefficient ( $r_S$ )

If the relationship between two variables is not linear, the correlation coefficient may prove to be a poor summary statistic. Thus, it is useful to supplement the linear correlation coefficient with another measure of the strength of the relationship, the rank correlation coefficient. To calculate the rank correlation coefficient, equation (2.40) is applied to the ranks of the data values rather than to the original sample values as shown in equation 3.27.

$$r_S = 1 - \frac{\sum_{i=1}^N (Rx_i - R\hat{x}_i)^2}{N(N^2 - 1)} \quad (3.28)$$

where  $R_{x_i}$  is the rank of  $x_i$  among all the other  $x$  values. The rank is calculated by sorting the  $x$  values in ascending order; the rank of a given value is equal to its order of appearance in the sorted list. Unlike the traditional correlation coefficient, the rank correlation coefficient is not strongly influenced by extreme pairs. Large differences between the two may be due to the location of extreme pairs on the scatter plot. Differences between  $(\rho)$  and  $(r_S)$  may also reveal that although the variables are correlated, their relation is not linear [12].

### 3.8 Inverse Distance Weight Method

A conceptually simple deterministic method is the so called inverse distance weighting (IDW). It is also known as *Shepard's* method from the name of its inventor. In spite of its simplicity, the method is recommended in the Hydrology Handbook, and it is commonly used for the estimation of missing data in the Earth sciences [9].

The IDW methods are often applied using a neighborhood of a user-determined radius around the prediction point  $u$  or a number of nearest neighbors to  $u$  (i.e. 3 nearest neighbors) to determine a number of  $N$  nearby data points with known values. This simple linear method of estimation assigns the linear weights  $\lambda_i, i = 1, 2, \dots, N$  according to the inverse of the distance  $r_{s_i, u}$  of  $s_i$  from the prediction point  $u$ . The greater the distance of  $s_i$  from  $u$ , the lower the value of the linear weight  $\lambda_i$  that corresponds to the data point  $s_i$  as shown in equation.

$$\hat{X}(u) = \frac{\sum_{i=1}^N \frac{x(s_i)}{r_{s_i, u}}}{\sum_{i=1}^N \frac{1}{r_{s_i, u}}} \quad (3.29)$$

Variations of the method use the inverse of the distance  $r_{s_i, u}$  raised to a power  $n$  as shown in equation 3.29 to calculate the values of the linear weights like the inverse distance squared weights (IDS) method that uses  $r_{s_i, u}^2$

$$\hat{X}(u) = \frac{\sum_{i=1}^N \frac{x(s_i)}{r_{s_i, u}^2}}{\sum_{i=1}^N \frac{1}{r_{s_i, u}^2}} \quad (3.30)$$

The benefit of using IDW methods is their computing simplicity. However the assumption that dependence of the value  $\mathbf{X}(\mathbf{u})$  on the values of its neighbors is reduced with the square of the distance or some other power leads to a less effective

predictor than the kriging predictors. IDW methods also do not give an estimate of the uncertainty of the estimation at each point [4] [35] [14] [15].

**Properties** The properties described in items 1–6 below are derived from the equations 3.29 and 3.30. The property in item (7) is due to the fact that IDW has a computational complexity that scales linearly with the sample size  $N$  [9].

1. Larger weights are assigned to data points that are closer to  $X$  than to more distant points.
2. Higher values of  $r$  increase the relative impact of sample values near  $X$ , whereas lower  $r$  values imply more uniform weights.
3. An "optimal"  $r$  value can be obtained using cross validation approaches.
4. If  $r = 0$  the IDW estimate reduces to the sample mean.
5. IDW weights are positive, i.e.,  $r_n > 0$ , and normalized so that their sum equals one, i.e.,  $\sum r_n = 1$ .
6. IDW is an exact and convex interpolation method.
7. The computational cost of IDW scales linearly with data size. A cut off radius may be required for larger data sets, i.e., for  $N > 10^3$ .
8. The method's shortcomings involve (i) the arbitrary choice of the weighting function (ii) relatively low accuracy (iii) the lack of an associated uncertainty measure and (iv) directionally independent weight functions.

IDW gives you explicit control over the influence that distance has over petrophysical properties; an advantage you don't have with Kriging.

This method also has its shortcomings such as,

- the assumption of interpolated result quality can decrease
- no account of clustering,
- variogram parameters and scale ignored and can over predict for positively skewed or high nugget effects.

In view of its shortcomings, Inverse Distance Weighting method is not reliable for all kinds of deposits hence the emphasis on some aspects.

# Chapter 4

## Relation Between Permeability-Porosity

Simpler theories are preferable to complex ones.

---

Occam's razor

### 4.1 Introduction

Reservoir characterization can be broadly defined as the process of various reservoir characteristics by use of all available data. The description can be qualitative or quantitative. For these reasons some characteristics include pore and grain-size distribution, reservoir permeability and porosity are going to be analyzed here.

Into this chapter, we are going to analyze the behaviour in Burbank oil reservoir, between the correlation of permeability and porosity, as its performed from data analysis in the lab of Geostatistics in Technical University of Crete. The data extracted from flow units have an interesting observation that have been used in such reservoir's like the Burbank one. It was a chance to understand how a reservoir is working if the para-metres of oil are not in a difficult situation to use. For instance, in a case of a reservoir with argillaceous rocks, the correlation will be completely different because the construction of shale's is not giving the opportunity to give away the oil so easily. As such, different results are going to occur if we have had a heavy oil with low API.

The analysis that follows with empirical models, has shown (based on the RMSE), the faults are very common with each other, which is being proved by the correlation

of porosity with the empirical models. All the parameters which are being used, remain constant, apart from the porosity, which is being changed in every model.

#### 4.1.1 Permeability importance for Data modeling

Permeability is one of the most important, most spatially variable, most uncertain, and hence least predictable transport properties of porous media. Various empirical models, such as Kozeni-Carman, Timur's and Coates equations, are widely used to quantify permeability from well- log calculations of porosity and irreducible water saturation. However, these models do not explicitly include the role played by rock structure, spatial fluid distribution in the pore space, wettability, or clay mineral distribution on permeability. We present a pore-scale approach to investigate the influence of these factors on the permeability of clastic rocks for explicit pore geometries of brine-saturated granular rocks [27].

Synthetic pore-scale models are constructed to represent granular sands with variable grain-size distributions. These models include the structural effects of compaction, cementation, and distribution of dispersed hydrated clay minerals. Irreducible water is geometrically distributed on grain surfaces of the synthetic rocks. Permeability is calculated from lattice-Boltzmann flow simulations. A nonlinear relationship between permeability, porosity, and irreducible water saturation is established for these computer- generated rocks. We compare calculated permeability values of computer-generated rocks and laboratory measurements of core samples to those estimated from different empirical approaches, such as Coates, Timur and Kozeni Carman models. It is found that the latter models cannot be applied to general cases of clastic rocks even if their free parameters are adjusted to fit core measurements. Our simulations also show that spatial distributions of clay minerals and irreducible water play a fundamental role in establishing an accurate correlation between permeability, porosity, and irreducible water saturation. Specific deterministic equations must be established for rock formations that exhibit distinct grain-size distributions, clay types, structural clay distributions, and grain cementation [32], [27].

#### 4.1.2 Permeability and importance of grain size

Permeability governs the displacement of fluids through the pore space of porous media. It is one of the most important and least predictable transport properties of porous media in reservoir characterization. Permeability is usually evaluated from core samples and/or well tests. However, core samples and well-test data are often only available from few wells in a reservoir while well logs are available from the majority of wells. Therefore, accurate and reliable evaluation of permeability from well-log data embodies a significant technical and economic advantage.

Various empirical models have been proposed to infer permeability from well-log data, based on calculations of porosity, water saturation, capillary pressure, and formation resistivity factor. Permeability is estimated via correlations among other rock petrophysical properties. In many cases, there may exist deterministic relationships among these properties, but such correlations usually are empirically derived for a given formation in a given area, are often statistical in nature and, therefore, cannot be applied to general cases [10], [27].

## 4.2 Permeability Empirical Models

### 4.2.1 Kozeny–Carman

**Kozeny–Carman** The unidirectional fluid flow in porous media is generally described using Darcy’s law, which is given by

$$u_{\beta,av} = -\frac{K_{\beta}}{\mu} \frac{\Delta p}{L} \quad (4.1)$$

where  $u_{\beta,av}$  is an average velocity in the medium,  $P$  is the pressure drop,  $\mu$  is the fluid viscosity,  $L$  is the length of the porous bead in the flow direction and  $K_{\beta}$  is the permeability. Darcy’s law is used in many applications ranging from petroleum engineering to hydraulic and chemical process modeling, and its broad applicability relies on its simplicity and dependence of only two system parameters, namely, the fluid viscosity  $\mu$  and the porous medium permeability  $k_{\beta}$ . While the determination of the fluid viscosity is nowadays a standard procedure with well calibrated instruments, the estimation of the permeability coefficient is still a challenging problem from both theoretical and experimental standpoints. This is the subject of much practical interest in medicine, chemical and environmental engineering and geology, among many other fields and on which a vast literature is available [19], [33].

Among the possible correlations Kozeny–Carman equation (or Carman–Kozeny equation or Kozeny equation) is a relation used in the field of fluid dynamics to calculate the pressure drop of a fluid flowing through a packed bed of solids. It is named after Josef Kozeny and Philip C. Carman. The equation is only valid for laminar flow. The equation was derived by Kozeny (1927) and Carman (1937, 1956) from a starting point of (a) modelling fluid flow in a packed bed as laminar fluid flow in a collection of curving passages/tubes crossing the packed bed and (b) Poiseuille’s law describing laminar fluid flow in straight, circular section pipes [33].

$$\frac{\Delta_p}{L} = \frac{180\mu_u}{\Phi^2 D_p^2} \frac{1 - \epsilon^2}{\epsilon^3} u_s \quad (4.2)$$

$\Delta_p$  is the pressure drop;  $L$  is the total height of the bed;  $u_s$  is the superficial or "empty-tower" velocity;  $\mu_u$  is the viscosity of the fluid;  $\epsilon$  is the porosity of the bed;  $\Phi_s$  is the sphericity of the particles in the packed bed;  $D_p$  is the diameter of the volume equivalent spherical particle.

However, the Carman–Kozeny and Ergun correlations do not fit the experimental data when the texture of the porous medium exhibits at least one of the following characteristics:

1. very high porosity,
2. particles very far from spherical shape,
3. consolidated porous medium,
4. multi-mode or very large grain or pore size distribution.

Combining these equations gives the final Kozeny equation for absolute (single phase) permeability.

$$k = a \frac{\epsilon^3 (\Delta_p)^2}{1 - \epsilon^2} \quad (4.3)$$

$\epsilon$  is the porosity of the bed (or core plug) [fraction] ,  $\Delta_p$  is average diameter of sand grains [mm = millimeter] ,  $\kappa$  is absolute (i.e. single phase) permeability [mD = millidarcy] ,  $\alpha$  is the proportionality and unity factor [mD / mm<sup>2</sup>]

## 4.2.2 Empirical models

Permeability has also been observed to be a strict function of porosity and residual water saturation in certain reservoirs. A general empirical relationship proposed by *Wyllie and Rose*, relates the permeability,  $\kappa$ , of a porous medium to its porosity  $\phi$  and irreducible water saturation,  $Sw_i$ , as where  $a$ ,  $b$ , and  $c$  are statistically determined model parameters. Based on this general expression, various empirical relationships have been proposed to calculate permeability from values of porosity and irreducible water saturation derived from well logs [27].

Laboratory studies have shown that permeability depends on a long list of parameters: porosity, pore size and shape, pore size distribution, clay content, fluid type, and saturation. The objective of this thesis is to investigate the influence of rock microstructure and spatial distribution of clay minerals on the permeability of clastic



rocks for explicit pore geometries of brine-saturated granular rocks. Hydrated clay minerals are responsible for the presence of excess irreducible water whose spatial distribution in the pore space further conditions the geometry of pore throats.9, 10 Therefore, presence of clays in sands can substantially affect the relationship between porosity, irreducible water saturation, and permeability in ways that depart from standard parametric models such as those of Timur and Coates where the unit of permeability is Darcy (D). The units of porosity and irreducible water saturation are expressed in terms of fraction of bulk volume and pore space volume, respectively. Despite their widespread use, existing models used to calculate permeability from porosity and irreducible water saturation do not explicitly include the role played by rock structure, grain geometry, grain-size distribution, wettability, and spatial distribution of irreducible water in the pore space [27].

#### Wyllie and Rose, the Base Model

$$k = a \frac{\epsilon^b}{S_{wi}^c} \quad (4.4)$$

and residual (irreducible) water saturation ( $S_w(r)$ )

#### Timur

$$k = 8.58 \frac{\epsilon}{S_{wi}^2} \quad (4.5)$$

#### Coates

$$k = 4.90 \frac{\epsilon^4 (1 - S_{wi})^2}{S_{wi}^4} \quad (4.6)$$

### 4.3 Preliminary data analysis

This research project evaluates the relation between *porosity* and *permeability* that follows an overall methodology to make conclusions for these correlation functions, in order to work out which has the best fitting in Oil field data. The data are from flow unit 5 (FU5) with porosity, permeability from 48 exploration wells in Burbank oil field.

Porosity and permeability generally decrease with increasing depth (thermal exposure and effective pressure). However, a significant number of deep (over 4 km, or 13,000ft) sandstone reservoirs worldwide are characterized by anomalously high porosity and permeability. Anomalous porosity and permeability can be defined

Flow Unit (5)	Mean	Median	St.Dev	Min	Max
Permeability (md)	737.67	528	723.85	0.04	4290
Porosity(%)	22.41	24.17	6.13	5,94	32

Table 4.1: Data statistics of flow unit 5

as being statistically higher than the porosity and permeability values occurring in typical sandstone reservoirs of a given lithology (composition and texture), age, and temperature history [24].

As presented in Figures 4.1 and 4.2 porosity and permeability, the data show significant divergence from the normal distribution. The statistical properties of Permeability and porosity in our data is shown in 4.1. The histograms of the two variables (porosity and permeability) are shown in Figures 4.4 and 4.3.

Pearson's correlation coefficient between measured permeability and porosity shows  $\rho_p$  a correlation of 0.6908 (69.1%). Pearson's correlation coefficient calculates the linear correlation. To investigate the monotonic correlation between porosity and permeability, the non-linear Spearman's rank correlation coefficient was estimated and found at  $\rho_{sp} = 92.4\%$  (Equation: 3.28). Since there is strong linear correlation between porosity and permeability, it is expected that the various non-linear models detailed above would perform even better.

## 4.4 Results and discussion

There are several empirical models discussed in section 4.2 that attempt to predict permeability from porosity. In this thesis, in order to investigate which model fits better for Burbank oil field, we used the data from the exploratory drill-holes. In those data, both permeability and porosity was measured. To validate the various models of section 4.2, the results of the estimated permeability were compared with the actual permeability. The results are shown in figure 4.5 and Table 4.2. In this analysis the model coefficients like  $\alpha$ ,  $S_w$  are considered constant.

In Figures 4.5a– 4.5c the estimated theoretical values for each model are presented along with the data. The RMSE and Pearson  $\rho_p$  was chosen in this investigation as the criterion for comparisons between the different models. As can be seen from Table 4.2, Timur's model has lower RMSE and higher Pearson  $\rho_p$  from all tested models.

Timur's model has slightly better fit according to table 4.2. This model is characterized by greater simplicity than the other two models. Thus, the results of our

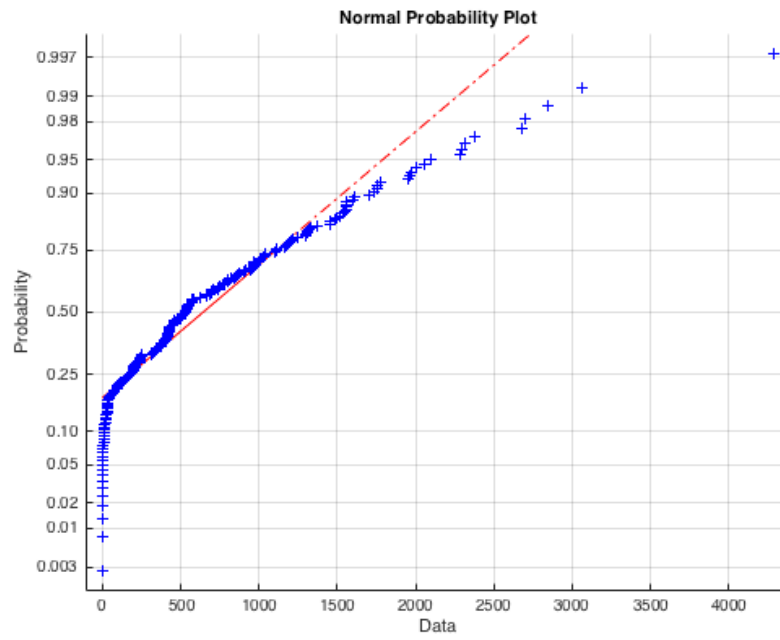


Figure 4.1: Permeability Norm Plot of Flow Unit 5

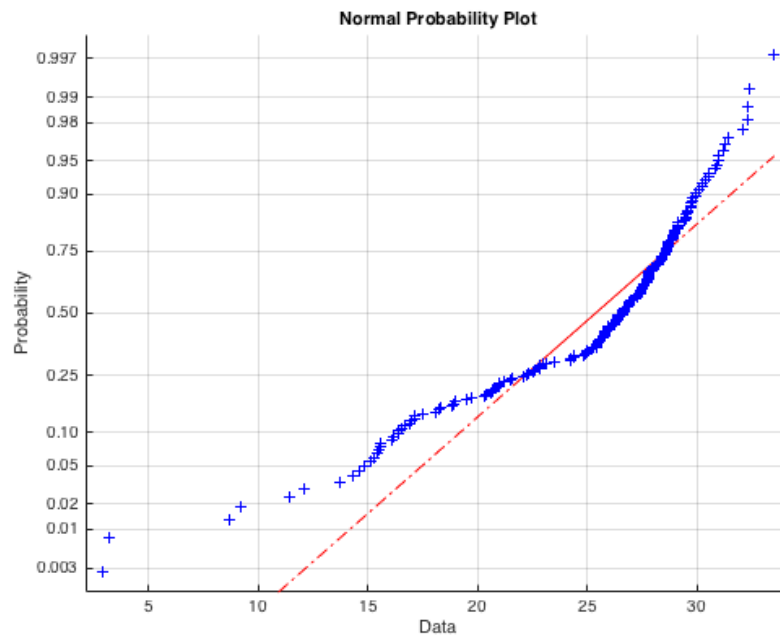


Figure 4.2: Porosity Norm Plot of Flow Unit 5

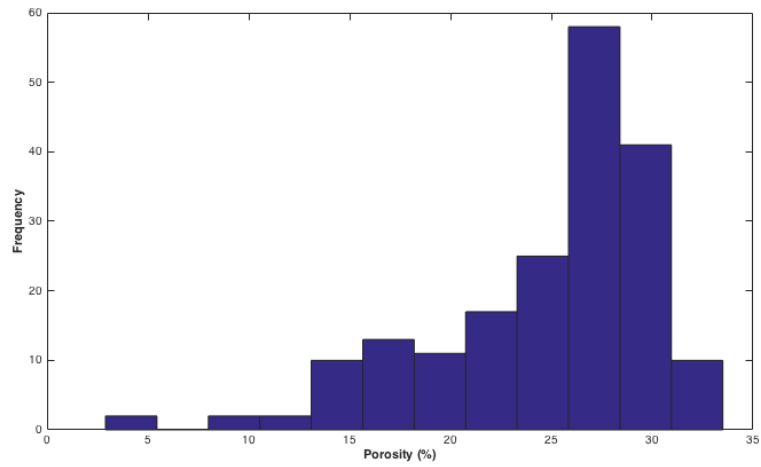


Figure 4.3: Porosity Histogram of Flow Unit 5

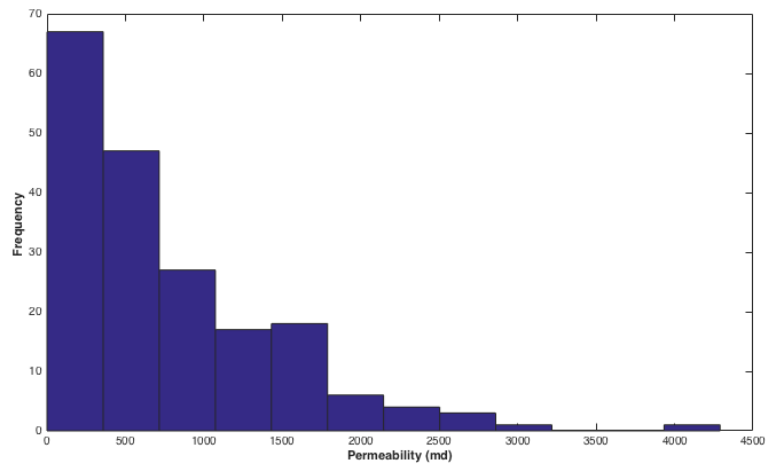
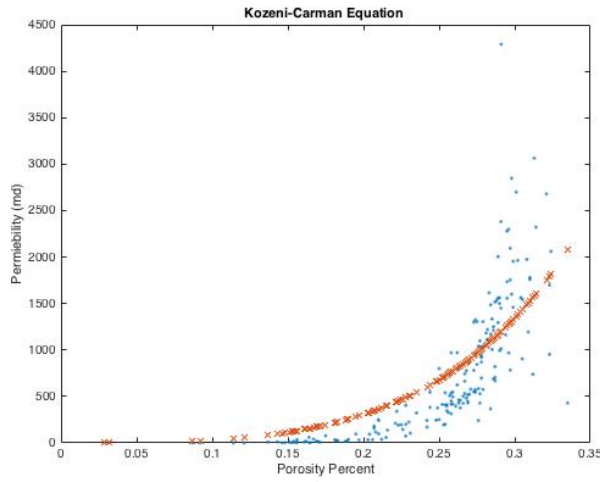
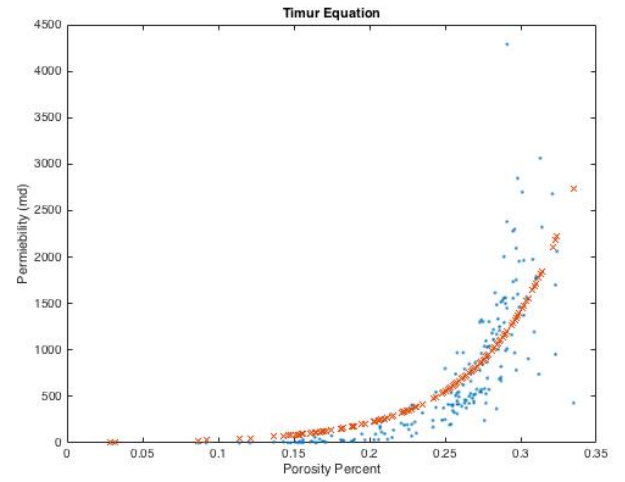


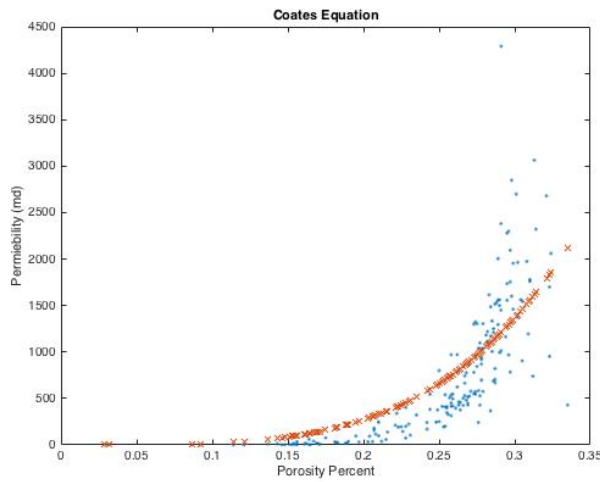
Figure 4.4: Permeability Histogram of Flow Unit 5



(a) Kozeni Carman Graph



(b) Timur Graph



(c) Coates Graph

Figure 4.5: Timur,Kozeni-Carman, Coates Equation

Flow Unit (5)	RMSE (md)	Pearson ( $\rho_p$ )
<b>Kozeny Carman Equation</b>	468.36	0.2521
<b>Timur Model</b>	456.31	0.8429
<b>Coates Equation</b>	460.76	0.5948

Table 4.2: Validation Measures (RMSE,Pearson) on Empirical Models

analysis indicate that for FU5 of Burbank oil field, Timur's equation should be used to estimate permeability from porosity.

This investigation highlights the steps and tools required in order to compare different models in order to correlate permeability and porosity.

# Chapter 5

## Use of Geostatistics in Reservoir Description

The man, who insists upon  
seeing with perfect clearness  
before he decides, never decides.

---

Frederic Amiel

### 5.1 Introduction

In this chapter, Stochastic and deterministic methods will be reviewed. One of these is Kriging, a very common and effective method in geosciences, that provides reliability information. The same applies for the Inverse Weighted Distance (IDW) discussed in in section [44](#) These methods will be applied to flow unit case studies, their performance will be compared with each other with the total amount of oil in place (OOIP) in a specific well in figure [5.1](#)

This case study involves a data-set of porosity and thickness in a specific reservoir and Flow Unit (FU5). The performance of IDW will be compared with the performance of kriging with an analysis of their respective differences. The Oil in Place (OOIP) will be estimated for FU5. This is the basic requirement for an oil company to know for a reservoir in a potential exploitation. The procedure is shown in figure [5.1](#)

This chapter is divided into several sections. The first section describes the importance of the assumptions of stationarity before the estimation of spatial relationships. These spatial relationships are based on observed sample data, and are important

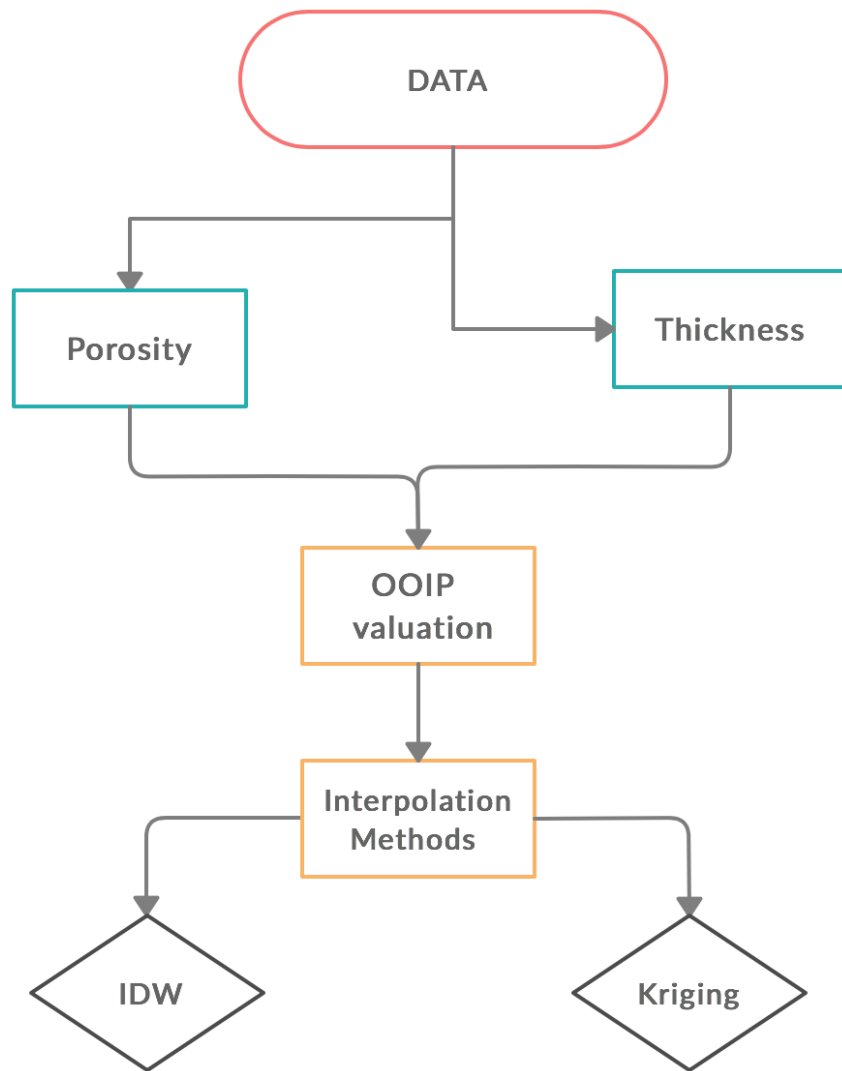


Figure 5.1: Flow Chart for Total Oil in Place (OOIP) Processing



to calculate the values in locations which there are no samples. If our assumption is accurate, we can estimate the values for a chosen grid. To assess the performance of the estimation, leave-one-out cross-validation can be used.

In the second section, we will present conventional summary statistics, which are used to describe spatial relationships. These relationships are based on the covariance and variogram as explained in Chapter 3. The empirical variogram and investigated models will be discussed in this section.

## 5.2 Preliminary data analysis

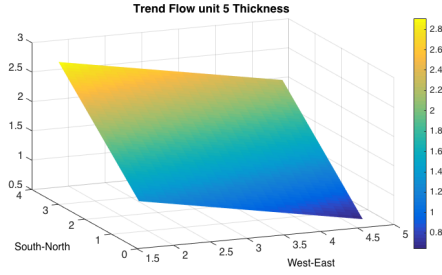
Summary statistics of flow unit (Fu5) data set for Burbank oil field are presented in tables 5.2 and 5.3. They include the mean value, the minimum, the maximum value, the standard deviation as well as the values for detrended Thickness (m) as shown in sections 5.3.2, detrended Porosity (%) 5.3.2 and the logarithm of Thickness $\times$  Porosity as shown in section 5.3.2. As we saw from trend removal (in figures : 5.2b 5.2a) we need to prove that data porosity and thickness has clearly and reflect the general space of flow unit, as a result predict stationary with removing of deterministic factors. Furthermore data are not close to the Gaussian distribution (in figures : 5.3a 5.3b), as we say from data analysis and Norm plots illustration. At this point its necessary to refer that this Flow unit (Fu5) coming not from the same exploration well like in Chapter 4 which has been flowing the procedure with porosity and permeability correlation.

Flow Unit (5)	a_0	a_1	a_2	RMSE	MAE	r%
Thickness (m)	1.6428	-0.2187	0.5249	11930	0.9055	0.4946
Porosity (%)	27.5685	-1.3698	-0.9621	5.3943	4.4946	0.4628

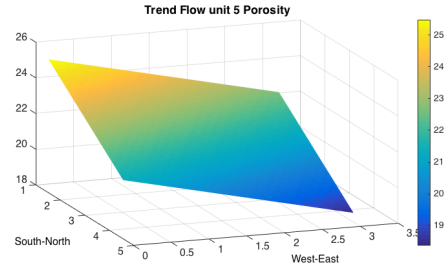
Table 5.1: Trend Values for data statistics of flow unit 5

Flow Unit (5)	Mean	Median	Min	Max
Thickness (m)	1.2192	1.538	0.0000	8.2296
Porosity(%)	22.4144	24.1750	5.9400	32.0000
Detrened Thickness	$-8.12 \cdot 10^{-12}$	-0.2615	-2.5015	5.1009
Detrened Porosity	$3.74 \cdot 10^{-15}$	1.7606	-16.4744	9.5856
log(Thickness*Porosity)	3.4357	3.4110	1.7658	5.0044

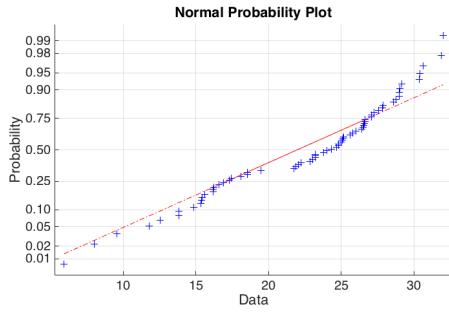
Table 5.2: Detrended data statistics of flow unit 5



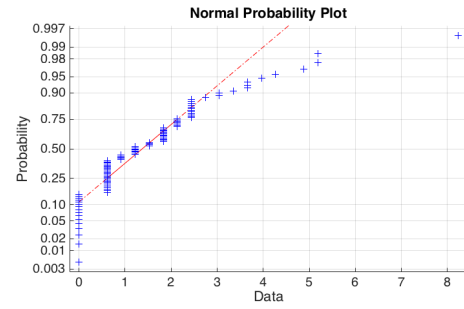
(a) Trend figure of Thickness (m)



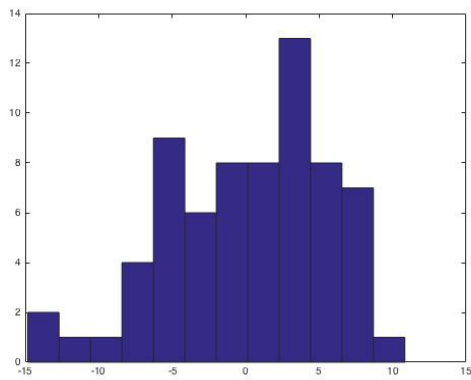
(b) Trend figure of Porosity (%)



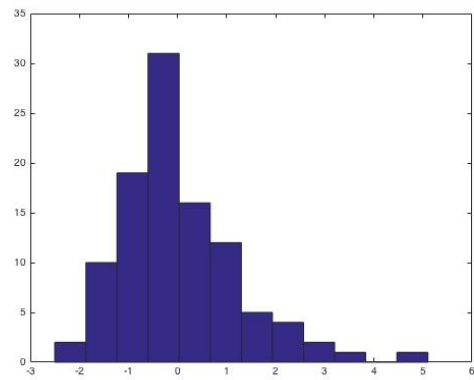
(a) Porosity Norm Plot of Flow unit 5



(b) Thickness Norm Plot of Flow unit 5



(a) Frequency of Porosity (%) Histogram of Flow unit 5



(b) Frequency of Thickness (m) Histogram of Flow unit 5

Flow Unit (5)	St.Dev	Kurtosis	Skewness
Thickness (m)	1.379	7.5825	1.6586
Porosity(%)	6.1304	2.6243	-0.6406
Detrended Thickness	1.199	5.68	1.237
Detrended Porosity	9.5856	6.13042	-0.6486
log(Thickness · Porosity)	0.7952	2.0583	0.082

Table 5.3: Detrended data statistics of flow unit 5

## 5.3 Kriging

### 5.3.1 Ordinary kriging implementation

In Thesis, after the statistical analysis of the data, in order to use Ordinary Kriging, we followed these four steps:

- calculating experimental isotropic variogram,
- fitting theoretical variogram models to the experimental variogram, Gaussian or Spherical (parameter inference),
- performing cross validation to choose the best model,
- estimating the missing values with ordinary kriging, respectively

The above procedures have been implemented to the investigated data by using software developed in the MATLAB programming environment.

### 5.3.2 Porosity and thickness trend analysis

In order to remove the trend from data, we performed multi-linear regression of the response, on the predictors, which contain porosity and thickness that composed in our flow unit. So, the result remaining after this procedure is clear and prepare for stochastic research and calculate remaining stock evaluation.

Cross validation performance measures calculated through leave-one-out cross validation for the precipitation data of flow unit (Fu5) for annual porosity and thickness data set. ME: Mean error (bias) (Equation 3.24, MAE: Mean absolute error (Equation 3.25), RMSE: Root mean square error (Equation 3.26), RP ( $\rho$ ): Pearson's linear correlation coefficient (Equation 3.27), Min: minimum prediction and minimum sample value, Max: maximum prediction and maximum sample value.

### 5.3.3 Variogram analysis

The estimation of variograms 3.6.6 requires great care and caution. In this section, we discuss several potential problems that can occur while estimating variograms and the practical solutions that can be implemented to minimize their effects. These problems include a number of pairs at a given lag distance. At the same time, estimates have shown that under the influence of outlier data and biased sampling, there are proposed solutions to all these problems. The process used to minimise the uncertainty, is described below.

To begin with, once the variogram is estimated, the next step is modeling the variogram to present it in a convenient format. Certain restrictions exist in modeling the estimated variogram. Then, we discuss these restrictions and the type of models used. The next section deals with construction of spatial relationships between two different variables situated at different locations in contrast with the previous sections. Both estimation and modeling procedures for these cross relationships are presented. The following section addresses these 2 methods for describing spatial relationships.

Firstly geostatistical analysis shows that variograms of thickness and porosity have some significant differences in their parameters and form. Specifically, we see that the thickness variogram (as shown in figure 5.5) is mostly nugget. However, the variogram for porosity as shown in figure 5.6 increases almost linearly. This is reflected in the values for sill and range (as shown in section 3.6.5) for all tested variogram models, as shown in table 5.5, 5.4.

To overcome those difficulties we contrast the logarithm of multiplication between thickness and porosity, (as shown in Figures: 5.6 and 5.5).5.7) in which the geostatistical analysis followed showed that the logarithm model show us better correlation with each other. (as shown in figures 5.75.8,5.9) The initial values and the boundaries of the parameters for each model used in the optimization/parameter are presented in Table . The estimated  $\sigma^2$ ,  $\xi$  and  $\phi$  for all the models (as saw in Tab 5.5 5.4,5.6 ) we except from Spherical are very close to the real, while the nugget effect ( $c_0$ ) is estimated with good accuracy only for flow unit 5 and after of many tries the error its was better.

Model	$\sigma^2$	$\xi$	$\phi$
Exponential	0,58	0,29	0.45
Gaussian	0,20	0,44	0.86
Spherical	0,30	0,53	0.76

Table 5.4: Variogram Parameters Thickness

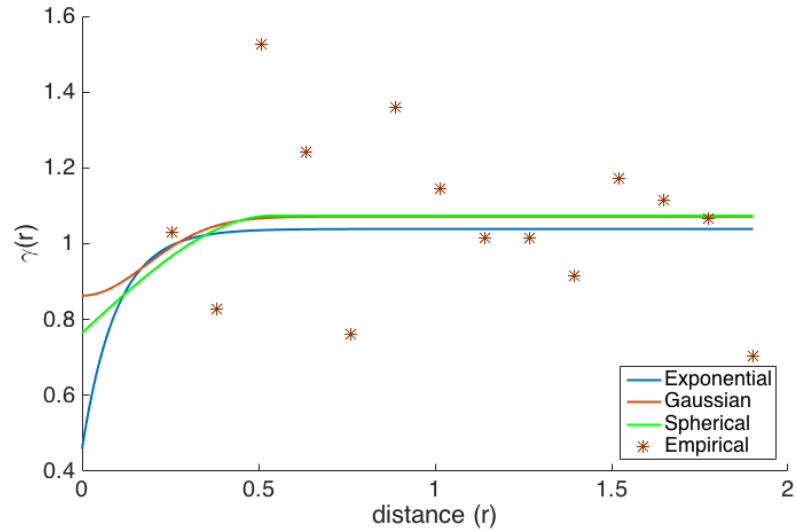


Figure 5.5: Thickness Variograms of Flow Unit 5

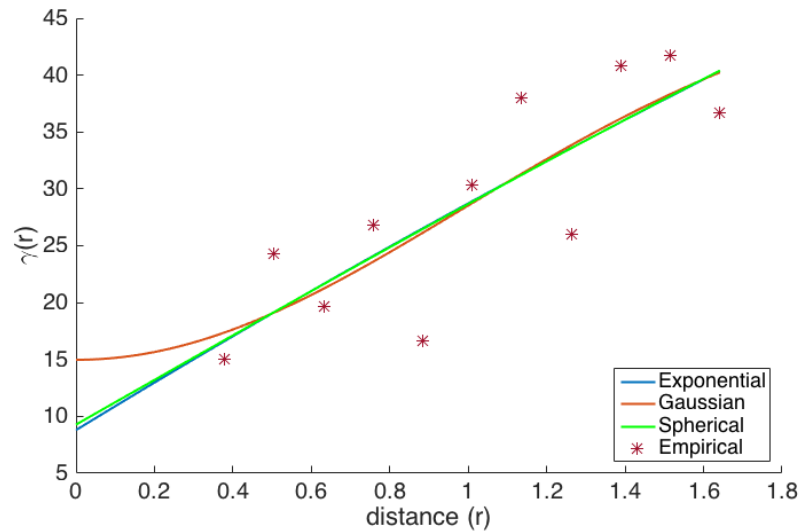


Figure 5.6: Porosity Variograms of Flow Unit 5

### 5.3.4 Kriging maps - reserves estimation

The method of regular kriging (Ordinary Kriging) was used to calculate the oil reserves in Burbank oil field, because as mentioned in Chapter 3.6.7 in Regular Kriging the average value remains constant in each neighborhood. Kriging is done with the corrected data, ie with the data that the trend has been removed. The

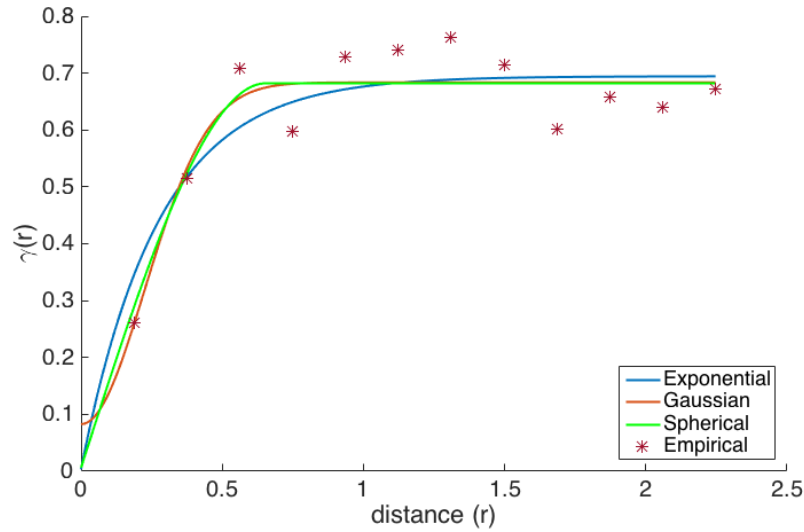


Figure 5.7: Multiplication Porosity and Thickness Variogram of Flow Unit 5

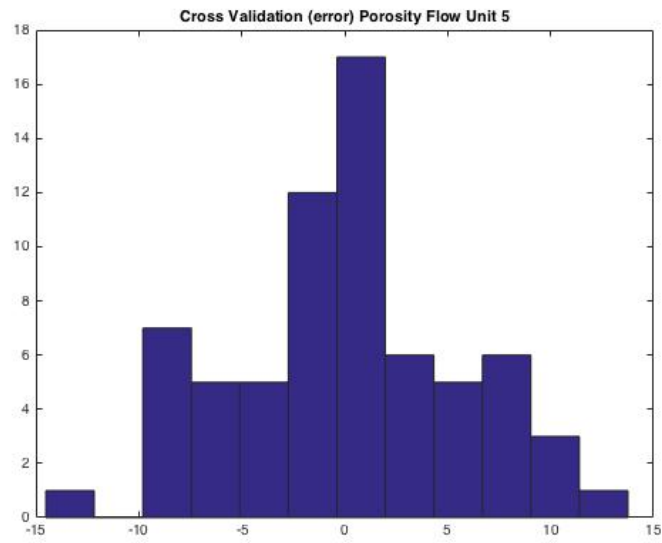
Model	$\sigma^2$	$\xi$	$\phi$
Exponential	182.28	25.91	8.79
Gaussian	33.63	4.41	14.97
Spherical	66.04	5.03	9.27

Table 5.5: Variogram Parameters Porosity

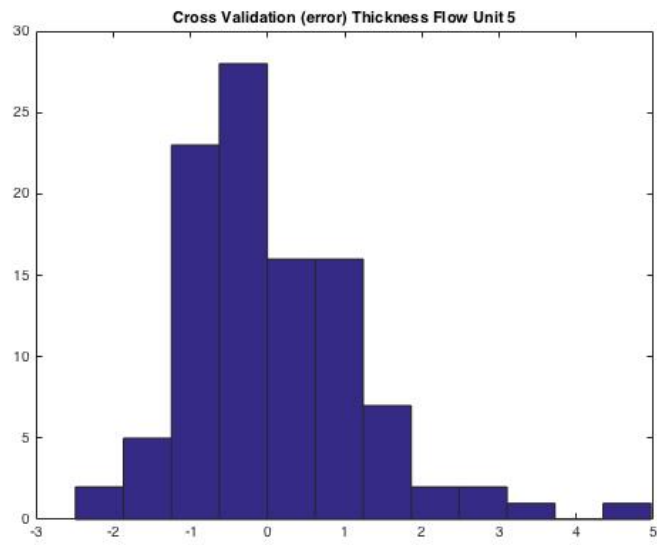
grid used consists of 50 x 50 cells, with a size of 60 m x 60 m. Considering, we adapted a empirical variogram, and next a theoretical spherical model. Also log of multiplication porosity and thickness took a part. Parameters resulting from the model (the length of correlation  $\xi$ , the nucleus effect), (as shown in section 3.6.5) and the scattering, estimates are made for each thickness and porosity values adopted to kriging method (as saw in Figures 5.11a, 5.11b, 5.10a, 5.10b) 5.9a, 5.9b). In addition estimates that obtained, the trend that was previously removed and in the final map that appears calculated final oil in place. Thus the final maps appears (as shown in Figures 5.9a 5.13) Histograms of assessments and real values are correlate nicely, they are close to zero and some of them leave the specified evaluation (as shown in figures 5.8a, 5.8b).

### 5.3.5 Total oil in place (OOIP) analysis

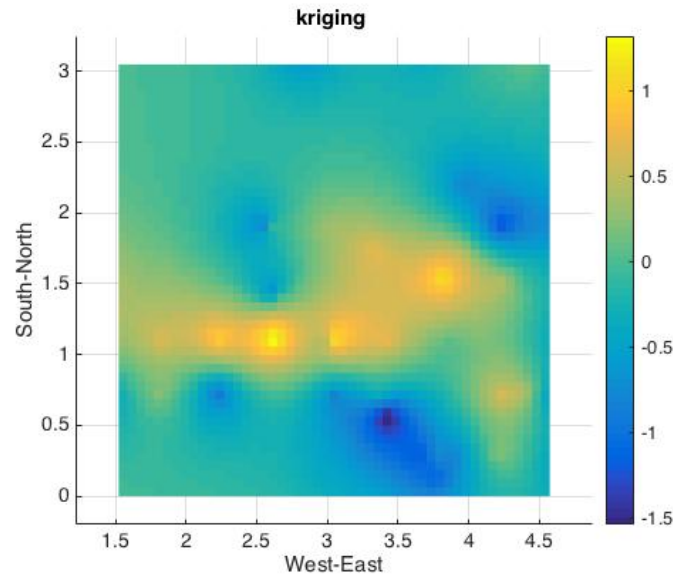
Knowing the amount of original oil in place 2.4 is the most important parameter for reservoir engineers to make a quick decision whether the discovered area is profitable



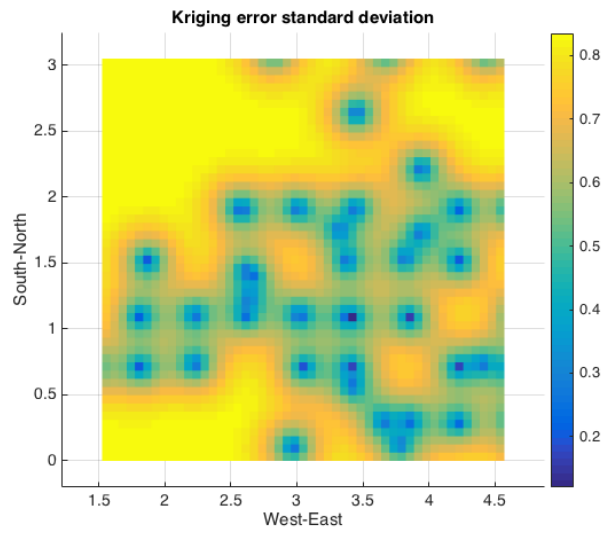
(a) Cross Validation Porosity Histogram of Flow unit 5



(b) Cross Validation Thickness Histogram of Flow unit 5

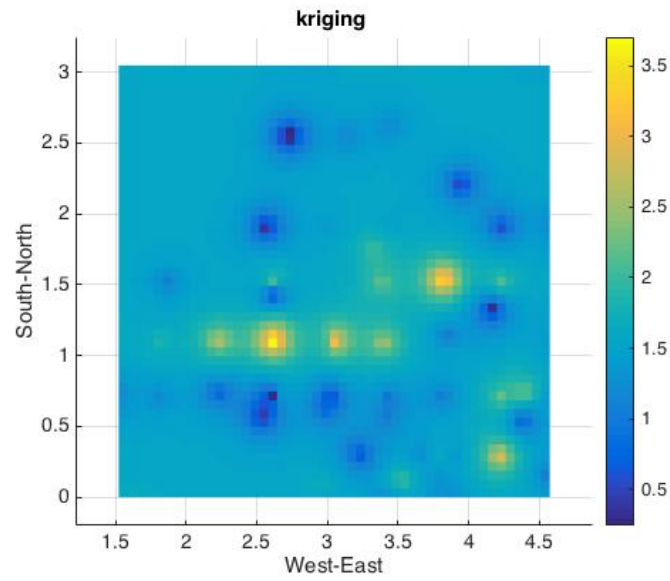


(a) Kriging of Flow Unit 5 multiplication

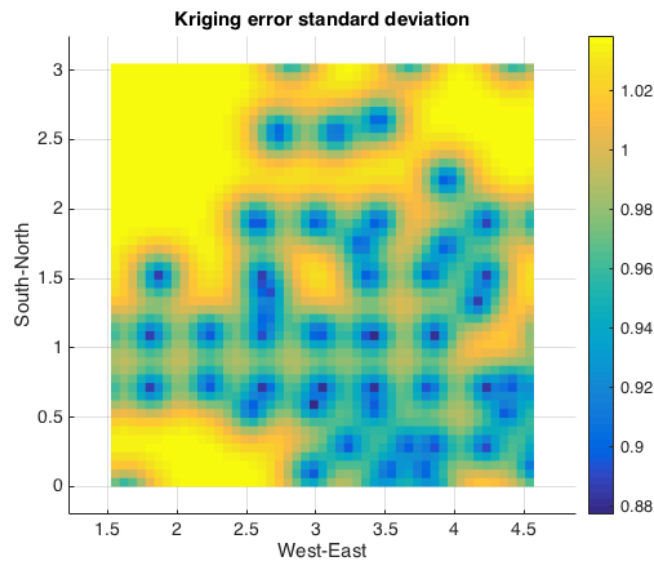


(b) Kriking error of Flow Unit 5 multiplication

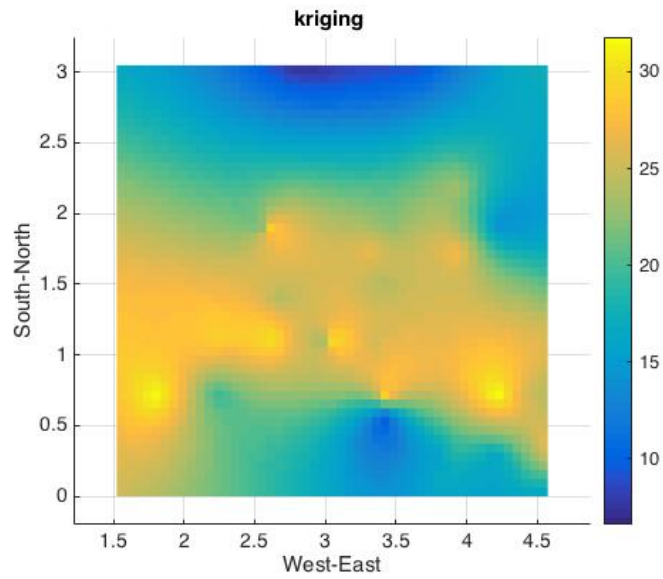




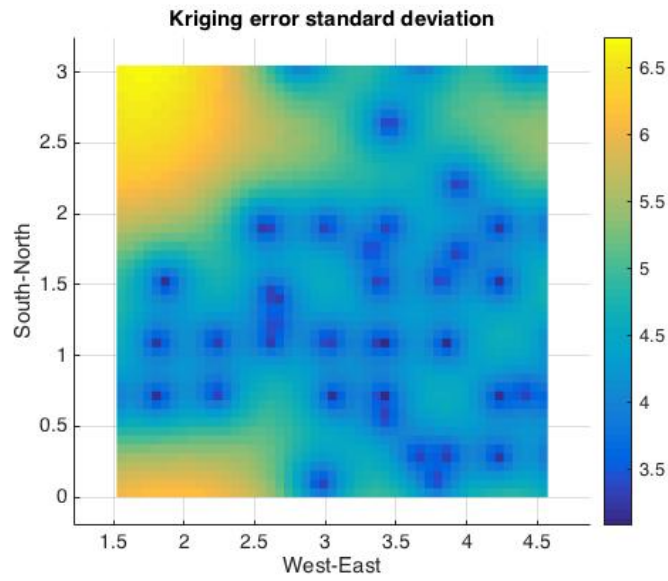
(a) Kriging Simulation of Flow Unit 5 Thickness



(b) Kriging Error Simulation of Flow Unit 5 Thickness



(a) Kriging Simulation of Flow Unit 5 Porosity



(b) Kriging Error Simulation of Flow Unit 5 Porosity

Model	$\sigma^2$	$\xi$	$\phi$
Exponential	0.69	0.82	0.003
Gaussian	0.60	0.55	0.082
Spherical	0.67	0.65	0.006

Table 5.6: Variogram Parameters with  $((\log(\%) \cdot (m)))$

Model	RMSE(m)
Spherical	0.6454
Gaussian	0.6527
Exponential	0.6652

Table 5.7: Thickness Variogram Errors (RMSE(m))

or not. This method depends on basic data of reservoir rock and reservoir fluid properties. However, the reservoir simulation needs a lot of information starts with geological history and ends with production history additional to reservoir rock and fluid properties. In this endeavor we realized the description of the reserve's. Porosity and thickness data (as is shown in figure 5.13) , at the end we point out that logarithm (porosity  $\cdot$  thickness) has better correlation for (OOIP) stock estimation method as shown in figure 5.12. Different geostatistical methods that took part showed the equation applies remarkably in both stochastic and deterministic methods. This was confirmed by validation measures and specify from with root mean squared method (RMSE) 5.13.

### 5.3.6 IDW and kriging comparison

The Inverse Distance Weighting method (IDW) is a simple at the same time effective method of estimation, which does not require as much data in comparison with Kriging. It has been proven to be effective and reliable in some aspects.

After defining the reservoir extent and fluvial faces, different variograms were computed to adequately quantify the variations in the distribution of porosity and permeability due to reservoir heterogeneity. Interpolation results, estimated from descriptive statistics, showed that IDW (in Figures 5.14a , 5.14b) and kriging (in tabs 5.10 5.11 5.9b), . The differences in the interpolated values were, however, insignificant but IDW with power index of 2.5 in porosity 5.16 and 1.5 in thickness 5.15 indicated the least error estimation.

Volume calculations also showed a marginal difference in (Pearson (R)) 3.27 of 0.48 about porosity and 0,1 about thickness between IDW power and kriging in the

Model	RMSE(%)
Spherical	381.7371
Gaussian	514.6989
Exponential	835.0983

Table 5.8: Porosity Variogram Errors (RMSE(%))

Model	RMSE( $\log(\%) \cdot (m)$ )
Spherical	0.032
Gaussian	0.050
Exponential	0.048

Table 5.9: Multiplication Porosity and Thickness Variogram Variogram Errors  
RMSE( $(\log(\%) \cdot (m))$ )

MAE	R	ME	RMSE	MaxAE
3.76	0.63	-0.19	4.86	13.08

Table 5.10: Kriging of Porosity (Validation Measures)

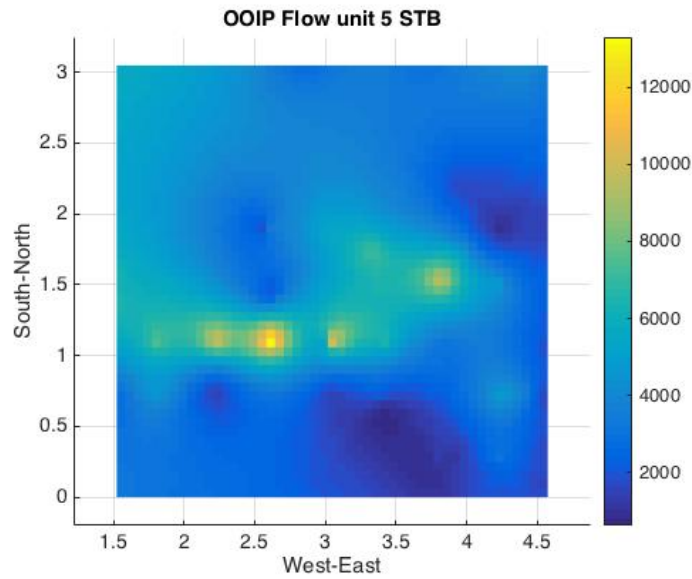


Figure 5.12: Total Oil in Place of Flow Unit 5 multiplication

reservoir zones. Cross validation of hydrocarbon volumes based on dividing the reservoir into fault segments resulted in an RMSE 3.26 of 1.12 for Thickness and

MAE	R	ME	RMSE	MaxAE
0.87	0.56	0.04	1.14	4.68

Table 5.11: Kriging of Thickness (Validation Measures)

MAE	R	ME	RMSE	MaxAE
0.53	0.59	-0.02	0.63	1.19

Table 5.12: Kriging of Multiplication ( $(\log(\%) \cdot (m))$ )

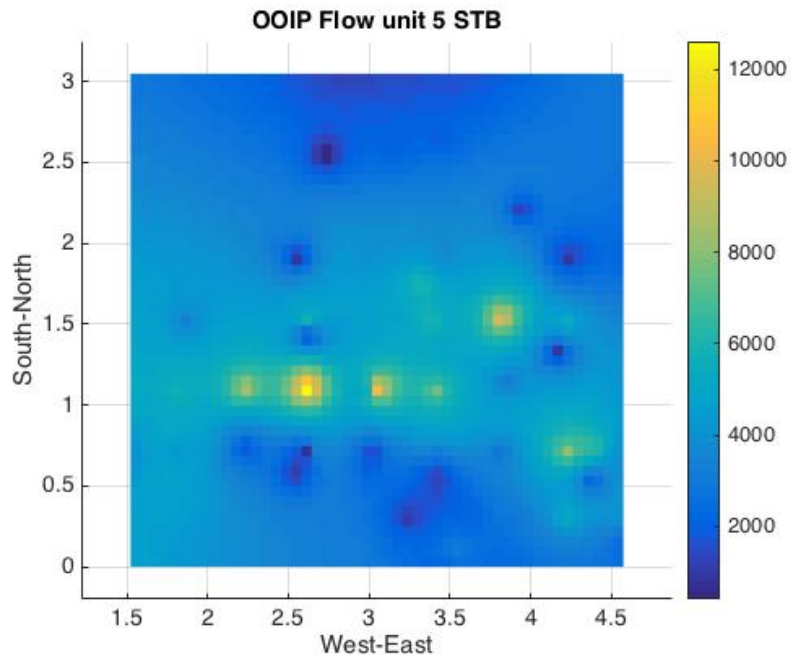


Figure 5.13: Total Oil in Place (bbl)

Original Oil in Place (OOIP) (bbl)	
Kriging	10,484,000
Kriging Multiplication	9,483,600
IDW	9,567,300

Table 5.13: Total Oil In Place in bbl for each method

5.44 for porosity. With inverse distance weight exhibiting least errors and higher accuracy, the volumetric and statistical results confirms that when there is less well data in a fluvial reservoir, the best porosity and permeability interpolation choice should be inverse distance weighting method with power index of 2.5 in table 5.15 for thickness and in table 5.17 1.5 for porosity.

n	MAE	R	ME	RMSE	MaxAE
1	0.94	0.52	0.07	1.25	6.09
1.5	0.90	0.55	0.08	1.18	5.39
2	0.88	0.57	0.07	1.13	4.61
2.5	0.90	0.58	0.06	1.12	4.01
3	0.92	0.58	0.06	1.14	3.64

Table 5.14: Validation Measures IDW of Thickness with Power index (1,1.5,2,2.5,3)

n	MAE	R	ME	RMSE	MaxAE
2.5	0.90	0.58	0.06	1.12	4.01

Table 5.15: Best Power index (2.5) Thickness

## 5.4 Synopsis

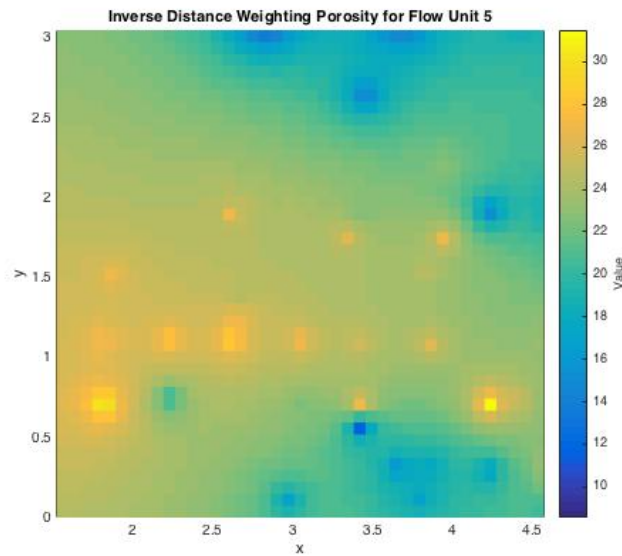
Uncertainty of the total flow units estimation of the above described analysis of the simple synthetic data set indicates that the developed codes can handle successively such data sets and provide relatively reliable and accurate results. It is achieved with collaboration between me and laboratory of geostatistics the comparison between two important methods (IDW,Kriging) the total oil in place for under study flow unit. It is found that deviation its remarkable and someone can take serious results if working with them. We need to point out that we tried our best effort to reach the maximum potential based on the given data. As a result, the analysis that took place was the best possible, because the results of these two methods are so close to each other.

n	MAE	R	ME	RMSE	MaxAE
1	4.49	0.47	-0.48	5.59	16.42
1.5	4.28	0.48	-0.78	5.44	16.01
2	4.09	0.50	-0.96	5.35	15.40
2.5	3.97	0.52	-1.04	5.31	16.02
3	3.94	0.53	-1.05	5.31	16.57

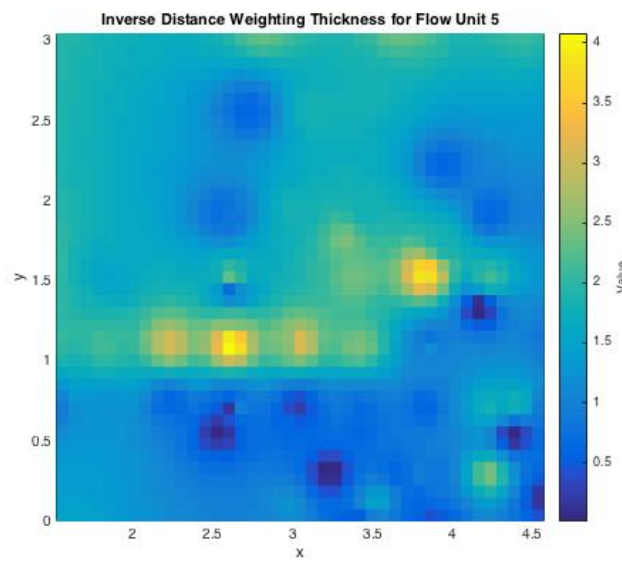
Table 5.16: Validation Measures IDW of Porosity with Power index (1,1.5,2,2.5,3)

n	MAE	R	ME	RMSE	MaxAE
1.5	4.28	0.48	-0.78	5.44	16.01

Table 5.17: Best Power index (2.5) Porosity



(a) IDW Simulation Flow Unit 5 Porosity



(b) IDW Simulation of Flow Unit 5 Thickness



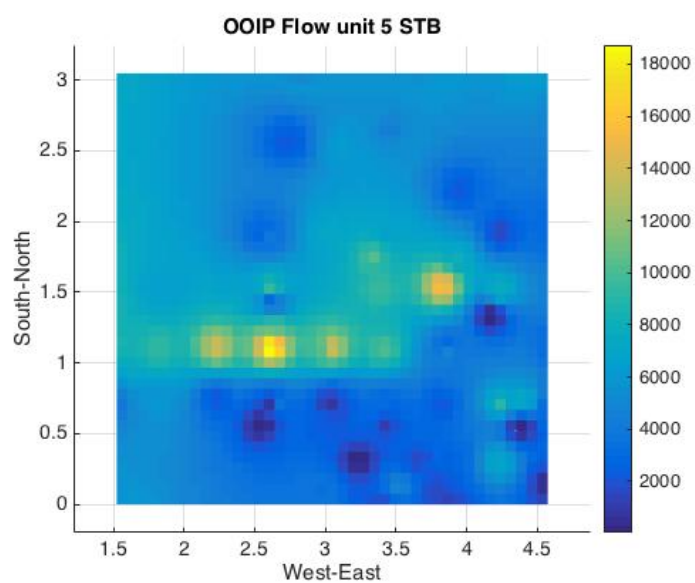


Figure 5.15: IDW OOIP of Flow Unit 5

Figure 5.16: IDW Simulations for flow units 5

# Chapter 6

## Conclusions and Suggestions for Further Research

### 6.1 Conclusions

This diploma thesis was designed to geostatistically analyze oil reserves with data from Burbank Oil Field in Oklahoma US , using the well-known programming language “Matlab”. Two methodologies were used to investigate the data. The first one was spatial interference with the standard kriging method, where the parameters of the phenomenon, sill, and correlation length used were evaluated by variograms. The second deterministic method used was the inverse distance weighting (IDW). A different task to aid the investigation was the usage of different methods that correlate the porosity and permeability, in order to understand the behavior of the oil field in this area.

During my thesis work, for technical reasons, boreholes with other Flow units were rejected because the procedure was the same and it’s not necessary to be analyzed further. From the field that emerged, the variogram for the study area was calculated and performed in specific boreholes with specific flow unit.

Corporation with specifications of empirical models such as Kozeny - Carman, Timur and Coates where the latter relate to terms such as porosity and permeability in formation conditions. According to our procedure these models they illustrate the characterization and relation with our terms. They gave us a fast brief, how our flow unit behave. It common to estimate the correlations of such data in order to end up at a specific standard curve with equation models defined by the literature. At this point it is worth pointing out that such models are widely used for quantitative determination of permeability in places where the calculation of water saturation

(Sw) cannot be evaluated. However, these models do not explicitly include the role played by the structure of the rocks, or the spatial distribution of liquids in the field of rock resources, or the distribution of clay minerals in permeability.

The second part of this project includes a correlation study between the thickness of an important qualification on behalf of the oil industry. The thickness of a specific flow unit combined with the porous contribute to calculating inventories and selecting the appropriate action plan for the production. Additionally, the extent and limitations factor of the reservoir was determined by calculating different variograms, in order to quantify the sufficient changes in the distribution of porosity and thickness for the heterogeneity of the reservoir. Finally, interpolation took place to fill the missing data, using one of the most widely used kriging interference algorithm, which with several drilling data is the best linear impartial assessment. That research tried to compare the applicability and the competitiveness of the inverse distance method (IDW), by using power indicators 1,1.5, 2, 2.5 and 3, where according to the data for that specific well for the specified Flow Unit, followed by a procedure that was applied and preceded by kriging for that determination of final volumes (OOIP). In the empirical bar graph, the exponential model was adapted, which was selected based on the square errors calculated after tests performed on the gaussian and spherical model. The spherical model was used in the kriging method.

In order to achieve our basic goal for this thesis, the calculation of the total Oil in Place into this flow unit reserves, the Standard method for (OOIP) and Kriging or IDW was used. Initially, a map was created with the estimates obtained, using a grid of 60 m x 60 m, and the total distance of 3000m. Knowing the new estimate of each cell, inventories were calculated approximately at 9,2 million STB. After that, it was compared with the estimates obtained using IDW. Stocks calculated at the average amounted to 9,5 million STB. In our procedure we focused on and played a serious task with the logarithm for our data, better validation measures appear with logarithm process in kriging method.

Stocks calculated are not very different from the other two methods. This happen because the average weights of all the measurements with the same weight compared to kriging using a different weight for each measurement and also the data that take part has not big amount. So the procedure between this method its wasn't so much how many its will be the Oil in Place but it's become known how this two methods work in Oil Field data and also with Kriging find the precisely error that kriging method gives.

### 6.1.1 Future work

A proposal for future research is to use different models than the ones already used and to compare the results. That is, to model the empirical variogram with a different model of a variogram, such as the Spartan, and to observe the changes that may occur in spatial inference. Also, kriging method can be used for simulation purposes in order to estimate confidence intervals, in order to make further work with other deterministic methods such as IDW, Voronoi or others. Last but not least, permeability and porosity are not able to correlate with low models, but they can guide us with the help of geostatistic tools, for a clearer image of how a reservoir behaves.

Another idea for this thesis deals with the comparison of models for predicting porosity and permeability. The implementation of these formulas its worth to apply in different formation and as a result will take more interpolation graphs. They can illustrate a correlation between permeability and porosity with the correct law model. These models has the same mathematical formula, but do not have the same characteristic parameters ( $S_w, B_o$  etc.). So, significant results about reservoir behavior will under estimated. Lastly do not expect that a simple correlation between permeability, porosity, and irreducible water saturation would work well for all rock formations with different values of porosity.

# Bibliography

- [1] M.Meister A. Cartellieri, J.Pragt. *Advantages and limitations of taking samples while drilling*. In SPWLA 53rd Annual Logging Symposium. Society of Petrophysicists and Well-Log Analysts, 2012.
- [2] Varouchakis Emmanouil Agou Vasiliki D and Hristopulos D.T. Geostatistical analysis of precipitation in the island of crete (greece) based on a sparse monitoring network. *Environmental Monitoring and Assessment*, 2019.
- [3] Yasir Albeatiy. What is the different between the net pay and resrvoir thickness. <https://www.slideshare.net/yoyoalbeatiy/what-is-the-different-between-the-net-pay-and-resrvoir-thickness>, 2008.
- [4] Jean-Paul Chile's and Pierre Delfiner. *Geostatistics Modeling Spatial Uncertainty*. John Wiley and Sons, Hoboken New Jersey, 2008.
- [5] J.P. Chilès and P. Delfiner. *Geostatistics: modeling spatial uncertainty*. Wiley series in probability and statistics. Wiley, 2012.
- [6] G. Christakos. *random field models in earth sciences*. Academic Press, Chapel Hill, North Carolina, 1992.
- [7] Schlumberger Oilfield Glossary Credits. Heteroneneity and fluid flow characteristics. <https://www.glossary.oilfield.slb.com/Terms/h/heterogeneity.aspx>.
- [8] N.A.C. Cressie. *Statistics for spatial data*. Wiley series in probability and statistics. Wiley, revised edition edition, 1993.
- [9] D.T.Hristopulos. *Random Fields for Spatial Data Modeling*. Springer, 2020.
- [10] Nnaemeka Ezekwe. Petroleum reservoir engineering practice. *Prentice Hall*, 2, 9 2014.

- [11] Panagiota Gafa. Geostatistical analysis of installed wind power production data. *Technical University of Crete*, 2020.
- [12] Andrew G.Pavlidis. Development of new geostatistical methods for spatial analysis and applications in reserves estimation and quality characteristics of coal deposits. *Technical University of Crete*, 2016.
- [13] Seni J. Grossman G., Agarwal Elder N., and H.Liu. *Ensemble methods in data mining: Improving Accuracy Through Combining Predictions*. Morgan and Claypool, 2010.
- [14] D.T Hristopulos. Spartan Gibbs random field models for geostatistical applications. *SIAM Journal on Scientific Computing*, 24(6):2125–2162, 2003.
- [15] D.T. Hristopulos. Applied geostatistics. Technical report, Technical University of Crete, 2012.
- [16] D.T. Hristopulos and S.N. Elogne. Analytical properties and covariance functions for a new class of generalized gibbs random fields. *IEEE Transactions on Information Theory*, 53(12):4667–4679, 2007.
- [17] Investing.com. Oil price today. <https://gr.investing.com/commodities/crude-oil>, 2018.
- [18] E.H. Isaaks and R.M. Srivastava. *Applied Geostatistics*. Oxford University Press, 1989.
- [19] S. Mauran, L. Rigaud, and O. Coudeville. Application of the carman–kozeny correlation to a high-porosity and anisotropic consolidated medium: The compressed expanded natural graphite. *Transport in Porous Media*, 43(2):355–376, May 2001.
- [20] Opuskinetic. What is reservoir characterization. <https://www.opuskinetic.com/2019/11/what-is-reservoir-characterisation/>, 2019.
- [21] Jim Pazos. Sweep efficiency. [https://oges.info/question/156694/What-is-sweep-efficiency\\_](https://oges.info/question/156694/What-is-sweep-efficiency_), 2019.
- [22] Hristopulos D.T. Petropoulos.G, Anagnostopoulos.P and Partsinevelos.P. An open source land biosphere extended for use with eo data for deriving spatiotemporally key biophysical parameters. *Geophysical Research*, 2019.
- [23] Stefan Z. Miska Robert F.Mitchell. *Fundamentals of Drilling Engineering*. Society of Petroleum Engineers, 2011.

- [24] Robert H. Lander Salman Bloch and Linda Bonnell. Anomalously high porosity and permeability in deeply buried sandstone reservoirs: Origin and predictability, 2002.
- [25] Jacob V. Brahmakulam (Schlumberger) Samy Serag El Din (ADCO Producing Co. Inc.) Chanh Cao Minh (Schlumberger) Douglas R. Murray (Schlumberger Oilfield Services). *Abu Dhabi International Petroleum Conference and Exhibition*. Society of Petroleum Engineers, 2012.
- [26] J. Melville SANDS. Burbank field, osage county, oklahoma. Technical report, Structure of Typical American Oil Fields, 1929.
- [27] Tatyana Sergeevna Torskaya, Guodong Jin, and Carlos Torres-Verdin. Pore-level analysis of the relationship between porosity irreducible water saturation and permeability of clastic rocks. *Proceedings - SPE Annual Technical Conference and Exhibition*, 2, 11 2007.
- [28] Off shore Engineering. The origin of oil and gas organic matter. <https://www.offshoreengineering.com>, 2019.
- [29] M.L. Stein. *Interpolation of Spatial Data: Some Theory for Kriging*. Springer, New York, 1999.
- [30] Sudhir and S. Richard. *Bias in error estimation when using cross-validation for model selection*. BMC Bioinformatics, 2006.
- [31] T.Darling. *Well Logging and Formation Evaluation*. Elsevier, 2005.
- [32] Tatyana Sergeevna Torskaya, Guodong Jin, Carlos Torres-Verdin, et al. Pore-level analysis of the relationship between porosity, irreducible water saturation, and permeability of clastic rocks. In *SPE Annual Technical Conference and Exhibition*. Society of Petroleum Engineers, 2007.
- [33] Francisco J. Valdes-Parada, J. Alberto Ochoa-Tapia, and Jose Alvarez-Ramirez. Validity of the permeability carman–kozeny equation: A volume averaging approach. *Physica A: Statistical Mechanics and its Applications*, 388(6):789 – 798, 2009.
- [34] Nicolaos. Varothis. Hydrocarbon reservoir mechanics. Technical report, Technical University of Crete, 2018.
- [35] E.A. Varouchakis, D.T. Hristopulos, and G.P. Karatzas. Improving kriging of groundwater level data using nonlinear normalizing transformations – a field application. *Hydrological Sciences Journal*, 57(7):1–16, 2012.

- [36] Bobby D. Weaver. Burbank Field. <https://www.okhistory.org/publications/enc/entry.php?entry=BU008>, 2008.
- [37] Weber. Types of reservoir heterogeneity. [https://www.researchgate.net/figure/Types-of-reservoir-heterogeneity-in-sandstone-bodies-that-occur-to-various-fig1\\_236833278](https://www.researchgate.net/figure/Types-of-reservoir-heterogeneity-in-sandstone-bodies-that-occur-to-various-fig1_236833278), 1986.
- [38] Wehitoil. Well logging. <https://wehitoil.com/well-logging-part-i/>, 2015.
- [39] Wikipedia. Volumetrics. <https://wiki.seg.org/wiki/Volumetrics>, 2018.
- [40] Anastasia Xenaki. Analysis of well log data using time series models and geostatistical methods. *Technical University of Crete*, 2020.
- [41] M. Žuković and D.T. Hristopulos. Spartan random processes in time series modeling. *Physica A-statistical Mechanics and Its Applications*, 387:3995–4001, 2008.



# Chapter 7

## Appendix

All algorithms for statistical and spatial analysis as well as the algorithms for the estimation of porosity ,thickness and permeability data, were developed and run in Matlab environment.

```
1
2
3 Thickness Procedure
4
5
6 %% Thickness FU3
7
8 load('FU3thickness.mat')
9 x=FU3thickness(:,1);
10 y=FU3thickness(:,2);
11 Th=FU3thickness(:,3);
12
13 [Fluct1,Mx,LinTren,QuaTren]=Detrend(x,y,Th,1); % Aferesh Prwtou Vathmou
14
15 % [Fluct2,Mx,LinTren,QuaTren]=Detrend(x,y,Th,2); %Aferesh Defterou
    Vathmou
16
17 % [Variogram1, lagcent, Pairsperclass]=Empeirvar(14,pi/2,pi/2, x,y,
    Fluct1,1,0.21);
18 % title('prwtou ba8mou')
19
20 % [Variogram2, lagcent, Pairsperclass]=Empeirvar(12,pi/2,pi, x,y,Fluct2
    ,1,0.25);
21 % title('deuterou ba8mou')
22 %
23 % [Variogram0, lagcent, Pairsperclass]=Empeirvar(12,pi/2,pi, x,y,Th
    ,1,0.25);
24 % title('xwris afairesh tashs')
```

```

25
26 % [Paramexp, lags, varioz, lagsn, variom]=Varexpon([x,y,Fluct1], 15, 0,
    0.22, 0);
27 % TO KALO
28
29 % [Paramexp, lags, varioz, lagsn, variom]=Varexpon([x,y,Fluct1], 14, 0,
    0.21, 0);% TO KALO
30
31
32 [Paramexp, lags, varioz, lagsn, variom]=Varexpon([x,y,Fluct1], 14, 0,
    0.22, 1);
33 [Paramgau, lags, varioz, lagsn, variom]=Vargauss([x,y,Fluct1], 14, 0,
    0.22, 0, 1);
34 [Paramsp, lags, varioz, lagsn, variom]=Varsph([x,y,Fluct1], 14, 0, 0.22,
    0, 1);
35
36
37 modsp=inline('betaexp1(3)+ betaexp1(1) ( betaexp1(1) betaexp1(1)
    *(1.5*x/betaexp1(2) 0.5* (x/betaexp1(2)).^3 ) ) .* (x<betaexp1(2)
    ) ','betaexp1','x');
38 ProblepshSpher=modsp(Paramsp, lags);
39 ErrSphe=sum((varioz ProblepshSpher).^2)
40
41 modga=inline('betaexp1(3)+betaexp1(1)*(1 exp( -x.^2/betaexp1(2).^2 ))',
    'betaexp1','x');
42 ProblepshGauss=modsp(Paramgau, lags);
43 ErrGauss=sum((varioz ProblepshGauss).^2)
44
45 modexpon=inline('betaexp1(3)+betaexp1(1)*(1 exp( -x/betaexp1(2) ))',
    'betaexp1','x');
46 ProblepExp=modsp(Paramexp, lags);
47 ErrExp=sum((varioz ProblepExp).^2)
48
49
50 % ***** CV *****
51
52 [EKTCV]=crossval(x,y,Fluct1,Paramexp,1,10);
53 A=[ones(length(x),1) x y];
54 TasDe= A * LinTren;% Tash stis 8eseis tw n dedomenwn
55
56 VALCV=TasDe + EKTCV;
57
58 ThCV=VALCV;
59 save CVALRESULTS ThCV Th
60
61 %*****
62 disp('**** CV Thickness ****')
63 Nk=length(Th);
64 MAECV=sum(abs(Th VALCV))/Nk

```

---

```

65 RCV=corrcoef(Th,VALCV)
66 MECV=sum((Th VALCV))/Nk
67 RMSECV=sqrt(sum((Th VALCV).^2)/Nk)
68 MaxAECV=max(abs(Th VALCV))
69 figure(2)
70 hist( (Th VALCV) , 12)
71 title('Cross Validation (error) Thickness Flow Unit 3')
72
73
74
75
76 disp('*****')
77 %%
78 %*****
79 [EKT, Xk, Yk, SF, PLG]=OrdKrig(83,50, x,y,Fluct1,Paramexp,1,11.2, 2);
80 Krigrids( Xk, Yk, EKT, SF );
81 figure(3)
82 colormap('parula')
83
84 %Ypologizw tash MM gia ton kanabo
85 % VAL= EKT + MM
86 %
87 [XI,YI] = meshgrid(Xk, Yk);
88 TASKAN=LinTren(1) + LinTren(2)*XI + LinTren(3)*YI;
89 figure(3)
90 surf(XI,YI,TASKAN)
91 shading flat
92 colormap('parula')
93 colorbar
94 title('Trend flow unit 3 Thickness')
95
96 VALTH=EKT+TASKAN;
97 Krigrids( Xk, Yk, VALTH, SF );
98 figure(4)
99 colormap('parula')
100 colorbar
101
102 % prepei na ginei cross validation sto VAL afou to bgaleis
103
104
105
106 Porosity Procedure
107
108
109 %% Porosity FU3
110 load('FU3por.mat')
111 x=FU3por(:,1);
112 y=FU3por(:,2);
113 Por=FU3por(:,3);

```

```

114
115 [Fluct1por,Mx,LinTrenPor,QuaTren]=Detrend(x,y,Por,1); % Aferesh Prwtou
    Vathmou
116
117 % [Fluct2,Mx,LinTren,QuaTren]=Detrend(x,y,Por,2); %Aferesh Defterou
    Vathmou
118
119
120 %[Paramexp, lags, varioz, lagsn, variom]=Varexpon([x,y,Fluct1por], 13,
    0, 0.19, 0);
121
122 [Paramexp, lags, varioz, lagsn, variom]=Varexpon([x,y,Fluct1por], 13, 0,
    0.19, 0);
123
124 [Paramgau, lags, varioz, lagsn, variom]=Vargauss([x,y,Fluct1por], 13, 0,
    0.19, 0);
125
126 [Paramsp, lags, varioz, lagsn, variom]=Varsph([x,y,Fluct1por], 13, 0,
    0.19, 0);
127
128
129 modsp=inline('betaexp1(3)+ betaexp1(1) ( betaexp1(1) betaexp1(1)
    *(1.5*x/betaexp1(2) 0.5* (x/betaexp1(2)).^3 ) ) .* (x<betaexp1(2)
    ) ','betaexp1','x');
130 ProblepshSpher=modsp(Paramsp,lags);
131 ErrSphe=sum((varioz ProblepshSpher).^2)
132
133 modga=inline('betaexp1(3)+betaexp1(1)*(1 exp( -x.^2/betaexp1(2).^2 ))',
    'betaexp1','x');
134 ProblepshGauss=modsp(Paramgau,lags);
135 ErrGauss=sum((varioz ProblepshGauss).^2)
136
137 modexpon=inline('betaexp1(3)+betaexp1(1)*(1 exp( -x/betaexp1(2) ))',
    'betaexp1','x');
138 ProblepExp=modsp(Paramexp,lags);
139 ErrExp=sum((varioz ProblepExp).^2)
140
141
142 [EKT, ~, ~, SF, PLG]=OrdKrig(83,50, x,y,Fluct1por,Paramexp,1,12.2, 2);
143
144 TASKAN=LinTrenPor(1) + LinTrenPor(2)*XI + LinTrenPor(3)*YI;
145 figure
146 surf(XI,YI,TASKAN)
147 shading flat
148 colormap('parula')
149 colorbar
150 title('Trend flow unit 3 Porosity')
151
152

```

---

```

153 VALPOR=EKT+TASKAN;
154 Krigrids( Xk, Yk, VALPOR, SF );
155 colormap( 'parula' )
156 hold off
157
158 SFPOR=SF;
159 %save KriPor5 VALPOR Xk Yk SFPOR
160
161 disp( '*****POR CV *****' )
162 [EKTcv,~,~,Err]=crossval(x,y,Fluct1por,Paramexp,1,10);
163
164 A=[ones(length(x),1) x y];
165 TasDe= A * LinTrenPor;
166
167 VALCV=TasDe + EKTcv;
168
169 Val_Err=VALCV Por;
170 figure
171 hist( Val_Err,14)
172 title( 'Cross Validation (error) Porosity Flow Unit 3' )
173
174 PorCV=EKTcv;
175 %save CVALRESULTS5 ThCV Th Por PorCV % swnw kai ta dyo Th kai Por kai
    CV
176
177 disp( '*****' )
178 %%
179 %
180 JJJ=VALTH.* VALPOR/100;
181 xcell=(Xk(2) Xk(1))*1000; ycell=(Yk(2) Yk(1))*1000;
182 %CUBICM=sum(sum(JJJ*xcell*ycell));
183 A=xcell*ycell; % A cubic metra
184 NG=0.7
185 Sw=0.20
186 Bo=1.2
187 metat=6.29 % kybiko metro se bbl
188 CelloOIP=JJJ*(A*NG*(1 Sw))/Bo * metat;
189 OOIIP=sum(sum(CelloOIP))
190
191 Krigrids( Xk, Yk, CelloOIP );
192 colormap( 'parula' )
193 title( 'OOIP flow unit 3 (bbl)' )
194 hold off

1 cle
2
3 %% Thickness FU5
4
5 load( 'FU5thickness.mat' )

```

```

6 x=FU5thickness (:,1);
7 y=FU5thickness (:,2);
8 Th=FU5thickness (:,3);
9
10 %%%%%%%%% Removal Trial trend%%%%%%%%%%%%%
11
12 [Fluct1,Mx,LinTren,QuaTren]=Detrend(x,y,Th,1); % Aferesh Prwtou Vathmou
13
14 %[Fluct1,Mx,LinTren,QuaTren]=Detrend(x,y,Th,0); % Aferesh Prwtou
    Vathmou
15
16
17 [MTHICK,Me,STHICK,AsymetriTHICK,kurtosisThick,minTHICK,maxTHICK] =
    GEOSTATh(Th)
18
19 %[MTHICK,Me,STHICK,AsymetriTHICK,kurtosisThick,minTHICK,maxTHICK] =
    GEOSTATh(Fluct1)
20
21
22
23 % [Fluct2,Mx,LinTren,QuaTren]=Detrend(x,y,Th,2); %Aferesh Defterou
    Vathmou
24
25 % [Variogram1, lagcent, Pairsperclass]=Empeirvar(14,pi/2,pi/2, x,y,
    Fluct1,1,0.21);
26 % title('prwtou ba8mou')
27
28 % [Variogram2, lagcent, Pairsperclass]=Empeirvar(12,pi/2,pi, x,y,Fluct2
    ,1,0.25);
29 % title('deuterou ba8mou')
30 %
31 %[Variogram0, lagcent, Pairsperclass]=Empeirvar(12,pi/2,pi, x,y,Th
    ,1,0.25);
32 %title('Without Remove of Trend Values')
33
34 [Paramexp, lags, varioz, lagsn,variome]=Varexpon([x,y,Fluct1], 15, 0,
    0.22, 1);
35 [Paramgau, lags, varioz, lagsn,variomg]=Vargauss([x,y,Fluct1], 15, 0,
    0.22, 0, 1);
36 [Paramsp, lags, varioz, lagsn,varioms]=Varsph([x,y,Fluct1], 15, 0,
    0.22, 0, 1);
37
38 figure(50)
39 hold on
40 plot(lagsn,variome,'Linewidth',2)
41 plot(lagsn,variomg,'Linewidth',2)
42 plot(lagsn,varioms,'g','Linewidth',2)
43 plot(lags,varioz,'*')
44 hold off

```

---

```

45 % legend('Exponential','Gaussian','Spherical','Empirical','Location','SouthEast')
46 xlabel('distance (r)')
47 ylabel('\gamma(r)')
48
49
50 modsp=inline('betaexp1(3)+ betaexp1(1) ( betaexp1(1) betaexp1(1)
    *(1.5*x/betaexp1(2) 0.5* (x/betaexp1(2)).^3 ) ) .* (x<betaexp1(2)
    ) ','betaexp1','x');
51 ProblepshSpher=modsp(Paramsp,lags);
52 ErrSphe=sum((varioz ProblepshSpher).^2)
53
54 modga=inline('betaexp1(3)+betaexp1(1)*(1 exp( -x.^2/betaexp1(2).^2 ))','betaexp1','x');
55 ProblepshGauss=modsp(Paramgau,lags);
56 ErrGauss=sum((varioz ProblepshGauss).^2)
57
58 modexpon=inline('betaexp1(3)+betaexp1(1)*(1 exp( -x/betaexp1(2) ))','betaexp1','x');
59 ProblepExp=modsp(Paramexp,lags);
60 ErrExp=sum((varioz ProblepExp).^2)
61
62
63 %[Paramexp, lags, varioz, lagsn, variom]=Varexpon([x,y,Fluct1], 14, 0, 0.21, 0, 1);
64
65
66 % ***** CV *****
67
68 [EKTCV]=crossval2(x,y,Fluct1,Paramsp,5,10);
69 A=[ones(length(x),1) x y];
70 TasDe= A * LinTren; % Tash stis 8eseis twn dedomenwn
71
72 %TasDe=Mx;
73 VALCV=TasDe + EKTCV;
74
75 ThCV=VALCV;
76 save CVALRESULTS ThCV Th
77
78 %*****
79
80
81 *****Cross Validation*****
82
83 disp('**** CV Thickness ****')
84 Nk=length(Th);
85 MAECV=sum(abs(Th VALCV))/Nk
86 RCV=corrcoef(Th,VALCV)
87 MECV=sum((Th VALCV))/Nk

```

```

88 RMSECV=sqrt(sum((Th VALCV).^2)/Nk)
89 MaxAECV=max(abs(Th VALCV))
90 figure(99)
91 hist( (Th VALCV), 12)
92 title('Cross Validation (error) Thickness Flow Unit 5')
93
94
95
96
97 disp('*****')
98
99
100 %%
101
102
103
104 %*****
105 %[EKT, Xk, Yk, SF, PLG]=OrdKrig(83,50, x,y,Fluct1,Paramexp,1,11.2, 2);
106 [EKT, Xk, Yk, SF, PLG]=OrdKrig(50,50, x,y,Fluct1,Paramsp, 5, 31.9, 2,
    [5 15]*0.3048, [0 10]*0.3048);
107 colormap('parula')
108 Krigrids( Xk, Yk, EKT, SF );
109 figure(3)
110 colormap('parula')
111
112 **** Trend Calculation with Matrix****
113 % VAL= EKT + MM
114 %
115
116
117
118 [XI,YI] = meshgrid(Xk, Yk);
119 TASKAN=LinTren(1) + LinTren(2)*XI + LinTren(3)*YI;
120 %TASKAN=Mx+0*XI+0*YI;
121
122
123
124
125 figure
126 surf(XI,YI,TASKAN)
127 shading flat
128 colormap('parula')
129 colorbar
130 title('Trend Flow unit 5 Thickness ')
131
132 VALTH=EKT+TASKAN;
133 Krigrids( Xk, Yk, VALTH, SF );
134 figure
135 colormap('parula')

```



---

```

136 colorbar
137
138
139
140
141
142 %%%%%%%%%% Porosity FU5 %%%%%%%%%%
143
144
145
146 load ( 'FU5por.mat' )
147 x=FU5por (:,1) ;
148 y=FU5por (:,2) ;
149 Por=FU5por (:,3) ;
150
151 [Mpor,Me,Spor,Asymetripor,kurtosispor,minpor,maxpor] = GEOSTAPor(Por)
152
153
154 %[ Fluct1por,Mx,LinTrenPor,QuaTren]=Detrend(x,y,Por,0); % Aferesh Mx
155 [ Fluct1por,Mx,LinTrenPor,QuaTren]=Detrend(x,y,Por,1); % Aferesh Prwtou
    Vathmou
156
157 %[Mpor,Me,Spor,Asymetripor,kurtosispor,minpor,maxpor] = GEOSTAPor(
    Fluct1por)
158
159 % [ Fluct2,Mx,LinTren,QuaTren]=Detrend(x,y,Por,2); %Aferesh Defterou
    Vathmou
160
161 [Paramexp, lags, varioz, lagsn,variomexp]=Varexpon([x,y,Fluct1por], 13,
    0, 0.19, 0);
162
163 [Paramgau, lags, varioz, lagsn,variomgaus]=Vargauss([x,y,Fluct1por],
    13, 0, 0.19, 0);
164
165 [Paramsp, lags, varioz, lagsn,variomsph]=Varsph([x,y,Fluct1por], 13, 0,
    0.19, 0);
166
167
168 figure(51)
169 hold on
170 plot(lagsn,variomexp,'Linewidth',2)
171 plot(lagsn,variomgaus,'Linewidth',2)
172 plot(lagsn,variomsph,'g','Linewidth',2)
173 plot(lags,varioz,'*')
174 hold off
175 % legend('Exponential','Gaussian','Spherical','Empirical','Location','
    SouthEast')
176 xlabel('distance (r)')
177 ylabel('gamma(r)')

```

```

178
179
180 modsp=inline('betaexp1(3)+ betaexp1(1) ( betaexp1(1) betaexp1(1)
      *(1.5*x/betaexp1(2) 0.5* (x/betaexp1(2)).^3 ) ) .* (x<betaexp1(2)
      ) ','betaexp1','x');
181 ProblepshSpher=modsp(Paramsp,lags);
182 ErrSphe=sum((varioz ProblepshSpher).^2)
183
184 modga=inline('betaexp1(3)+betaexp1(1)*(1 exp( -x.^2/betaexp1(2).^2 ))',
      'betaexp1','x');
185 ProblepshGauss=modsp(Paramgau,lags);
186 ErrGauss=sum((varioz ProblepshGauss).^2)
187
188 modexpon=inline('betaexp1(3)+betaexp1(1)*(1 exp( -x/betaexp1(2) ))',
      'betaexp1','x');
189 ProblepExp=modsp(Paramexp,lags);
190 ErrExp=sum((varioz ProblepExp).^2)
191
192
193
194 %[EKT, ~, ~, SF, PLG]=OrdKrig(83,50, x,y,Fluct1por,Paramexp,1,12.2, 2);
195 [EKT, Xk, Yk, SF, PLG]=OrdKrig(50,50, x,y,Fluct1por,Paramsp, 5, 31.9,
      2, [5 15]*0.3048, [0 10]*0.3048);
196
197 TASKAN=LinTrenPor(1) + LinTrenPor(2)*XI + LinTrenPor(3)*YI;
198 figure
199 surf(XI,YI,TASKAN)
200 shading flat
201 colormap('parula')
202 colorbar
203 title('Trend Flow unit 5 Porosity')
204
205 TASKAN=Mx+0*XI+0*YI; % Kanw overwrite thn linear me Mx
206
207 VALPOR=EKT+TASKAN;
208 Krigrids( Xk, Yk, VALPOR, SF );
209 colormap('parula')
210 hold off
211
212 SFPOR=SF;
213 %save KriPor5 VALPOR Xk Yk SFPOR
214
215 [EKTCV,~, ~, Err]=crossval2(x,y,Fluct1por, Paramsp, 5,10);
216
217 A=[ones(length(x),1) x y];
218 TasDe= Mx; %A * LinTrenPor;
219 %TasDe= A * LinTrenPor;
220 VALCV=TasDe + EKTCV;
221

```

---

```

222 Val_Err=VALCV Por;
223
224 figure
225 hist(Val_Err,12)
226 title('Cross Validation (error) Porosity Flow Unit 5')
227
228 PorCV=EKTCV;
229 %save CVALRESULTS5 ThCV Th Por PorCV % swnw kai ta dyo Th kai Por kai
    CV
230
231 *****Cross Validation*****
232
233
234 disp('*****Porosity CV *****')
235 Nk=length(Por)
236 MAECV=sum(abs(Por VALCV))/Nk
237 RCV=corrcoef(Por,VALCV)
238 MECV=sum((Por VALCV))/Nk
239 RMSECV=sqrt(sum((Por VALCV).^2)/Nk)
240 MaxAECV=max(abs(Por VALCV))
241
242
243 disp('*****')
244 %%
245
246
247 %%%%%%%%%%%Stocks%%%%%%%%%%
248
249 JJJ=VALTH.* VALPOR/100;
250 xcell=(Xk(2)-Xk(1))*1000; ycell=(Yk(2)-Yk(1))*1000;
251 %CUBICM=sum(sum(JJJ*xcell*ycell));
252 A=xcell*ycell; % A cubic metra
253 NG=0.7
254 Sw=0.20
255 Bo=1.2
256 metat=6.29 % kybiko metro se bbl
257
258 CelloOIP=JJJ*(A*NG*(1-Sw))/Bo * metat;
259
260 OIP=sum(sum(CelloOIP))
261
262 Krigrids(Xk, Yk, CelloOIP);
263 colormap('parula')
264 title('OIP Flow unit 5 STB')
265 hold off

```

1 Flow Unit 8

2

3 Thickness Procedure

```

4
5 %% Thickness FU8
6
7 load('FU8thickness.mat')
8 x=FU8thickness(:,1);
9 y=FU8thickness(:,2);
10 Th=FU8thickness(:,3);
11
12 [Fluct1,Mx,LinTren,QuaTren]=Detrend(x,y,Th,1); % Aferesh Prwtou Vathmou
13
14 % [Fluct2,Mx,LinTren,QuaTren]=Detrend(x,y,Th,2); %Aferesh Defterou
    Vathmou
15
16 % [Variogram1, lagcent, Pairsperclass]=Empeirvar(14,pi/2,pi/2, x,y,
    Fluct1,1,0.21);
17 % title('prwtou ba8mou')
18
19 % [Variogram2, lagcent, Pairsperclass]=Empeirvar(12,pi/2,pi, x,y,Fluct2
    ,1,0.25);
20 % title('deuterou ba8mou')
21 %
22 % [Variogram0, lagcent, Pairsperclass]=Empeirvar(12,pi/2,pi, x,y,Th
    ,1,0.25);
23 % title('xwris afairesh tashs')
24
25 % [Paramexp, lags, varioz, lagsn,variom]=Varexpon([x,y,Fluct1], 15, 0,
    0.22, 0);
26 % TO KALO
27
28 [Paramexp, lags, varioz, lagsn,variom]=Varexpon([x,y,Fluct1], 14, 0,
    0.21, 0);
29
30 % ***** CV *****
31
32 [EKTCV]=crossval(x,y,Fluct1,Paramexp,1,10);
33 A=[ones(length(x),1) x y];
34 TasDe= A * LinTren;% Tash stis 8eseis tw n dedomenwn
35
36 VALCV=TasDe + EKTCV;
37
38 ThCV=VALCV;
39 save CVALRESULTS ThCV Th
40
41 %*****
42 disp('**** CV Thickness ****')
43 Nk=length(Th);
44 MAECV=sum(abs(Th - VALCV))/Nk
45 RCV=corrcoef(Th,VALCV)
46 MECV=sum((Th - VALCV))/Nk

```

---

```

47 RMSECV=sqrt(sum((Th VALCV).^2)/Nk)
48 MaxAECV=max(abs(Th VALCV))
49 figure(2)
50 hist( (Th VALCV) , 12)
51 title('CV error Porosity')
52
53
54
55
56 disp('*****')
57 %%
58 %*****
59 [EKT, Xk, Yk, SF, PLG]=OrdKrig(83,50, x,y,Fluct1,Paramexp,1,11.2, 2);
60 Krigrids( Xk, Yk, EKT, SF );
61 figure(3)
62 colormap('parula')
63
64 %Ypologizw tash MM gia ton kanabo
65 % VAL= EKT + MM
66 %
67 [XI,YI] = meshgrid(Xk, Yk);
68 TASKAN=LinTren(1) + LinTren(2)*XI + LinTren(3)*YI;
69 figure(3)
70 surf(XI,YI,TASKAN)
71 shading flat
72 colormap('parula')
73 colorbar
74 title('Tash')
75
76 VALTH=EKT+TASKAN;
77 Krigrids( Xk, Yk, VALTH, SF );
78 figure(4)
79 colormap('parula')
80 colorbar
81
82 % prepei na ginei cross validation sto VAL afou to bgaleis
83
84
85 Porosity Procedure
86
87 %% Porosity FU8
88 load('FU8por.mat')
89 x=FU8por(:,1);
90 y=FU8por(:,2);
91 Por=FU8por(:,3);
92
93 [Fluct1por,Mx, LinTrenPor, QuaTren]=Detrend(x,y,Por,1); % Aferesh Prwtou
    Vathmou
94

```

```

95 % [Fluct2,Mx,LinTren,QuaTren]=Detrend(x,y,Por,2); %Aferesh Defterou
    Vathmou
96
97
98 [Paramexp, lags, varioz, lagsn, variom]=Varexpon([x,y,Fluct1por], 13, 0,
    0.19, 0);
99
100 [EKT, ~, ~, SF, PLG]=OrdKrig(83,50, x,y,Fluct1por,Paramexp,1,12.2, 2);
101
102 TASKAN=LinTrenPor(1) + LinTrenPor(2)*XI + LinTrenPor(3)*YI;
103 figure
104 surf(XI,YI,TASKAN)
105 shading flat
106 colormap('parula')
107 colorbar
108 title('Tash Porod')
109
110
111 VALPOR=EKT+TASKAN;
112 Krigrids( Xk, Yk, VALPOR, SF );
113 colormap('parula')
114 hold off
115
116 SFPOR=SF;
117 %save KriPor5 VALPOR Xk Yk SFPOR
118
119 disp('*****POR CV *****')
120 [EKTCV,~, ~, Err]=crossval(x,y,Fluct1por,Paramexp,1,10);
121
122 A=[ones(length(x),1) x y];
123 TasDe= A * LinTrenPor;
124
125 VALCV=TasDe + EKTCV;
126
127 Val_Err=VALCV Por;
128 figure
129 hist(Val_Err,14)
130 title('CV error Porosity')
131
132 PorCV=EKTCV;
133 %save CVALRESULTS5 ThCV Th Por PorCV % swnw kai ta dyo Th kai Por kai
    CV
134
135 disp('*****')
136 %%
137 %
138 JJJ=VALTH.* VALPOR/100;
139 xcell=(Xk(2) Xk(1))*1000; ycell=(Yk(2) Yk(1))*1000;
140 %CUBICM=sum(sum(JJJ*xcell*ycell));

```

---

```
141 A=xcell*ycell; % A cubic metra
```

```
142 NG=0.7
```

```
143 Sw=0.20
```

```
144 Bo=1.2
```

```
145 metat=6.29 % kybiko metro se bbl
```

```
146 CellOOIP=JJJ*(A*NG*(1 Sw))/Bo * metat;
```

```
147 OOIP=sum(sum(CellOOIP))
```

```
148
```

```
149 Krigrids( Xk, Yk, CellOOIP );
```

```
150 colormap( 'parula' )
```

```
151 title( 'OOIP (bbl)' )
```

```
152 hold off
```

```
1
```

```
2
```

```
3 Flow Unit 10
```

```
4
```

```
5 Thickness Procedure
```

```
6
```

```
7 %%%%%%%%% Thickness FU10
```

```
8
```

```
9 load( 'FU10thickness.mat' )
```

```
10 x=FU10thickness(:,1);
```

```
11 y=FU10thickness(:,2);
```

```
12 Th=FU10thickness(:,3);
```

```
13
```

```
14 [Fluct1,Mx,LinTren,QuaTren]=Detrend(x,y,Th,1); % Aferesh Prwtou Vathmou
```

```
15
```

```
16 %[Fluct2,Mx,LinTren,QuaTren]=Detrend(x,y,Th,2); %Aferesh Defterou  
Vathmou
```

```
17
```

```
18 % [Variogram1, lagcent, Pairsperclass]=Empeirvar(14,pi/2,pi/2, x,y,  
Fluct1,1,0.21);
```

```
19 % title('prwtou ba8mou')
```

```
20
```

```
21 % [Variogram2, lagcent, Pairsperclass]=Empeirvar(12,pi/2,pi, x,y,Fluct2  
,1,0.25);
```

```
22 % title('deuterou ba8mou')
```

```
23 %
```

```
24 % [Variogram0, lagcent, Pairsperclass]=Empeirvar(12,pi/2,pi, x,y,Th  
,1,0.25);
```

```
25 % title('xwris afaresh tashs')
```

```
26
```

```
27 % [Paramexp, lags, varioz, lagsn, variom]=Varexpon([x,y,Fluct1], 15, 0,  
0.22, 0);
```

```
28 % TO KALO
```

```
29
```

```
30 [Paramexp, lags, varioz, lagsn, variom]=Varexpon([x,y,Fluct1], 14, 0,  
0.21, 0);
```

```

31 % [Paramexp, lags, varioz, lagsn, variom] = Varexpon([x, y, Fluct2], 14, 0,
    0.21, 0);
32
33
34 % ***** CV *****
35
36 [EKTCV] = crossval(x, y, Fluct1, Paramexp, 1, 10);
37 A = [ones(length(x), 1) x y];
38 TasDe = A * LinTren; % Tash stis 8eseis tw n dedomenwn
39
40 VALCV = TasDe + EKTCV;
41
42 ThCV = VALCV;
43 save CVALRESULTS ThCV Th
44
45 %*****
46 disp('**** CV Thickness ****')
47 Nk = length(Th);
48 MAECV = sum(abs(Th - VALCV)) / Nk
49 RCV = corrcoef(Th, VALCV)
50 MECV = sum((Th - VALCV).^2) / Nk
51 RMSECV = sqrt(sum((Th - VALCV).^2) / Nk)
52 MaxAECV = max(abs(Th - VALCV))
53 figure(2)
54 hist(Th - VALCV, 12)
55 title('Cross Validation (error) Thickness Flow Unit 10')
56
57
58
59
60 disp('*****')
61 %%
62 %*****
63 % [EKT, Xk, Yk, SF, PLG] = OrdKrig(83, 50, x, y, Fluct1, Paramexp, 1, 0.7, 2);
64 [EKT, Xk, Yk, SF, PLG] = OrdKrig(40, 40, x, y, Fluct1, Paramexp, 1, 31.9, 2, [5
    15]*0.3048, [0 10]*0.3048);
65 Krigrids(Xk, Yk, EKT, SF);
66 figure(3)
67 colormap('parula')
68
69 % Ypologizw tash MM gia ton kanabo
70 % VAL = EKT + MM
71 %
72 [XI, YI] = meshgrid(Xk, Yk);
73 TASKAN = LinTren(1) + LinTren(2)*XI + LinTren(3)*YI;
74 figure(3)
75 surf(XI, YI, TASKAN)
76 shading flat
77 colormap('parula')

```



---

```

78 colorbar
79 title('Trend flow unit 10 Thickness')
80
81 VALTH=EKT+TASKAN;
82 Krigrids( Xk, Yk, VALTH, SF );
83 figure(4)
84 colormap('parula')
85 colorbar
86 %title('Kriging Standard Deviation flow unit 10 Thickness')
87 % prepei na ginei cross validation sto VAL afou to bgaleis
88
89
90 Porosity Procedure
91
92
93 %% Porosity FU10
94
95 % #####
96 % #####
97
98
99 load('FU10por.mat')
100 x=FU10por(:,1);
101 y=FU10por(:,2);
102 Por=FU10por(:,3);
103
104 figure
105 [Fluct1por,Mx,LinTrenPor,QuaTren]=Detrend(x,y,Por,1); % Aferesh Prwtou
    Vathmou
106
107 % [Fluct2,Mx,LinTren,QuaTren]=Detrend(x,y,Por,2); %Aferesh Defterou
    Vathmou
108
109
110 % [Paramexp, lags, varioz, lagsn, variom]=Varexpon([x,y,Fluct1por], 13,
    0, 0.19, 0);
111 % [EKT, ~, ~, SF, PLG]=OrdKrig(83,50, x,y,Fluct1por,Paramexp,1,12.2, 2)
    ;
112
113 [Paramexp, lags, varioz, lagsn, variom]=Varexpon([x,y,Por], 13, 0, 0.19,
    0);
114 % [EKT, ~, ~, SF, PLG]=OrdKrig(83,50, x,y,Por,Paramexp,1,0.7, 2);
115 [EKT, ~, ~, SF, PLG]=OrdKrig(40,40, x,y,Por,Paramexp,1,31.9, 2, [5
    15]*0.3048, [0 10]*0.3048);
116
117 TASKAN=LinTrenPor(1) + LinTrenPor(2)*XI + LinTrenPor(3)*YI;
118 figure
119 surf(XI,YI,TASKAN)
120 shading flat

```

```

121 colormap('parula')
122 colorbar
123 title('Trend flow unit 10 Porosity')
124
125
126 VALPOR=EKT; %TASKAN;
127 Krigrids( Xk, Yk, VALPOR, SF );
128 colormap('parula')
129 hold off
130
131 SFPOR=SF;
132 %save KriPor5 VALPOR Xk Yk SFPOR
133
134 disp('*****POR CV *****')
135 %[EKTCV,~,~,Err]=crossval(x,y,Fluct1por,Paramexp,1,10);
136 [EKTCV,~,~,Err]=crossval(x,y,Por,Paramexp,1,10);
137
138 A=[ones(length(x),1) x y];
139 TasDe= A * LinTrenPor;
140
141 VALCV=EKTCV; % +TasDe;
142
143 Val_Err=VALCV Por;
144 figure
145 hist(Val_Err,14)
146 title('Cross Validation (error) Porosity Flow Unit 10')
147
148 PorCV=EKTCV;
149 %save CVALRESULTS5 ThCV Th Por PorCV % swnw kai ta dyo Th kai Por kai
    CV
150
151 disp('*****')
152 %%
153 %
154 JJJ=VALTH.* VALPOR/100;
155 xcell=(Xk(2) Xk(1))*1000; ycell=(Yk(2) Yk(1))*1000;
156 %CUBICM=sum(sum(JJJ*xcell*ycell));
157 A=xcell*ycell; % A cubic metra
158 NG=0.7
159 Sw=0.20
160 Bo=1.2
161 metat=6.29 % kybiko metro se bbl
162 CelloOIP=JJJ*(A*NG*(1 Sw))/Bo * metat;
163
164 OOIIP=nansum(nansum(CelloOIP))
165
166 figure
167 Krigrids( Xk, Yk, CelloOIP );
168 colormap('parula')

```

---

```

169 title('OOP flow unit 10 (bbl)')
170 hold off
171
172 %%
173 %
174 %PorCV; Por
175 %ThCV 91; Th 91
176
177 SYNTE= 1/100* (A*NG*(1 Sw))/Bo * metat;
178 Nk=min([length(Th), length(Por)]); % pairnoyme to elaxisto mikos apo ta
    dyo dianismata
179
180 GINOM=Por(1:Nk,1).*Th(1:Nk,1)*SYNTE;
181 GINOMCV=PorCV(1:Nk,1).*ThCV(1:Nk,1)*SYNTE;
182
183 Val_Err=GINOMCV/GINOM;
184
185 MAECV=sum(abs(GINOM GINOMCV))/Nk
186 RCV=corrcoef(GINOM,GINOMCV)
187 MECV=sum((GINOM GINOMCV))/Nk
188 RMSECV=sqrt(sum((GINOM GINOMCV).^2)/Nk)
189 MaxAECV=max(abs(GINOM GINOMCV))
190 RelEr=abs(GINOM GINOMCV)./GINOM; % An 8elw na dw ta relative errors se
    ena ena shmeio
191 MARE=sum(abs(GINOM GINOMCV)./GINOM )/Nk
192 figure
193 hist( (GINOM GINOMCV), 12)
194 title('Cross Validation (error) GINOMENO Flow Unit 10')

```

```

1 cle
2
3 load('FU5thickness.mat')
4 xt=FU5thickness(:,1);
5 yt=FU5thickness(:,2);
6 Th=FU5thickness(:,3);
7
8 load('FU5por.mat')
9 xp=FU5por(:,1);
10 yp=FU5por(:,2);
11 Por=FU5por(:,3);
12
13 %[MTHICK,Me,STHICK,AsymetriTHICK,kurtosisThick,minTHICK,maxTHICK] =
    GEOSTATh(Th)
14 %[Mpor,Me,Spor,Asymetripor,kurtosispor,minpor,maxpor] = GEOSTAPor(Por)
15
16
17 LT=round([xt yt]*1000)/1000;
18
19 LP=round([xp yp]*1000)/1000;

```

```

20
21 [C,ITh,IPor] = intersect(LT,LP,'rows');
22
23 Porth = log(Por(IPor).* Th(ITh)); % Porosity x thickness koina
24 x = xt(ITh);
25 y = yt(ITh);
26
27
28 %[Variogram0, lagcent, Pairsperclass]=Empeirvar(12,pi/2,pi, x,y,Th
    ,1,0.25);
29 %title('Without Remove of Trend Values')
30
31 [Fluct1,Mx,LinTren,QuaTren]=Detrend(x,y,Porth,0); % Aferesh mhd Vathmou
32
33 [Mpor,Me,Spor,Asymetripor,kurtosispor,minpor,maxpor] = GEOSTAPor(Porth)
34
35
36
37 % *****
38
39 [Paramexp, lags, varioz, lagsn,variomexp]=Varexpon([x,y,Fluct1], 12, 0,
    0.26, 0, 1);
40 [Paramgau, lags, varioz, lagsn,variomgaus]=Vargauss([x,y,Fluct1], 12,
    0, 0.26, 0, 1);
41 [Paramsp, lags, varioz, lagsn,variomsph]=Varsph([x,y,Fluct1], 12, 0,
    0.26, 0, 1);
42
43
44
45 figure(51)
46 hold on
47 plot(lagsn,variomexp,'Linewidth',2)
48 plot(lagsn,variomgaus,'Linewidth',2)
49 plot(lagsn,variomsph,'g','Linewidth',2)
50 plot(lags,varioz,'*')
51 hold off
52 legend('Exponential','Gaussian','Spherical','Empirical','Location','
    SouthEast')
53 xlabel('distance (r)')
54 ylabel('\gamma(r)')
55
56
57 modsp=inline('betaexp1(3)+ betaexp1(1) ( betaexp1(1) betaexp1(1)
    *(1.5*x/betaexp1(2) 0.5* (x/betaexp1(2)).^3 ) ) .* (x<betaexp1(2)
    ) ','betaexp1','x');
58 ProblepshSpher=modsp(Paramsp,lags);
59 ErrSphe=sum((varioz ProblepshSpher).^2)
60
61 modga=inline('betaexp1(3)+betaexp1(1)*(1 exp( -x.^2/betaexp1(2).^2 ))',

```

---

```

        'betaexp1','x');
62 ProblepshGauss=modsp(Paramgau,lags);
63 ErrGauss=sum((varioz ProblepshGauss).^2)
64
65 modexpon=inline('betaexp1(3)+betaexp1(1)*(1 exp( -x/betaexp1(2) ))','x',
        'betaexp1','x');
66 ProblepExp=modsp(Paramexp,lags);
67 ErrExp=sum((varioz ProblepExp).^2)
68
69
70
71 % *****
72
73 [EKTCV]=crossval2(x,y,Fluct1,Paramexp,5,10);
74 % disp('-----')
75 % disp('gauss')
76 % [EKTCV]=crossval(x,y,Fluct1,Paramgau,2,10);
77 %
78
79
80 %A=[ones(length(x),1) x y];
81 %TasDe= A * LinTren; % Tash stis 8eseis twn dedomenwn
82
83 A=[ones(length(x),1) x y x.^2 y.^2 x.*y];
84 TasDe= A * QuaTren; % Tash stis 8eseis twn dedomenwn
85
86 TasDe=Mx;
87 VALCV=TasDe + EKTCV;
88
89 Err=VALCV Porth;
90 Nk=length(Porth);
91 mean(Err)
92 MAECV=mean(abs(Porth VALCV))
93 RMSECV=sqrt(mean((Porth VALCV).^2))
94 RCV=corrcoef(Porth,VALCV)
95 MECV=sum((Porth VALCV))/Nk
96 %%
97
98 [EKT, Xk, Yk, SF, PLG]=OrdKrig(50,50, x,y,Fluct1,Paramsp, 5, 15, 2, [5
        15]*0.3048, [0 10]*0.3048);
99 Krigrids( Xk, Yk, EKT, SF );
100 figure(3)
101 colormap('parula')
102 figure(4)
103 %title('kriging Variance')
104
105
106 %*****
107 disp('**** CV Porth ****')
```

```

108 disp('apologar')
109 Nk=length(Porth);
110 Porth2=exp(Porth); VALCV2=exp(VALCV);
111
112 MAECV=sum(abs(Porth2 VALCV2))/Nk
113 RCV=corrcoef(Porth2,VALCV2)
114 MECV=sum((Porth2 VALCV2))/Nk
115 RMSECV=sqrt(sum((Porth2 VALCV2).^2)/Nk)
116 MaxAECV=max(abs(Porth2 VALCV2))
117 figure(99)
118 hist( (Porth2 VALCV2), 12)
119 title('Cross Validation (error) Thickness Flow Unit 5')
120 %%%%%%%%%%%%%%%%%%%%%%%%%%%%%%%%%%%%%%%%%%%%%%%%%%%%%%%%%%%%%%%%%%%%%%%%%
121
122
123 [XI,YI] = meshgrid(Xk, Yk);
124 TASKAN=LinTren(1) + LinTren(2)*XI + LinTren(3)*YI;
125 %TASKAN=Mx+0*XI+0*YI;
126 %TASKAN=QuaTren(1) + QuaTren(2)*XI + LinTren(3)*YI +QuaTren(4)*XI.^2 +
    +QuaTren(5)*YI.^2 + +QuaTren(6)*XI.*YI;
127
128 %
129 % figure(3)
130 % surf(XI,YI,TASKAN)
131 % shading flat
132 % colormap('parula')
133 % colorbar
134 % title('Trend Flow unit 5 Thickness ')
135 %
136 VALTH=exp(EKT+TASKAN);
137 Krigrids( Xk, Yk, VALTH, SF );
138 figure(5)
139 colormap('parula')
140 colorbar
141
142 JJJ=VALTH/100;
143 %JJJ=VALTH.* VALPOR/100;
144 xcell=(Xk(2) Xk(1))*1000; ycell=(Yk(2) Yk(1))*1000;
145 %CUBICM=sum(sum(JJJ*xcell*ycell));
146 A=xcell*ycell; % A cubic metra
147 NG=0.7
148 Sw=0.20
149 Bo=1.2
150 metat=6.29 % kybiko metro se bbl
151 CelloOIP=JJJ*(A*NG*(1 Sw))/Bo * metat;
152 OOIP=sum(sum(CelloOIP))
153
154 Krigrids( Xk, Yk, CelloOIP );
155 colormap('parula')

```

---

```

156 title('OOP Flow unit 5 STB')
157 hold off

1 cle
2
3
4 %% Setup and construct interpolation grid
5
6 % Interpolation size and step
7 xint_min = 5*0.3048; %min(x);
8 xint_max = 15*0.3048;%max(x);
9 xint_step = (xint_max - xint_min)/41;
10
11 %[5 15]*0.3048, [0 10]*0.3048 Vima
12
13 yint_min = 0*0.3048;
14 yint_max = 10*0.3048;
15 yint_step = (yint_max - yint_min)/41;
16
17 % Prepare meshgrid in which the interpolation will be computed
18 % This is required by griddata
19 [xint, yint] = meshgrid(xint_min:xint_step:xint_max,...
20                         yint_min:yint_step:yint_max);
21
22
23
24 for CASDED=1:2
25
26
27
28
29 %% Porosity FU5
30
31 if CASDED==1
32 load('FU5por.mat')
33 x=FU5por(:,1);
34 y=FU5por(:,2);
35 z=FU5por(:,3);
36 else
37 load('FU5thickness.mat')
38 x=FU5thickness(:,1);
39 y=FU5thickness(:,2);
40 z=FU5thickness(:,3);
41 end
42
43
44
45 %% Interpolate
46

```

```

47 % IDW exponent
48
49 if CASDED==1
50     exponent = 1.5;    %Poro
51 else
52     exponent = 2.5;    %Thic
53 end
54
55
56
57 % Interpolate using griddata and nearest neighbors method
58 %interpolation = griddata(x, y, z, xint, yint, 'natural');
59
60 % Interpolate using IDW
61 interpolation_IDW = griddataIDW(x, y, z, xint, yint, exponent);
62
63
64 %% CV
65
66 N=length(x);
67 VALCV(N,1)=0;
68
69 for i=1:N
70     xt=x; xt(i)=[]; xs=x(i);
71     yt=y; yt(i)=[]; ys=y(i);
72     zt=z; zt(i)=[]; zs=z(i);
73
74
75     VALCV(i) = griddataIDW(xt, yt, zt, xs, ys, exponent);
76 end
77
78 if CASDED==1
79     disp('*****POR CV *****');
80 else
81     disp('*****THI CV *****');
82 end
83
84
85 MAECV=sum(abs(z VALCV))/N
86 RCV=corrcoef(z,VALCV)
87 MECV=sum((z VALCV))/N
88 RMSECV=sqrt(sum((z VALCV).^2)/N)
89 MaxAECV=max(abs(z VALCV))
90
91 disp(' ----- ')
92
93
94
95 %%

```



---

```

96
97
98 % Inverse Distance Weighting interpolation
99 figure;
100 pcolor(xint, yint, interpolation_IDW);
101 axis('equal', 'tight')
102 shading('flat');
103 hold('on');
104 %scatter(x, y, 20*abs(z+1), z, 'filled', 'MarkerEdgeColor', 'k');
105 c_obj = colorbar;
106 c_obj.Label.String = 'Value';
107
108 if CASDED==1
109 title(['Inverse Distance Weighting Porosity for Flow Unit 5'])
110 else
111 title(['Inverse Distance Weighting Thickness for Flow Unit 5'])
112 end
113 xlabel('x');
114 ylabel('y');
115
116 if CASDED==1
117 InterPOR=interpolation_IDW; % Kanavos tou porodous
118 else
119 InterTHI=interpolation_IDW; % kanavos tou Thickness
120 end
121
122
123 end
124
125
126 JJJ=InterPOR.* InterTHI/100;
127 xcell=xint_step*1000; ycell=yint_step*1000;
128 A=xcell*ycell; % A cubic metra
129 NG=0.7
130 Sw=0.20
131 Bo=1.2
132 metat=6.29 % kybiko metro se bbl
133 CelloOIP=JJJ*(A*NG*(1 Sw))/Bo * metat;
134 OOIP=sum(sum(CelloOIP))
135
136 Krigrids( xint_min:xint_step:xint_max, yint_min:yint_step:yint_max,
           CelloOIP );
137 colormap('parula')
138 title('OOIP Flow unit 5 STB')
139 hold off

1 function vq = griddataIDW(x, y, v, xq, yq, p)
2
3 % Interpolate 2 D scattered data using inverse distance weighting

```

```
4
5 % Compute all pairwise distances
6 r = pdist2([xq(:), yq(:)], [x, y]);
7
8 % Compute weights
9 W = 1./r.^p;
10
11 % Set weights to one for distances equal to zero
12 W(r==0) = 1;
13
14 % Interpolate
15 vq = W*v ./ sum(W, 2);
16
17 % Reshape to match matrix dimensions
18 [nxq, nyq] = size(xq);
19 vq = reshape(vq, nxq, nyq);
```

```
1
2 cle
3
4 %% GRID
5 % Grid apo kanabo porodous
6 load('FU5por.mat')
7 x=FU5por(:,1);
8 y=FU5por(:,2);
9
10 nx=146; % gia keli 60x60m
11 ny=82;
12
13 minx=min(x) - 0.15;
14 maxx=max(x) + 0.15;
15 miny=min(y) - 0.15;
16 maxy=max(y) + 0.15;
17
18 Xk=linspace(minx, maxx, nx);
19 Yk=linspace(miny, maxy, ny);
20 [XI, YI] = meshgrid(Xk, Yk);
21
22 Ax=reshape(XI, nx*ny, 1);
23 Ay=reshape(YI, nx*ny, 1);
24 A=[Ax, Ay];
25
26 %% Thickness
27
28 load('FU5thickness.mat')
29 %load Kanavos
30
31 x=FU5thickness(:,1);
32 y=FU5thickness(:,2);
```

---

```

33 Th=FU5thickness (:,3);
34
35 [ArWeiTh] = Vorongrap(x, y,Th, 0.15);
36
37 c_obj = colorbar;
38 c_obj.Label.String = 'Thickness (m)';
39 xlabel('x (km)');
40 ylabel('y (km)');
41
42 [idTh] = knnsearch([x y],A,'k',1);
43 VORONKANth=Th(idTh);
44 VORONKANth=reshape(VORONKANth,ny,nx);
45
46
47
48 %% Porosity
49
50 load('FU5por.mat')
51 x=FU5por(:,1);
52 y=FU5por(:,2);
53 Por=FU5por(:,3);
54
55 [ArWei] = Vorongrap(x, y,Por, 0.1);
56
57 c_obj = colorbar;
58 c_obj.Label.String = 'Porosity (%)';
59 xlabel('x (km)');
60 ylabel('y (km)');
61
62 [idPor] = knnsearch([x y],A,'k',1);
63
64 VORONKANPor=Por(idPor);
65 VORONKANPor=reshape(VORONKANPor,ny,nx);
66
67 %% Sxhmata
68
69 figure(3)
70 surf(XI,YI,VORONKANth)
71 shading flat
72 colormap('parula')
73 colorbar
74 title('Voronoi Estimation for Thickness')
75 c_obj = colorbar;
76 c_obj.Label.String = 'Thickness (m)';
77 xlabel('x (km)');
78 ylabel('y (km)');
79 view(2)
80
81 figure(4)

```

```

82 surf(XI,YI,VORONKANPor)
83 shading flat
84 colormap('parula')
85 colorbar
86 title('Voronoi Estimation for Porosity')
87 c_obj = colorbar;
88 c_obj.Label.String = 'Porosity (%)';
89 xlabel('x (km)');
90 ylabel('y (km)');
91
92 view(2)
93
94
95 %%
96
97 VALTH=VORONKANth;
98 VALPOR=VORONKANPor;
99
100 JJJ=VALTH.* VALPOR/100;
101 Krigrids( Xk, Yk, JJJ );
102 colormap('parula')
103 hold off
104 xcell=(Xk(2)-Xk(1))*1000; ycell=(Yk(2)-Yk(1))*1000;
105 %CUBICM=sum(sum(JJJ*xcell*ycell));
106 A=xcell*ycell; % A cubic metra
107 NG=0.7
108 Sw=0.20
109 Bo=1.2
110 metat=6.29 % kybiko metro se bbl
111 CellOOIP=JJJ*(A*NG*(1-Sw))/Bo * metat;
112 OOIP=sum(sum(CellOOIP))
113 %title('OOIP flow unit 5 (bbl)')
114 %hold off

```

```

1 % cle
2 % load('FU5PERM.mat')
3 % FU5PERM(951,:)=[];
4 % e=(FU5PERM(:,3));
5 % e(e<=10^(7))=0.0000001;
6 % K=FU5PERM(:,4);
7 % %K(K<=10^(5))=0.00001;
8 %
9 % f1=fittype('a*x.^3+b')
10 % [F1, G1, L1] = fit(e,K,f1)
11 %
12 % f2=fittype('a*x.^3')
13 % [F2, G2, L2] = fit(e,K,f2)
14 % K=FU5PERM(:,4);
15 % f3=fittype('(a*((x.^3)))/((1-x)^2)') % K=a*(e^3*Dp^2)/(1-e)^2

```

---

```

16 % [F3, G3, L3] = fit(e,K,f3)
17 % myfit = fit(e/100,K,f3)
18 %
19 % KabiliTasis=f3(174.3,e/100);
20 %
21 % figure;
22 % plot(e/100,K, '. ')
23 % hold on;
24 % plot(e/100,KabiliTasis, '. ')
25 % xlabel('Porosity Percent')
26 % ylabel('Permiebility')
27 %%
28 cle
29 load('FU5PERM.mat')
30 %FU5PERM(951,:)=[];
31 e=(FU5PERM(:,3));
32 e(e<=10^(7))=0.0000001;
33 K=FU5PERM(:,2);
34
35
36 %% Coates Equation
37 f1=fitttype('a*x.^4')
38 [F1, G1, L1] = fit(e,K,f1)
39 [myfit1,myfit1_gof] = fit(e/100,K,f1)
40
41 KabiliTasis1=f1(myfit1.a, e/100);
42 g = inline('P1*x.^4', 1)
43 j=linspace(10^5,0.23,100);
44 a=myfit1.a
45
46 t=g(j,a)
47
48 figure(1);
49 plot(e/100,K, '. ')
50 hold on;
51 %plot(j,t)
52 title('Coates Equation')
53 plot(e/100,KabiliTasis1, 'x')
54 xlabel('Porosity Percent')
55 ylabel('Permiebility (md)')
56 hold off
57
58 %% Timur Equation
59
60 f2=fitttype('a*exp(x.*b)')
61 [F2, G2, L2] = fit(e,K,f2)
62 [myfit2,myfit2_gof] = fit(e/100,K,f2)
63
64 KabiliTasis2=f2(myfit2.a, myfit2.b, e/100);

```

```

65
66 figure(2);
67 plot(e/100,K, '. ')
68 hold on;
69 plot(e/100,KabiliTasis2, 'x')
70 title('Timur Equation')
71 xlabel('Porosity Percent')
72 ylabel('Permiebility (md)')
73 hold off
74
75
76
77 %% Kozeni Carman Equation
78
79 %K=FU9PERM(:,4);
80 f3=fittype(' (a*((x.^3)))/((1 x)^2) '); % K=a*(e^3*Dp^2)/(1 e)^2
81 [F3, G3, L3] = fit(e,K,f3)
82 [myfit3, myfit3_gof] = fit(e/100,K,f3)
83
84 KabiliTasis3=f3(myfit3.a, e/100);
85
86 figure(3);
87 plot(e/100,K, '. ')
88 hold on;
89 title('Kozeni Carman Equation ')
90 plot(e/100,KabiliTasis3, 'x')
91 xlabel('Porosity Percent')
92 ylabel('Permiebility (md)')
93 hold off
94 % cle
95 % load('FU3PERM.mat')
96 % %FU3PERM(951,:)=[];
97 % e=(FU3PERM(:,3));
98 % e(e<=10^(7))=0.0000001;
99 % K=FU3PERM(:,4);
100 % %K(K<=10^(5))=0.00001;
101 %
102 % f1=fittype('a*x.^3+b')
103 % [F1, G1, L1] = fit(e,K,f1)
104 %
105 % f2=fittype('a*x.^3')
106 % [F2, G2, L2] = fit(e,K,f2)
107 % K=FU3PERM(:,4);
108 % f3=fittype(' (a*((x.^3)))/((1 x)^2) ') % K=a*(e^3*Dp^2)/(1 e)^2
109 % [F3, G3, L3] = fit(e,K,f3)
110 % myfit = fit(e/100,K,f3)
111 %
112 % KabiliTasis=f3(72.4, e/100);
113 %

```

---

```
114 % figure; % Rotaw andrea ti pws vazw grammi tashs mesa sta dedomena kai
    na moy enfanizetai mazi tous sto plot!!!
115 % plot(e/100,K, '. ')
116 % hold on;
117 % plot(e/100,KabiliTasis, '. ')
118 % xlabel('Porosity Percent ')
119 % ylabel('Permiebility ')
120 %
```